UNIVERSITAT POLITÈCNICA
DE CATALUNYA
BARCELONATECH

From the production of the single cell to the end of life of the battery module: the development of parameter variation of lithium-ion cells

David Oeser

Universitat Politècnica de Catalunya

Departament d'Enginyeria Elèctrica

PhD thesis

From the Production of the Single Cell to the End of Life of the Battery Module: The Development of Parameter Variation of Lithium-Ion Cells

Author: **David Oeser**

Directors: **Daniel Montesinos i Miracle**
Ansgar Ackva

Barcelona, September 2022

Universitat Politècnica de Catalunya
Departament d'Enginyeria Elèctrica
Centre d'Innovació Tecnològica en Convertidors Estàtics i Accionament
Av. Diagonal, 647. Pl. 2
08028 Barcelona

Acknowledgement

First of all, I would like to thank my supervisors Ansgar Ackva and Daniel Montesinos-Miracle for their confidence and continuous support during this thesis. Both always listened to my technical and organisational problems and helped me to overcome them. It was their advice and critical questions that helped me to stay on the right path in the last few years.

I would also like to thank my reviewers Prof. Gunther Bohn and Prof. Bernhard Arndt. Their invested time enabled me to further improve this thesis. I would also like to thank Prof. Francisco Díaz González, Prof. Andreas Sumper and Prof. Johannes Teigelkötter for their support and willingness to participate in the committee.

Special thanks go to my colleagues Andreas Ziegler, who has accompanied and supported me since the beginning of my study in 2012, and to Thiemo Hein. Our extensive discussions about test procedures, ageing mechanisms and the interpretation of test results have contributed significantly to the success of this thesis. I would also like to thank them for supporting me in monitoring my long-term tests when I was on holiday or sick. This important task can hardly be managed alone. Furthermore, I would like to thank all the other colleagues and students at TTZ-EMO who supported me.

I would also like to thank my parents Elisabeth and Anton. You have supported me all my life and thus created the basis for my academic education. Without you, this thesis would not have been possible.

My final thanks go to my wife Michelle, who had to put up with me, especially at the end of this thesis. You often listened to me with understanding and encouraged me to keep going when things weren't going well. Despite and thanks to you, I was able to write this thesis. Thank you for your loving support.

Abstract

In lithium-ion batteries, depending on the requirements, many individual cells are connected in series and parallel. Despite very similar individual cell parameters after production, they can develop differently during the subsequent ageing process due to intrinsic and extrinsic influences. A pronounced parameter variation of the assembled cells ultimately leads to a reduced utilisation of the lithium-ion battery and thus also to a reduced lifetime. The aim of this work is therefore to gain a better understanding of the origin and development of parameter variation during the ageing process. The work is divided into three major parts.

At the beginning, parameters such as capacity and internal resistance of 480 brand-new cells of one production batch are recorded. The obtained values allow the calculation of the production-related parameter variation of the cells. In order to investigate the development of the parameter variation during cell ageing, numerous ageing tests are carried out in this work. These are divided into single cell tests and module tests.

With the help of single cell ageing tests, the development of the parameter variation of unconnected cells is investigated. Here, several cells are combined into groups and aged under identical conditions. In order to show the influence of different operating conditions on the parameter variation during single cell ageing, the cell groups are aged at different temperatures and different load currents.

Finally, by ageing various self-built modules, the development of the parameter variation of cells connected in series and in parallel is investigated. By varying the load current and the number of cells connected in parallel, further dependencies are investigated.

The measured data show that both the load on the cells and the ambient temperature have a decisive influence on the development of parameter variation. Operating conditions near the lithium plating boundary are particularly problematic. Since the onset of lithium plating varies slightly between the ageing cells, there are extreme differences in the ageing rate over a certain period of time. This ultimately leads to large parameter variations in the tests carried out.

The cells used in this work are cylindrical cells in 18650 format with a nominal capacity of 2.6 Ah (Samsung ICR18650-26J). The high-energy cells consist of a Lithium Nickel Manganese Cobalt Oxide (NMC) cathode and a graphite anode.

Resum

Les bateries de ions de liti estan formades per l'associació sèrie i paralel de diferents cel·les en funció dels requeriments. Malgrat que els procesos productius asseguren molt poques variacions en la fabricació, aquestes poden evolucionar en el temps de manera diferent degut a les influències internes o externes. Si aquesta variació dels paràmetres de cada cel·la és molt gran es reduirà la capacitat i la vida útil de la bateria. L'objectiu d'aquest treball és aprofondir en el coneixement de l'origen dels fenòmens que provoquen la variació dels paràmetres característics de la bateria durant el seu ús i el pas del temps. El treball està dividit en tres grans parts.

Inicialment, s'han mesurat parametres com la capacitat o la resistència interna de 480 cel·les noves del mateix lot. Els valors obtinguts han permès calcular la variació de paràmetres deguda al procés productiu. Per tal d'investigar la variació dels paràmetres també durant l'ús i envelliment de les cel·les s'han realitzat tests tant de cel·les individuals com de mòduls de bateries. Amb l'ajut de l'envelliment de cel·les individuals s'investiga l'envelliment de cel·les no connectades entre elles. A partir d'aquest punt, diferents cel·les s'han convinat en grup i s'han envellit en les mateixes condicions. Per tal de poder observar la influència de les diferents condicions d'operació en la variació dels parametres durant l'envelliment, altres grups s'han envellit en diferents condicions de temperatura i càrrega.

Finalment, mitjançant l'envelliment de diferents grups de cel·les connectades en sèrie i en paral·lel formant una bateria s'han envellit i monitoritzat els seus paràmetres.

Les dades obtingudes mostren que tant el nivell de càrrega de les cel·les com la temperatura ambient tenen una influència decisiva en la variació dels paràmetres. Condicions d'operació properes a la metalització del liti (*lithium plating*) són particularment problemátiques. Atès que l'inici de la metalització del liti varia lleugerament entre les cèl·lules envellides, existeixen diferencies extremes entre cel·les. Això provoca grans variacions dels paràmetres de les cel·les envellides.

Les cel·les usades en aquest treball són cilindriques del tipus 18650 amb una capacitat nominal de 2.6 Ah (Samsung ICR18650-26J). Les cel·les, d'alta energia, consisteixen un càtode NMC i un anode de grafit.

Contents

List of Figures

List of Tables

Acronyms

AML	Areal Mass Loading.
BMS	Battery Management System.
BOL	Begin Of Life.
BOT	Begin Of Test.
CC	Constant Current.
CID	Current Interrupt Device.
CL	Cell Level.
COV	Coefficient Of Variation.
C-Rate	Current Rate.
CTS	Cell Test System.
CV	Constant Voltage.
DOD	Depth Of Discharge.
DVA	Differential Voltage Analysis.
EFC	Equivalent Full Cycles.
EIS	Electrochemical Impedance Spectroscopy.
EOC	End Of Charge.
EOD	End Of Discharge.
EOL	End Of Life.
EOT	End Of Test.
EV	Electric Vehicle.
HF	Hydrofluoric Acid.
HPS	High Power System.
LAAM	Loss of Anode Active Material.
LCO	Lithium Cobalt Oxide.
LFP	Lithium Iron Phosphate.

Li/Li$^+$	Lithium Reference.
LiBF$_4$	Lithium Tetrafluoroborate.
LIC	Lithium-Ion Cell.
LiPF$_6$	Lithium Hexafluorophosphate.
LLI	Loss of Lithium Inventory.
LTO	Lithium Titanate Oxide.
NCA	Lithium Nickel Cobalt Aluminium Oxide.
NMC	Lithium Nickel Manganese Cobalt Oxide.
OCV	Open-Circuit Voltage.
PC	Propylene Carbonat.
PLA	Polylactic Acid.
RPT	Reference Parameter Test.
SEI	Solid Electrolyte Interphase.
SHE	Standard Hydrogen Electrode.
SOC	State Of Charge.
SOH	State Of Health.
SPI	Solid Permable Interphase.

List of Symbols

$C_{\mathrm{DCH,CV}}$	Discharge Capacity with CV-Phase.
C_{DCH}	Discharge Capacity.
C_{N}	Nominal Capacity.
C_{rel}	Relative Capacity.
E^0	Standard Electrode Potential.
I_{cell}	Cell Current.
I_{p}	Cell Current during Pulse.
Q_1	Charge Quantity for Determining the Loss of Anode Capacity.
Q_2	Charge Quantity for Determining the Loss of Lithium.
Q_{Ah}	Total Charged and Discharged charge quantity.
R_{CT}	Charge Transfer Resistance (Determined in Frequency Domain).
$R_{\mathrm{DC,t_p}}$	Internal Resistance Obtained by Current Step Response at Time t_{p} (Determined in Time Domain).
R_{Im0}	Pure Ohmic Resistance (Determined in Frequency Domain).
R_{rel}	Relative Internal Resistance.
T_{amb}	Ambient Temperature.
T_{cell}	Cell Temperature (Surface).
U_{EOC}	Voltage at End Of Charge.
U_{EOD}	Voltage at End Of Discharge.
U_{cell}	Voltage of the Full Cell.
η_{anode}	Overpotential at the Anode.
κ_x	Coefficient of Variation of the Variable x.
μ_x	Mean Value of the Variable x.
ω	Angular Frequency.
ϕ	Phase Shift.

$\rho_{x,y}$	Correlation Coefficient of Variable x and y.
σ_x	Standard Deviation of the Variable x.
φ_{anode}	Anode Potential.
φ^0_{anode}	Equilibrium Potential of the Anode.
φ_{cathode}	Cathode Potential.
f	Frequency.
m_{cell}	Cell Mass (with Shrink Sleeve and Isolation Ring).
n	Quantity.
t_0	Begin of Discharge.
t_{DCH}	Discharge Duration.
t_{p}	Pulse Duration.

Chapter 1

Introduction

1.1 Background

Lithium-ion batteries consist of many individual Lithium-Ion Cells (LICs). Depending on the requirements, different numbers of cells are connected in series and parallel. Through the number of serially connected cells, the voltage of the lithium-ion battery can theoretically be arbitrarily increased. The capacity can be increased by connecting cells in parallel. In principle, the desired energy content of a lithium-ion battery can be achieved by connecting the cells in any way. However, for reasons of efficiency, higher battery voltages are preferably realised, if possible. For a required power, higher system voltages reduce the required currents and thus minimise losses. Whereas a few years ago the system voltage of Electric Vehicles (EVs) was a maximum of 400 V, nowadays more and more vehicles are operated at 800 V. The trend for EVs is therefore clearly towards higher system voltages. However, the ageing of the serially connected cells is problematic. A diverging ageing behaviour among the serially connected cells inevitably leads to unused capacity in the better cells during operation and to a shortened lifetime due to a premature reaching of the End Of Life (EOL) criterion, caused by the weaker cells.

Due to a non-ideal production process, a parameter variation exists already after the production of the cells. This results in slightly varying values for the capacity and the internal resistance. Usually the values are normally distributed.

When assembling a lithium-ion battery, the individual cells are connected by various methods. For example, the cells can be screwed together or welded. Since these processes are also subject to a certain variation, different contact resistances add to the different internal cell resistances, which can also lead to varying cell parameters during operation.

Finally, the module design plays a major role in the operation of a lithium-ion battery. The chosen arrangement of the cells automatically results in different cell temperatures during operation, since, for example, inner cells become warmer than outer cells. Even using an additional cooling/heating system does not lead to optimally homogeneous temperature conditions for all cells. The prevailing temperature differences thus promote the development of a parameter variation. The greater the temperature differences, the severe the effects.

Due to a variety of influences from production, module assembly and module design to the operating conditions, a parameter variation of the individual cells during the operation of lithium-ion batteries must therefore be considered as given. Especially the severity of the evolving parameter variation is of high interest.

This thesis therefore focuses on the investigation of the described parameter variation on an empirical level. The findings should provide a better understanding of the development of parameter variation and, if possible, help to minimise it.

1.2 Motivation of Research

Since the cut-off voltages must always be maintained for all cells of a lithium-ion battery, the weakest cell of a series connection during the discharge process leads to the End Of Discharge (EOD). The more similar the individual parameters of the serially connected cells in a lithium-ion battery are, the more available energy can be extracted. A high variation in cell parameters, on the other hand, leads to large amounts of residual energy that cannot be extracted from the lithium-ion battery. Pronounced parameter variations should therefore be minimised as far as possible during operation. Although there are a few studies that show the development of parameter variation for individual cells and modules, no recommendations are given on how the parameter variation can be influenced.

A parameter variation is basically the result of different ageing rates of the installed cells inside a lithium-ion battery module. Since cell ageing depends on many factors such as temperature, load, Depth Of Discharge (DOD) etc., the parameter variation also depends on these factors. This relationship has not yet been sufficiently researched in the literature. This thesis therefore aims to make a contribution to this area by examining in more detail how parameter variation occurs as a function of different operating conditions.

For this purpose, groups of unconnected, identical cells are first aged with different temperatures and loads in this thesis. Here, the dependence of the parameter variation on the test conditions will initially be investigated without interactions. These measurements create the basis for further investigations. Finally, the parameter variation will also be empirically investigated for modules. For this purpose, both the number of cells connected in parallel and the load are varied. This type of study can rarely be found in literature.

By excluding damaging operating conditions that lead to increased parameter variation during ageing, the capacity utilisation and lifetime of lithium-ion batteries could be improved.

1.3 Objectives of Research

The aim of this work is to gain a deeper understanding of the development of parameter variation in lithium-ion batteries by means of an empirical approach. The variation of new cells, of ageing single cells as well as of ageing modules will be investigated. For this purpose, 480 new cylindrical cells in 18650 format are available for the planned investigations. The objective is further to find out whether or not the capacity utilisation and thus also the lifetime of lithium-ion batteries can be increased with help of the knowledge gained. The following objectives are derived from this aim:

- Obtain a deeper insight into the functionality and the ageing behaviour of LICs based on the literature.
- Review the current state of the literature regarding parameter variation of new cells, aged single cells and aged modules.
- Reveal the effects of production on parameter variation of new LICs.
- Investigate the influence of temperature and load on the parameter variation of single cells during ageing.
- Analyse the parameter variation behaviour of modules depending on cell configuration and load during ageing.
- Derive recommendations for minimising parameter variation on the basis of the measured data.

1.4 Contributions of Research

The scientific contribution of this work can be summarised as follows:

- This thesis presents various parameters of 480 brand-new cells with the help of common measuring methods. With the help of these parameters, statistical values are calculated (e.g. standard deviation, mean value, coefficient of variation). Correlations between the parameters are examined. On the one hand the measurement of the 480 cells serves as a basis for comparison for all further measurements in this thesis. On the other hand this study extends the existing literature. In order to increase comparability, this work also records parameters used in the literature.
- To investigate the parameter variation of unconnected single cells, a total of 80 cylindrical cells in 18650 format were aged in 10 different groups. For each group, the load (0.5C and 1.0C) and the ambient temperature (0°C to 40°C) were varied. During the ageing process, the condition of all cells was periodically recorded using various measuring methods. At End Of Test (EOT), further measurement methods such as Differential Voltage Analysis (DVA) and Electrochemical Impedance Spectroscopy (EIS) provide additional insights into the ageing state of all cells. With help of the collected data, it is possible to calculate and show the progressive development of the parameter variation for all 10 operating conditions. Finally, it is possible to determine operating conditions that are particularly prone to the development of a strong variation.
- To investigate the parameter variation of cells in modules, a total of 6 self-designed and self-built modules were aged. The number of cells connected in parallel (1p to 4p) and the load (0.5C and 1.0C) were varied. By self-assembling the modules, the condition and thus also the parameter variation of all cells used can be checked before Begin Of Test (BOT). At EOT, the modules are disassembled and all individual cells are measured again. This enables a direct comparison of the cell parameters and their variation at different times. In addition, the data of the individual cells are displayed in the form of colour maps depending on the module design. In this way, valuable insights into module ageing can be gained.

  Overall, this work offers new and valuable insights into the development of parameter variation of single cells and modules that cannot be found in the literature.

1.5 Thesis Outline

This thesis is divided into 7 chapters, which are summarised below.

Chapter 1 gives a introduction to the topic and briefly explains the background of this thesis. It also summarises the motivation, objectives and contributions of this work.

Chapter 2 explains how LICs work and summarises important ageing mechanisms. In addition to common electrode materials, various cell formats and typical terminology are introduced.

Chapter 3 summarises measuring methods for determining battery-relevant parameters. These are the determination of the capacity, the determination of the internal resistance in the time and frequency domain and the Differential Voltage Analysis (DVA). DVA can be used to examine the conditions and balancing of the electrodes.

Chapter 4 first presents the production process of LICs and possible sources of production variations that can lead to deviations among cell parameters. Then, various parameters of 480 brand-new cells are recorded and presented. Using this data, variation values are calculated and correlations among the parameters are examined.

Chapter 5 describes the ageing process of a total of 80 individual cells, which are aged in 10 groups under different test conditions. With help of the empirical data, the ageing behaviour and the development of the parameter variation during ageing is shown.

Chapter 6 shows, in analogy to chapter 5, the ageing behaviour and the development of the parameter variation of cells in modules. For this purpose, a total of 6 modules are aged under different conditions and disassembled after completion of the test. A second measurement of the installed individual cells allows the parameter variation to be evaluated after the test has been completed.

Chapter 7 concludes and summarises the results of the thesis, highlights the contributions of this work and provides opportunities and suggestions for further research. A list of all publications and patent applications of the author can be found at the end of this chapter.

Chapter 2

Fundamentals of Lithium-Ion Cells

This chapter focuses on the introduction of LIC technology, its cell structure and the associated functional principle. It also includes possible degradation mechanisms that occur during ageing.

2.1 Terms and Definitions

- Nominal capacity (C_N)
  The nominal or rated capacity C_N of a cell describes the amount of electrical charge in Ah that a fully charged new cell can deliver under certain conditions. The conditions include the minimum discharge voltage, the discharge current and the temperature of the cell [1]. This information can be found in the manufacturer's data sheet.
- C-rate
  The Current Rate (C-Rate) indicates the charge or discharge current as a function of C_N. For a cell with C_N= 2.6 Ah, 1C means a charge or discharge current of 2.6 A. In other words and theoretically, a discharge with 1C is completed after exactly one hour. The C-Rate is used to make it easier to compare the currents of cells with different C_N.
- State Of Health (SOH) and usable capacity (C_DCH)
  The SOH is a relative percentage value that indicates the usable capacity C_DCH as a function of C_N. C_DCH can be calculated with the integral of the discharge current i over the duration of the complete discharge process (t_0 to t_DCH).

$$\mathrm{SOH} = \frac{C_\mathrm{DCH}}{C_\mathrm{N}} \cdot 100$$

$$C_\mathrm{DCH} = \int_{t_0}^{t_\mathrm{DCH}} i(t)\mathrm{d}t \tag{2.1}$$

- State Of Charge (SOC) and Depth Of Discharge (DOD)
  The SOC describes the actual percentage state of charge of a cell in relation to its currently usable capacity C_{DCH}. The DOD, on the other hand, indicates the percentage state of discharge of a cell in relation to its currently usable capacity C_{DCH}. It follows:

$$\mathrm{SOC} = \frac{C_{\mathrm{DCH}} - \int_{t_0}^{t_1} i(t)\mathrm{d}t}{C_{\mathrm{DCH}}} \tag{2.2}$$

$$\mathrm{SOC} = 1 - \mathrm{DOD},\ \mathrm{DOD} = 1 - \mathrm{SOC}. \tag{2.3}$$

- Begin Of Life (BOL) and End Of Life (EOL)
  The BOL of a cell is defined by the time of production, The EOL describes the end of the lifetime of a cell. The EOL is not further defined, but usually set to about 80% - 70% SOH. However, the EOL is not equivalent to a defective cell. The cell can still be used beyond the EOL.
- Begin Of Test (BOT) and End Of Test (EOT)
  According to BOL and EOL, BOT and EOT are defined by the begin and end of an experimental test a cell or a module is running through.
- Equivalent Full Cycles (EFC)
  The charge and discharge capacity of a cell depends on the operating conditions (e.g. load current and temperature of the cell). In order to ensure comparability between cells with different operating conditions, EFC can be used to specify the actual charge throughput of the cell:

$$\mathrm{EFC} = \frac{Q_{\mathrm{Ah}}}{2 \cdot C_{\mathrm{N}}}.$$

  The sum of the total charged and discharged charge quantity Q_{Ah} of the cell is thereby related to its nominal capacity C_{N}.

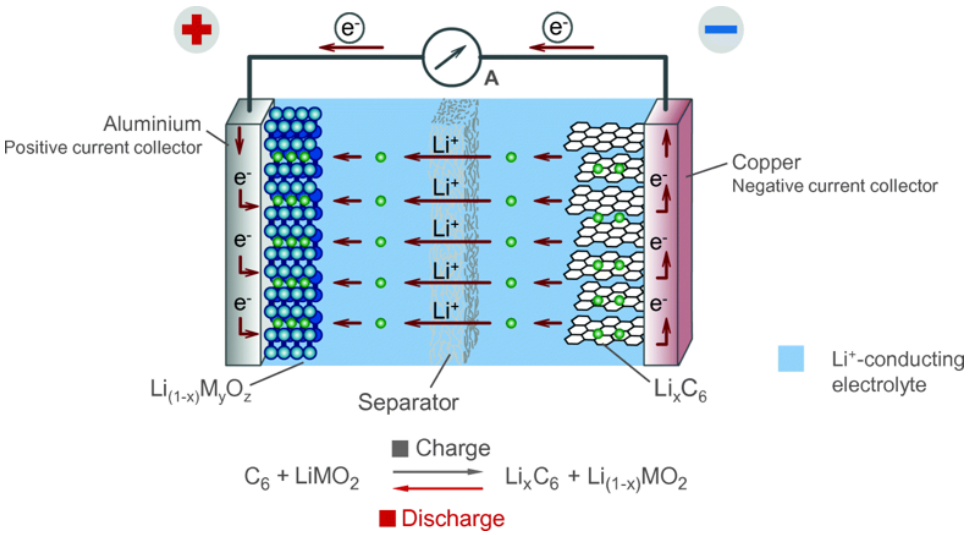

Figure 2.1: Schematic arrangement of the components of a LIC. The designation $LiMO_2$ used in the chemical equation generally describes the functional principle on the basis of layered oxides. [3]

2.2 Components of Lithium-Ion Cells

A LIC consists of two electrodes, which are separated and electrically isolated from each other by a porous membrane, the so-called separator. Both the pores of the electrodes and the pores of the separator are completely filled with electrolyte, which in commercial applications is often based on a solvent such as acetonitrile or Propylene Carbonat (PC). It is mixed with additional conducting salts such as Lithium Hexafluorophosphate ($LiPF_6$) or Lithium Tetrafluoroborate ($LiBF_4$) and has an ion-conductive property. [2]

The cathode, called positive electrode in the following work, consists in most cases of an aluminium foil with a transition metal oxide active material. On the anode, in the following referred to as the negative electrode, the active material graphite or amorphous carbon, is applied to a copper foil. The materials of the current collectors are selected to provide good electrical conductivity combined with good chemical stability. [3]

The schematic arrangement and the functional principle of the cell components is shown in Figure 2.1. The movement direction of the electrons and lithium-ions results from a discharge process of the LIC.

The first cathode material Lithium Cobalt Oxide (LCO) ($LiCoO_2$), intro-

duced by John B. Goodenough, is still used in many LICs today due to its high storage capacity, a low self-discharge and its cyclic stability [4]. Disadvantages of LCO are its low thermal stability, lattice distortion during deep cycling and the high costs due to the high content of cobalt. Further commonly used cathode materials, also for use in EVs, are NMC ($LiNiCoMnO_2$) and Lithium Nickel Cobalt Aluminium Oxide (NCA) ($LiNiCoAlO_2$). The use of nickel, manganese and aluminium results in improved properties compared to pure LCO. Besides improved thermal stability, this also includes a reduction in costs due to the lower content of cobalt. The cathode material Lithium Iron Phosphate (LFP) ($LiFePO_4$) is more suitable for use in home storage systems, but is increasingly used for EVs as well. LFP is characterised primarily by its thermal stability and thus by its low flammability. At the same time, however, the specific gravimetric discharge capacity is only a fraction of the previously mentioned materials (LFP: 150 mAh/g, NMC: 234 mAh/g, NCA: 200 mAh/g, LCO: 274 mAh/g). [5] Due to the high safety of LFP cells, extensive research is done to improve the energy density further.

Graphite as anode material has several advantages, such as a high lithium diffusivity, an electrically high conductivity and a small volume change during lithiation. It is available in large quantities and therefore relatively inexpensive. Furthermore, power and energy density, as well as the cyclic stability of the material result in a good overall compromise with regard to availability and low price [5]. The theoretical gravimetric storage capacity of graphite, with a value of about 372 mAh/g, is higher than that of most cathode materials [2]. Compared to graphite, amorphous carbons (hard carbons, soft carbons) are hardly used in consumer cells. Due to a slightly more positive potential compared to the Lithium Reference (Li/Li^+) (amorphous carbon: 0.1 V - 0.7 V, graphite: 0.1 V - 0.2 V), slightly higher charging currents are possible, as the risk of metallic lithium deposition decreases. In the case of an alloy with metals, the storage capacity of amorphous carbon can significantly exceed that of graphite. The structure is considered more stable and safer in compounds with novel electrolytes and cathode materials, but further research on these materials is needed [3]. Lithium Titanate Oxide (LTO) is characterized by high cyclic and thermal stability. The change in volume during lithiation is only 0.2% (volume change in graphite: approx. 10%), which contributes significantly to its cyclic stability. An advantage and disadvantage at the same time is the voltage of the material compared

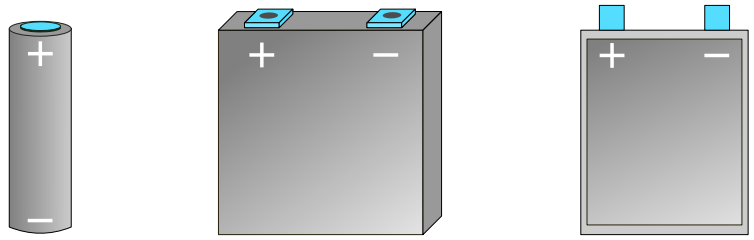

Cylindircal Prismatic Pouch

Figure 2.2: The different cell formats vary in their external form and dimensions. Moreover, the form of the cells results in different possibilities for connecting a cooling system.

to Li/Li^+ of approximately 1.55 V. On the one hand, lithium plating is hardly an issue, even at high C-Rate during charging. But on the other hand the energy density is limited by the low total voltage of the cell [6].

2.3 Cell Formats

LICs exist in various formats. There are cylindrical cells, prismatic cells and pouch cells (see Figure 2.2). The chemical function of the different types does not differ. For all formats, metal-based packaging or cases are used to prevent the penetration of moisture and the exchange of substances with the environment. There are solid metal housings, as in the case of cylindrical and prismatic cells, but also plastic housings coated with aluminium, as in the case of pouch cells. [7]

Each format has some specific properties. Especially with regard to the cooling connection and the heat development in the cell, there are significant differences where the anisotropic thermal conductivity has to be taken into account. Thus, the appropriate cooling concept must be designed individually for each cell type. [8, 9]

Further differences exist in the production of the electrode-separator composite. While cylindrical winding is used for cylindrical cells, there are other possibilities for prismatic and pouch cells. These include, for example, stacking, prismatic winding and z-folding. [10]

Nowadays, all formats are used in traction batteries of electric vehicles. Due to the significantly lower energy content of the smaller cylindrical cells, many

cells are often connected in parallel to increase the capacity. However, the possible volumetric energy density of the formats differs only slightly. [9]

2.4 Function of Lithium-Ion Cells

The function of a LIC is explained using the charging process of the full cell. By applying an electrical voltage across the two electrodes, the charging process is initiated and a cell-external flow of electrons from the positive to the negative electrode occurs. In order for the crystal lattice of the positive electrode to retain its electrical neutrality, a balancing process takes place inside the cell simultaneously. Under energy input lithium-ions are dissolved from the crystal of the positive electrode and migrate into the electrolyte, which solvates the ions with the help of solvent molecules. This process is called deintercalation. At the same time, the crystal lattice of the positive electrode releases an electron via the external circuitry. The reaction equation is as follows [2]:

$$\mathrm{LiM^{III}}_{1-x}\mathrm{O_2} \longrightarrow \mathrm{Li}_{1-x}\mathrm{M^{IV}O_2} + \mathrm{xLi^+} + \mathrm{xe^-}. \tag{2.4}$$

The factor x is material-dependent and describes the amount of lithium which can be removed from the crystal. A complete removal means x=1, while x=0 therefore means no removal. For NMC, for example, x=0.66 should not be exceeded for reasons of structure stability. [3]

The designation $\mathrm{LiMO_2}$ used in the chemical equation generally describes the functional principle on the basis of layered oxides. These are often used as cathode material. In the equation, M can be substituted by suitable metals such as cobalt, nickel, manganese or aluminium, as well as combinations of these metals (e.g. $\mathrm{Li}_{1-x}(\mathrm{Ni}_{1/3}\mathrm{Mn}_{1/3}\mathrm{Co}_{1/3})\mathrm{O_2}$ (NMC)). [3]

The dissolved lithium-ions now migrate through the separator to the negative electrode. In case of the first charging process after production, the Solid Electrolyte Interphase (SEI) is formed on the negative graphite electrode. During this process a small amount of the lithium-ions reacts with degradation products of the liquid electrolyte and deposits as an insoluble layer on the graphite electrode surface. Further decomposition of the electrolyte by reaction with the anode is thus limited [11,12]. This layer serves to separate the lithium-ions from the solvent molecules and to allow them to enter the

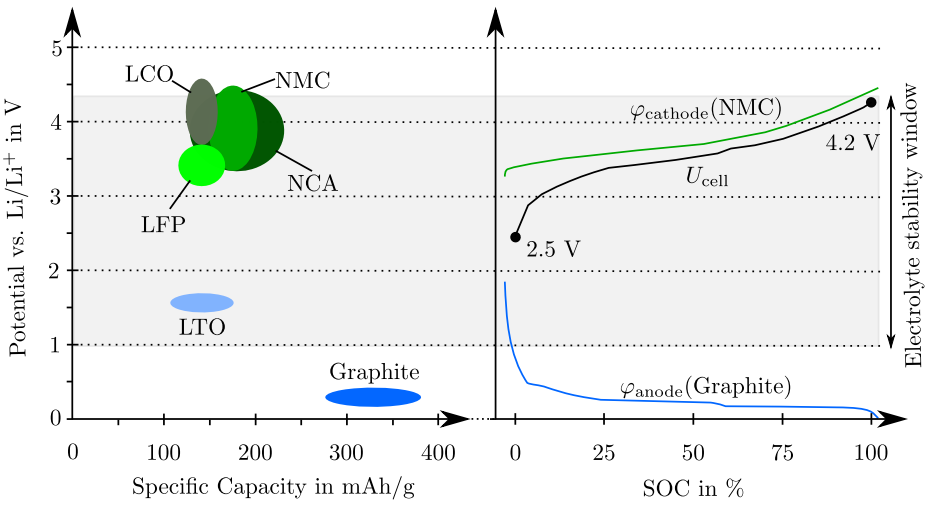

Figure 2.3: Operating range of common electrode materials vs. Li/Li^+. Blue toned materials are suitable anode materials, green toned materials are used as cathode material. Based on [5].

graphite lattice of the negative electrode [3]. Most cells use carbon-based anode materials, which usually form a stable SEI [12]. The SEI plays a role not only in protecting the anode, but also in cell ageing [13]. During the intercalation of lithium-ions into the anode an electron is taken up. The resulting lithium is intercalated in the carbon structure of the anode. For the intercalation of one lithium atom, six carbon atoms are needed. The reaction equation is as follows [2]:

$$C_6 + xLi^+ + xe^- \longrightarrow Li_xC_6. \tag{2.5}$$

When the LIC gets discharged, the entire process described above is reversed.

2.4.1 Operating Range of Electrodes

The cell voltage U_{cell} depends on the materials used and is calculated from the difference between the cathode and anode potential:

$$U_{cell} = \varphi_{cathode} - \varphi_{anode}. \tag{2.6}$$

The potential of the cathode and anode material is not constant. Depending on the degree of lithiation, a certain potential vs. Li/Li^+ develops for the re-

spective electrode. U_{cell} changes accordingly. Figure 2.3 shows the potential vs. Li/Li^+ for some common cathode and anode materials. Each material covers a certain potential range due to different degrees of lithiation. Based on an NMC cathode and a graphite anode, the resulting cell voltage U_{cell} is qualitatively presented.

Furthermore, the grey area in Figure 2.3 shows the electrochemical stability window of common organic electrolytes. These cover a voltage range of approximately 4.35 V to 1 V vs. Li/Li^+. Below 1 V reduction takes place, above 4.35 V oxidation of the electrolyte starts. The reduction of the electrolyte below 1 V at the anode is an essential part of the formation of the SEI. When the SEI is formed, in theory the electrolyte is protected from further reactions with the anode. [2]

The notation of the electrode potential versus Li/Li^+ as a reference potential is advantageous in LIC technology, since lithium is the reference point for the electrodes used. Normally, the standard electrode potential E^0 of a specific electrode is determined by the Standard Hydrogen Electrode (SHE). In chemistry, hydrogen is considered the zero point of the standard potential scale (potential vs. SHE) [14]. For pure lithium E^0 = -3.04 V, which is the lowest potential of the standard potential scale. To transfer the SHE notation to the notation versus Li/Li^+, the potential of -3.04 V must be subtracted from the SHE potential.

2.5 Ageing Mechanisms

The following subsections describe ageing mechanisms of different LIC components. In general, ageing can be divided into two fields. Cyclic ageing takes place during use and calendar ageing during storage. In reality, these two fields overlap and cannot be separated. Regardless of the field of ageing, the ageing process is characterized by a decrease in usable capacity, as well as a decrease in performance caused by an increase in cell impedance. Since the LICs investigated in this work are based on a NMC cathode and a graphite anode, the ageing process is described based on these materials.

2.5.1 Ageing of Active Anode Material

Despite the fact that not only graphite but also other materials are used, there are considerably more scientific studies on the ageing processes of graphite anodes, due to its heavy use in consumer cells [15]. The ageing

of graphite anodes is mainly affected by changes in the SEI, lithium plating and mechanical stress [13]. These mechanisms are described on the following pages.

2.5.1.1 Solid Electrolyte Interphase

The operating range of a graphite anode comprises a voltage that lies outside the stability window of the electrolyte used (see Figure 2.3). Therefore, the anode surface has a strong reducing effect on the electrolyte, especially in charged state, due to the low anode potential. Thus, when solvated lithium-ions enter the anode, the electrolyte is reduced and decomposes into its components [16]. Under consumption of lithium, this decomposition products cause organic layers to form on the anode surface, the so-called SEI. An ideally formed SEI is electrically insulating and can only be passed by lithium-ions. With an ideal SEI, further reactions of the anode surface with the electrolyte would be prevented [15]. After the initial formation, the SEI serves to desolvate the solvated lithium-ions.

The composition of the SEI depends strongly on the anode material and the electrolyte used in the LIC. In the case of the electrolyte, for example, it depends on the solvent contained, the conducting salt and the additives used. When using graphite and electrolytes based on PC with $LiPF_6$ as conducting salt, reaction products such as Li_2CO_3, $ROCO_2Li$, $(CH_2OCO_2Li)_2$ and LiF are often reported. [11, 17]

Since the structure of the SEI is only perfect in theory, further reactions occur during use of the LIC. For example, the volume change of the anode during intercalation of lithium can damage the SEI. At the exposed areas of the anode surface SEI is reformed which irreversibly consumes lithium. This lithium is no longer available and the cell capacity is reduced. The thickening of the SEI also increases the cell impedance, as the intercalation of lithium-ions becomes increasingly difficult. In addition, the conductivity of the electrolyte decreases due to the decomposition at the anode surface. The thickness of the SEI is initially in the range of some 10 nm up to some 100 nm in aged state [18–20].

Continuous, extensive growth of the SEI can also lead to penetration into the structure of the separator or the anode, reducing the accessible active anode surface area. The penetration of the SEI into the anode affects the porous structure, which ultimately leads to local lithium plating during charging, even at low current levels. Yang et al. have investigated this phenomenon

and assign the non-linear rapid capacity loss at the EOL to this phenomenon. [21]

2.5.1.2 Lithium Plating

Lithium plating is an undesirable side reaction that can occur during the charging process of a LIC. Instead of the desired intercalation of lithium, deposition occurs on the anode surface below the SEI. The condition for the occurrence of lithium plating is controversial. However, it is often assumed that lithium is deposited when the anode potential φ_{anode} is below 0 V vs. Li/Li^+ [22].

$$\varphi_{\text{anode}} \leq 0\ V \tag{2.7}$$

The anode potential φ_{anode} results from the equilibrium potential of the anode φ^0_{anode} and the overvoltage at the anode η_{anode} [23]. It follows:

$$\varphi_{\text{anode}} = \varphi^0_{\text{anode}} - |\eta_{\text{anode}}|. \tag{2.8}$$

Various circumstances influence the equilibrium potential of the anode by an overpotential and thus can lead to lithium plating. Lithium plating is favoured by high charging currents, low ambient temperatures and a high SOC [21, 24, 25]. Bach et al. report that local mechanical pressure within the anode can lead to local lithium plating, too [26].

Graphite anodes are in principle particularly susceptible to lithium plating, as the intercalation potential of lithium is barely above the deposition potential for lithium [3, 21, 27, 28]. Thicker anodes with larger graphite particles are even more susceptible to lithium plating than thinner anodes with smaller particles [21, 29].

The occurrence of lithium plating ($\varphi_{\text{anode}} \leq 0\ V$) can lead to various effects, which are explained in more detail below. Here, a differentiation is made between reversible and irreversible lithium plating. Figure 2.4 summarises the different effects in a qualitative illustration.

If lithium has deposited on the anode surface during the charging process, it can subsequently intercalate into the graphite by diffusion. No lithium is lost during this process. Another reversible process is given by so-called lithium stripping. When the charging process is completed and the LIC is subsequently discharged, the plated lithium (Li^0) can become an ion again (Li^+) by releasing an electron and participate normally in the discharging

process. Lithium stripping is possible because the oxidation potential of lithium, lies below the potential of lithium de-intercalation [27, 30]. A requirement for lithium stripping is the electrical contact between lithium and the graphite particle, as well as the location below the SEI.

If there is a higher concentration of deposited lithium, it can get into contact with the electrolyte outside of the SEI, causing formation of new SEI (SEI reformation) [25]. As already mentioned, the new formation of the SEI under consumption of lithium leads to significant capacity loss, to a decrease of the electrolyte conductivity and to a reduction of the anode porosity. This in turn leads to an increase in current density at the concerned areas and thus increases the probability of further lithium plating. Therefore, especially aged LICs, which already show structural changes at the anode, have a stronger tendency to lithium plating, even at higher temperatures [21, 28].

The deposited lithium tends to form needle-shaped structures. These so-called dendrites can become a safety risk, for example by damaging the separator and leading to internal short circuits. [21, 24, 31]

Also, in the case of extensive plating, lithium that is directly on the graphite surface can be dissolved faster than lithium that is deeper in the SEI. As a result, parts of the deposited lithium may lose electrical contact to the graphite. Due to the reaction of the loose lithium with the electrolyte, it becomes electrically isolated and turns into dead lithium. [32]

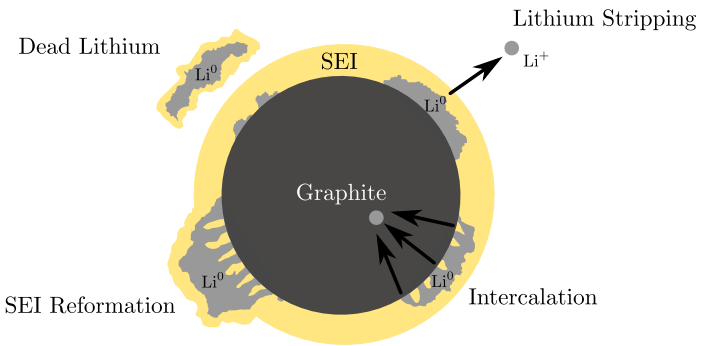

Figure 2.4: Schematic illustration of lithium stripping, lithium intercalation, SEI reformation and the formation of dead de-contacted lithium. Based on [22].

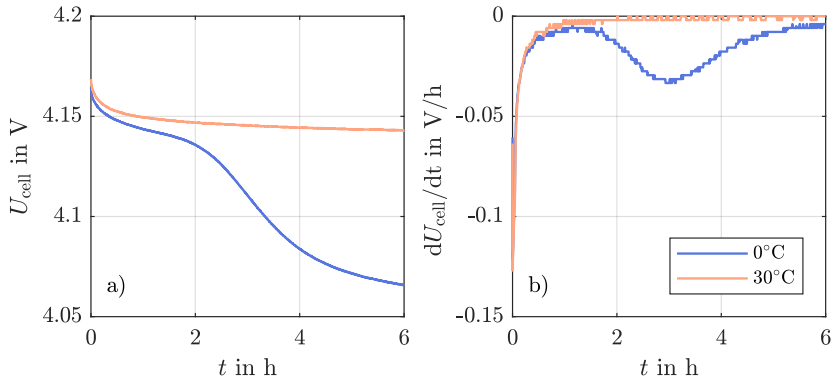

Figure 2.5: Relaxation measurement of two identical LICs, both charged with 1.0C followed by a Constant Voltage (CV) phase at 4.175 V. a) relaxation behaviour of both LICs after charging. b) corresponding derivatives.

Detection of Lithium Plating

There are various methods to detect lithium plating in LICs. For example, after disassembling, the anode material can be examined optically with the aid of a microscope or by material analysis for metallic lithium. A more simple and non-invasive method is given by the relaxation measurement. This was used in [33] and verified in parallel with help of in situ neutron diffraction.

To carry out the relaxation measurement, the LIC is charged under the condition to be investigated (e.g. 1.0C/0°C). The measurement begins immediately after the charging current is switched off. From this point on, U_{cell} is observed for several hours. If lithium plating has taken place in the previous charging process under the selected condition, the curve shows a clear voltage drop with an additional inflection point. This indicates that plated lithium is subsequently intercalated in the anode. By deriving the associated voltage curve, the inflection point can be visualised and evaluated as an extremum. In [33] a direct correlation between the position of the extremum and the amount of plated lithium was demonstrated. The later the extremum, the more plating has taken place in the previous charging process. Figure 2.5 shows a relaxation measurement for two different conditions with identical LICs. At 0°C, plating can be detected (extremum at ca. 3 h), at 30°C there is no plating.

2.5.1.3 Mechanical Stress

Theoretically, the intercalation and de-intercalation of lithium in and from the anode over the entire SOC range results in a volume change of the active material of about 10% [5, 15]. If the SOC range of the cell is not fully utilized, the value is correspondingly lower [34]. However, SOCs where the anode is weakly lithiated are significantly more harmful than areas of higher lithiation [35]. Lithium plating leads to an even stronger volumetric expansion [36].

The volumetric expansion of a LIC can be measured with suitable measuring instruments. This was proven by an high-resolution interferometric measurement in an own separate experiment [37].

The mechanical damage caused by the volume change is problematic. The expansion and contraction of the material causes cracks in the already formed SEI. Thus, areas of the anode are uncovered again and can react with electrolyte to form a new SEI. [38]

The anode itself is also damaged. If the binder material used is not able to withstand the mechanical stress, particles may be detached or the carbon-carbon bond may be lost [15,35] . This leads to a loss of accessible active material and a corresponding reduction in capacity [15]. In addition, graphite can be detached from the current collector. This increases the impedance of the cell and therefore limits its performance [39].

2.5.2 Ageing of Active Cathode Material

The cathode is also suffering from similar ageing mechanisms as the anode. The loss of capacity or power through the cathode is caused by structural changes, film formation on the cathode surface and dissolution reactions. These mechanisms are highly dependent on the combination of materials, the SOC and the temperature of the cell. [15, 40, 41]

Structural changes in the cathode can have various causes. For example, a strong discharge of the cathode leads to a phase transformation with strong volumetric expansion, which can lead to crystal defects when recharging [42]. NMC is also known for a change of the layer structure. Nickel and lithium can exchange places in the crystal lattice due to their similar atomic radii. This leads to a blockage of the diffusion channels resulting in an increase of the cathode impedance and a loss of active lithium [43].

In addition to structural changes, chemical decomposition of the electrolyte

and film formation take place due to exceeding the stability window of the electrolyte (see Figure 2.3). Therefore, when storing LICs, high temperatures as well as high SOCs should be avoided since they lead to electrolyte decay through oxidation on the cathode surface [15, 40]. The layer that forms in this process is called Solid Permable Interphase (SPI) [44]. It is reported that the formation of the SPI also leads to a significant cathode related impedance increase [40].

Another ageing factor of the cathode is metal dissolution. Here, above all, a dissolution of manganese in the electrolyte takes place, which is favoured by high temperatures [40, 41, 45]. This leads to an irreversible loss of capacity, as well as a loss of power, due to an electrical contact loss in the active material. Furthermore the manganese in the electrolyte can move to the anode and contribute to the growth of the SEI. It has been reported that even small amounts of manganese negatively affect the lifetime of LICs [40].

2.5.3 Electrolyte

In most commercial cells, $LiPF_6$ is found in the electrolyte, which is used to improve the ionic conductivity. As a side effect it is able to form the SEI during the reaction with the anode, which is necessary for the cyclic stability of the cell. [46]

However, the stability of $LiPF_6$ is problematic. At elevated temperatures, and even with the smallest impurities through water decay occurs (hydrolysis) [47]. The reaction products resulting from the decomposition increase the impurity of the electrolyte and lead to further decomposition products, which cause the electrolyte to age. In the decomposition chain, Hydrofluoric Acid (HF) is also produced, which can dissolve the SEI or the electrodes.

If there are no impurities in the electrolyte, the ageing process takes place very slowly [48, 49]. However, due to the highly hygroscopic properties of $LiPF_6$ and the electrode materials used, there are smallest traces of water in the electrolyte which lead to hydrolysis [46, 50, 51]. It is therefore almost impossible to produce completely water-free cells during production [48]. Any kind of decomposition in the electrolyte affects the ionic conductivity and thus the impedance of the entire cell.

2.5.4 Separator

Separators are used to electrically isolate the two electrodes from each other, but must also enable a high ionic conductivity. This is guaranteed by the high porosity of the materials used [3]. Various ageing and abrasion mechanisms are mentioned in the literature. One of the mechanisms is clogging of the pores. For example visco-elastic creep of the separator can lead to the closure of the pores. This phenomenon worsens at higher temperatures [52, 53]. Decomposition products in the electrolyte can also clog the pores [54]. Mechanical stress also has a negative effect on the separator. Waldmann et al. investigated the deformation of the jelly roll induced by cyclic ageing. The deformation of the jelly roll also causes a deformation of the separator [55]. The higher the intensity of the deformation, the greater the effect on the ion conductivity of the separator and thus on the impedance of the cell [56]. Vetter et al. even report that the SEI can grow into the separator, which also leads to clogging of the pores and a reduction in the ionic conductivity [15].

Chapter 3

Methods for Determining Electrochemical Cell Parameters

In chapter 2.5 different ageing mechanisms of LICs were described. Besides different causes, all mentioned ageing mechanisms lead either to a reduction of the usable capacity or to an increased internal resistance. Therefore, capacity and internal resistance are the most important parameters to determine the status of a LIC. There are various methods for this purpose which are described in this chapter. In addition, methods such as EIS and DVA are discussed. They provide additional information about the electrochemical cell behaviour.

Independent of the measuring method, important points must be considered when determining the cell parameters reliably and repeatedly. To ensure the comparability of measurements, they must always be carried out identically. This includes keeping the measurement method and the selected conditions for measurement unchanged, such as current and temperature. In the literature, a temperature of 25°C is often chosen as a basis for comparison. This can only be guaranteed, for example, with a temperature chamber.

In addition to the temperature of the cell, accurate contacting also plays an important role. A 4-point measurement with the lowest possible resistance should be used for all measurements, so that the voltage of the cell can be determined independently of the load-carrying cables. If the contact resistance of the connection is too high, the cell may heat up additionally and falsify the results. The reproducibility of the contacting also is very important, especially when comparing the internal resistance values. For example, spring-loaded contacts that connect the cell with a defined pressure after clamping are suitable for this purpose.

3.1 Determination of Capacity

To determine the discharge capacity (C_{DCH}), a fully charged cell is discharged with a defined Constant Current (CC) until the minimum permissible voltage is reached. The discharge current is integrated up to EOD to determine the amount of charge contained in the cell. The previous charge is also important in this process. Depending on the choice of the charging parameters, the capacity C_{DCH} that can be removed in the following discharge can vary significantly. The standard charging procedure is a combination of a CC charge and a subsequent CV phase at the value of the maximum permitted voltage. The CV phase is used to minimize the influence of the internal resistance and to fully charge the cell. During the CV phase, the charge current decreases continuously. The termination criteria for the current in the CV phase and other important values for determining the capacity, such as minimum and maximum voltage or the current to be selected can be found in the data sheet of a LIC.

The method just described for determining C_{DCH} using just CC discharge has a dependence on the internal resistance of the cell. The voltage drop on the internal resistance depends on the selected discharge current. Thus the lower voltage limit (EOD) depends on the discharge current as well. As a result, a quantity of unremovable charge remains in the cell. The maximum capacity of the cell can therefore not be determined with CC discharge only. In order to reduce the influence of the internal resistance, an additional CV phase with defined cut-off thresholds can be added to the CC discharge. With the help of the CV phase it is possible to determine the maximum capacity of the cell ($C_{\mathrm{DCH,CV}}$). It can be advantageous to determine both C_{DCH} and $C_{\mathrm{DCH,CV}}$ as both values can be measured and no additional test is required (see Figure 3.1). Furthermore the capacity values obtained can be used to determine the SOH of the cell. In this work, the SOH refers to the discharge capacity without an additional CV-discharge phase C_{DCH}. It follows:

$$\mathrm{SOH} = \frac{C_{\mathrm{DCH}}}{C_{\mathrm{N}}} \cdot 100 \ . \tag{3.1}$$

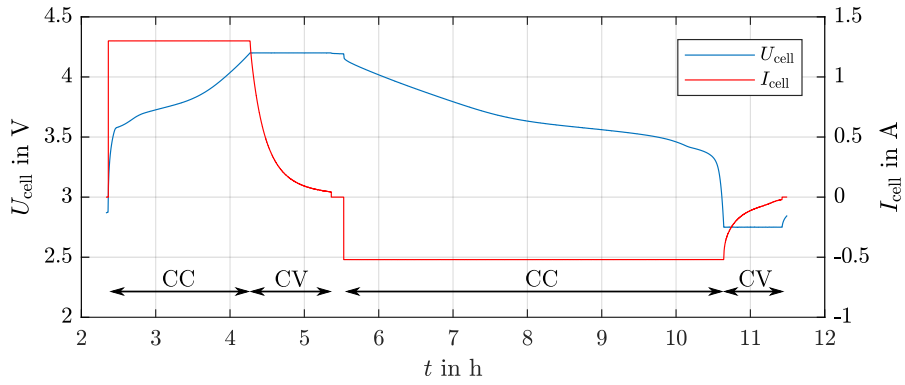

Figure 3.1: Procedure for determining the capacity (at 25°C). Both capacity values C_{DCH} and $C_{\text{DCH,CV}}$ can be taken from this procedure.

3.2 Determination of Internal Resistance

The performance of a LIC can be influenced by a variety of components within the cell. Even passive components such as the electrolyte or the separator can contribute to an increase in internal resistance (compare chapters 2.5.3 and 2.5.4). The determination of the internal resistance can be done by a current step response method in the time domain or by using a frequency dependent impedance measurement. Both methods are explained in the following subsections.

3.2.1 Current Step Response

In the current step response measurement, a change in the cell voltage ΔU is caused by the application of a current pulse of the intensity I_{p} and the duration t_{p} (see Figure 3.2). The measurement can be carried out by a charging or a discharging pulse ($I_{\text{p}} > 0$ or $I_{\text{p}} < 0$). The resistance is calculated as follows:

$$R_{\text{DC,t}_{\text{p}}} = \frac{U_1 - U_0}{I_{\text{p}}} = \frac{\Delta U}{I_{\text{p}}} \tag{3.2}$$

The duration and the intensity of the pulse are not specified. However, the product of pulse intensity I_{p} and pulse duration t_{p} should be small, in order not to change the SOC of the cell significantly during the measurement. This is problematic in terms of evaluation, since the internal resistance is a SOC

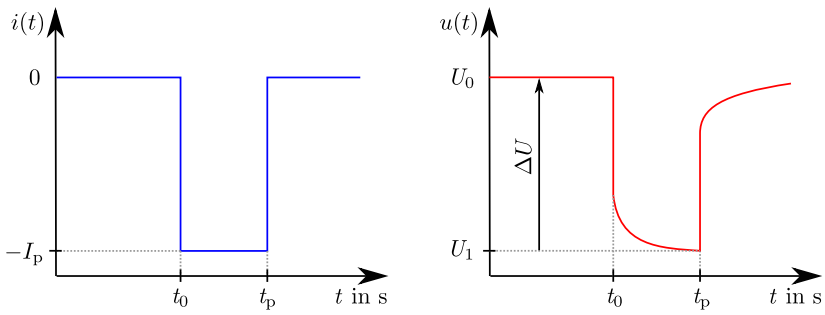

Figure 3.2: Current step response measurement with a discharge pulse. The voltage drop ΔU caused by the discharge current pulse with intensity I_p is used to calculate the internal resistance after the time t_p.

dependent variable. An evaluation of the internal resistance at a certain SOC is thus associated with an error. Typically, the maximum possible load current specified by the manufacturer is selected as I_p. The duration of the pulse amounts to a few seconds. In the literature, durations between some ms and 10 s are usually chosen [57–60].

The current step response measurement determines the sum of the pure ohmic resistance and the polarization resistance which represents slow cell processes [61]. This can be seen by transient processes in the falling voltage curve between t_0 and t_p, especially caused by charge transfer and diffusion of lithium-ions into the active material [62]. Phenomena of faster cell processes (e.g. the pure ohmic resistance) cannot be determined separately since the sampling rate of the measurement device is usually too low [63].

The advantage of this measurement method is its easy feasibility and the simple integration into the test plan. Furthermore, the cells do not need to be connected to an additional measuring device. Thus, influences of poor reproducibility on the contacting can be avoided.

3.2.2 Electrochemical Impedance Spectroscopy

EIS is a method that allows the dynamic behaviour of LICs to be investigated over a wide frequency range [62, 64]. A sinusoidal signal with the angular frequency $\omega = 2\pi f$ is used to excite the investigated cell. The signal can be a sinusoidal voltage with the peak value $\hat{U}$ (potentiostatic measurement) or also a sinusoidal current with the peak value $\hat{I}$ (galvanostatic measurement)

[2]. Furthermore, there are hybrid methods in which the measurement is carried out galvanostatically, but the current amplitude $\hat{I}$ is continuously adjusted so that a previously defined change in the voltage amplitude $\hat{U}$ is obtained.

Since the impedance of a LIC is a SOC dependent parameter, the galvanostatic or hybrid method is normally used for the measurement. They do not change the SOC on average, since the charge quantities of the first and second half-wave of the sinusoidal signal are equalized by each other. [63,65]

Assuming that a LIC is a time-invariant, linear, causal system, the response signal is also a sinusoidal signal with the same angular frequency ω and phase shift ϕ [66]. The impedance of the cell is then calculated as follows [67]:

$$i(t) = \hat{I} \cdot sin(\omega \cdot t) \tag{3.3}$$

$$u(t) = \hat{U} \cdot sin(\omega \cdot t + \phi(\omega)) \tag{3.4}$$

$$\underline{Z}(\omega) = \frac{\hat{U}(\omega)}{\hat{I}(\omega)} \cdot e^{j\phi(\omega)} = \mathrm{Re}(\underline{Z}(\omega)) + j \cdot \mathrm{Im}(\underline{Z}(\omega)). \tag{3.5}$$

At high frequencies the impedance of a LIC shows an inductive behaviour, at lower frequencies it behaves capacitive. Furthermore, in the capacitive range, the curve is characterized by two semicircles, followed by a 45° slope. Figure 3.3 shows an EIS measurement using the example of a Samsung ICR18650-26J in a Nyquist plot. The red markers show the different areas of EIS. These are explained in more detail in the following pages.

At high frequencies the cell behaves inductive. This behaviour is mainly caused by metallic parts in the cell, as well as the connecting cables of the measuring instrument [62]. Furthermore, at higher frequencies an increase of the real part can be observed, which can be ascribed to the skin effect [64]. With cylindrical cells, as in Figure 3.3, the skin effect is more pronounced due to the spiral winding and thus a higher inductance compared to other cell formats [68]. The inductive area is less relevant for the investigation of ageing effects within LICs.

In contrast to the current step response method, the purely ohmic part of the cell can be determined with the help of the EIS. At the transition from inductive behaviour to capacitive behaviour the curve crosses the real axis. At this point of intersection $\mathrm{Im}(\underline{Z})=0$ is given. Thus, the cell has

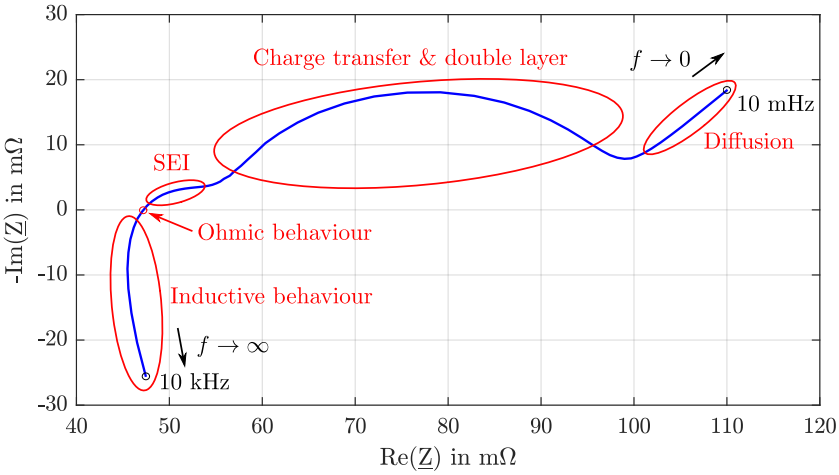

Figure 3.3: Impedance spectrum in a Nyquist plot of a Samsung ICR18650-26J cell with a nominal capacity of 2.6 Ah. The cell was tested at 100% SOC and a temperature of 25°C in a frequency range from 10 kHz to 10 mHz. Characteristic areas are marked.

a purely ohmic behaviour here. For new cells this point is usually around $f = 1$ kHz and is called R_{Im0} in this work. The ohmic behaviour at this point is influenced by several components within the cell. In [64] R_{Im0} is described as the sum of the electolyte resistance, the resistance of the current collectors, the resistance of the active material and the transition resistance of active material and current collector. In [62, 69] the separator is also mentioned as a further influence. As the cell ages, R_{Im0} continues to increase, resulting in a shift in the direction of the real axis. One reason is the loss of conductivity of the electrolyte. Therefore, R_{Im0} is well suited for the investigation of electrolyte degradation (see chapter 2.5.3) [48, 49, 63].

When conducting a EIS with a new LIC, the two semicircles often overlap in such a way that they cannot be separated. With increasing age, depending on the operating conditions, further growth of the SEI occurs, which makes the two semicircles more clearly distinguishable from each other by a stronger expression of the first semicircle, which is caused by the anodic part of the EIS. The cell in Figure 3.3 is already strongly aged (approximately 60% SOH) and is therefore well suited to show the influence of the growing SEI. The two semicircles contain information about the charge transfer resistances of both electrodes, which is linked to the slow lithium-ion interfacial transfer,

and the double layer capacities which are created by the interface between surface films and particles of the electrodes [15, 70].

The low frequency area of the EIS is characterised by a steep 45° increase, which is caused by restrictions of mass transfer and ion diffusion [64, 71]. Diffusion takes place in several processes inside the cell, for example the movement of the ions in the electrolyte, the transfer of ions through the SEI and the movements in the porous electrode [64].

Figure 3.4 shows qualitatively some characteristic processes within the cell that can be captured with help of EIS measurement.

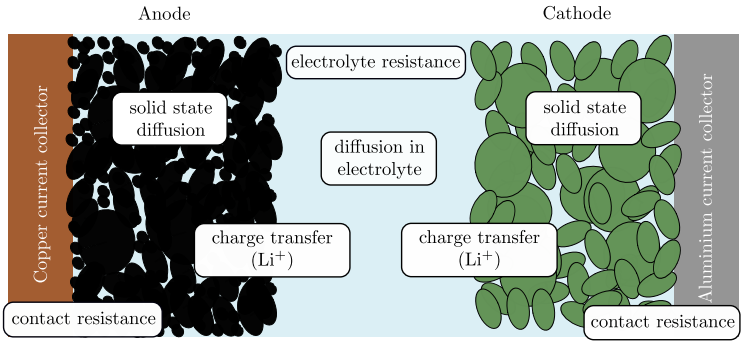

Figure 3.4: Schematic illustration of several cell-internal processes that can be measured with the help of EIS. All depicted areas are associated with losses and therefore contribute to the internal resistance of the cell. Based on [72].

In this work, for the evaluation of the EIS measurement, characteristic points of the recorded impedance spectrum are selected according to [73]. These points can be determined reliably and thus reproducibly from EIS measurements and are used for comparing the cells before and after ageing.

In the first step, the measured values during EIS are interpolated to obtain a continuous curve between the minimum and the maximum frequency. The purely inductive part of the measurement is ignored, since it does not provide information about cell-internal processes (see Figure 3.5).

As described, R_{Im0} results from the intersection of the curve with the imaginary axis and represents the purely ohmic behaviour of the cell. R_{CT} is calculated from the distance of the local minimum to R_{Im0}. If the first semicircle is negligibly small compared to the second semicircle, R_{CT} corresponds approximately to the charge transfer resistance of the cell. When the first semicircle appears during cell ageing, triggered by the growth of the SEI,

R_{CT} also includes the impedance part of the SEI.

The defined values R_{Im0} and R_{CT} are also often used for cell modelling due to their ability to describe important characteristics of the cell [61]. Also, these points provide a good complement to R_{DC,t_p} described in chapter 3.2.1, which is only able to resolve cell-internal processes in the low-frequency range due to the usually too low sample rate with the current step response method.

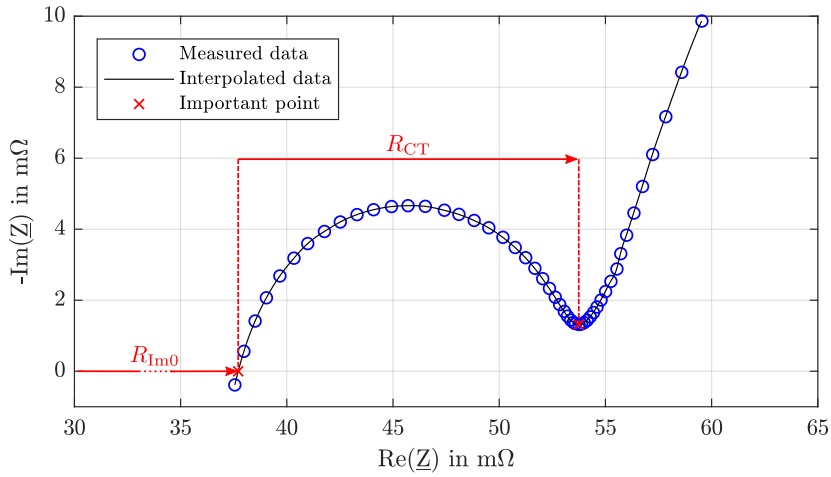

Figure 3.5: EIS measurement of a new Samsung ICR18650-26J LIC. The plot is limited to the capacitive range. After interpolation of the measured data, characteristic points can be determined.

EIS measurements show a dependence on the time since the last SOC change. This time between the last SOC change and the EIS measurement is called relaxation time, or equilibration time. During this phase, equilibration processes take place within the cell, which significantly influence the outcome of the EIS [69, 74, 75]. The reasons for these balancing processes are relaxation of ions within the double layer, electrolyte ionic concentration gradient redistribution and solid state diffusion of lithium atoms within the active materials [69].

Figure 3.6 shows the effect of the relaxation time on the EIS measurement. The more time elapses since the last SOC change, the smaller are the changes between the measurements, since the relaxation processes are mostly completed. While the first measurements still show significant shifts along the real axis after hours, hardly any changes occur between the measurements

after 100 h and 179 h.

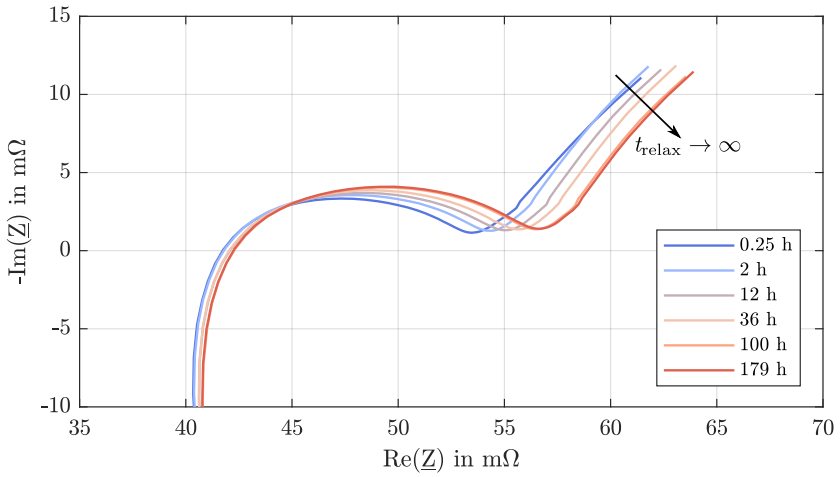

Figure 3.6: Dependence of the EIS measurement on the relaxation time. The cell was tested at 100% SOC and 25°C in a frequency range from 10 kHz to 10 mHz. It is shown clearly that there is a shift in the direction of the real axis depending on the relaxation time.

The relaxation time has a varying influence on different frequency ranges. In theory, frequencies in the range of f=1 kHz, which often describe the purely ohmic part of the cell (electrolyte, separator, current collector, etc.) are independent of the relaxation time [69]. At lower frequencies, it is assumed that balancing currents in the electrodes are responsible for the relaxation effect [74].

A closer examination of the relaxation process has shown that it is mainly the anode that contributes to changes in signal behaviour during EIS [74]. Due to the porosity of the material there is a varying current density distribution within the anode [75]. Therefore there is initially also a voltage difference between the individual anode particles. The only slowly occurring equalization process in the anode is owed to the flat curve of the anode potential, since the potential gradient between differently lithiated areas is extremely low (see Figure 2.3 anode potential). The equalization process within the cathode is much faster due to the steeper Open-Circuit Voltage (OCV) curve (see Figure 2.3 cathode potential) [74].

There are many recommendations in the literature on relaxation time, ranging from a few hours to a few days. In addition, the relaxation time also

depends on the temperature and the SOC of the cell [74]. Which relaxation time is sufficient in the end has to be determined individually for each cell.

In addition to the relaxation time, the temperature of the cell is very important for the EIS measurement. To ensure the comparability of the measured values, cells must always be tested at the same temperature. Therefore a climate chamber is recommended. Since the differences in the measurement results are very pronounced at different temperatures, the EIS measurement has already been used as a method for determining the temperature of LICs [76, 77]. Figure 3.7 shows the dependency of the EIS measurement on the temperature in a range of 10°C to 50°C. There is a strong dependence on temperature in the area of diffusion and charge transfer. Especially when examining aged cells, it is therefore important to keep the cells at the same temperature during measurement, as the changes in EIS measurement curve due to temperature deviations can be more pronounced than ageing-related changes [63].

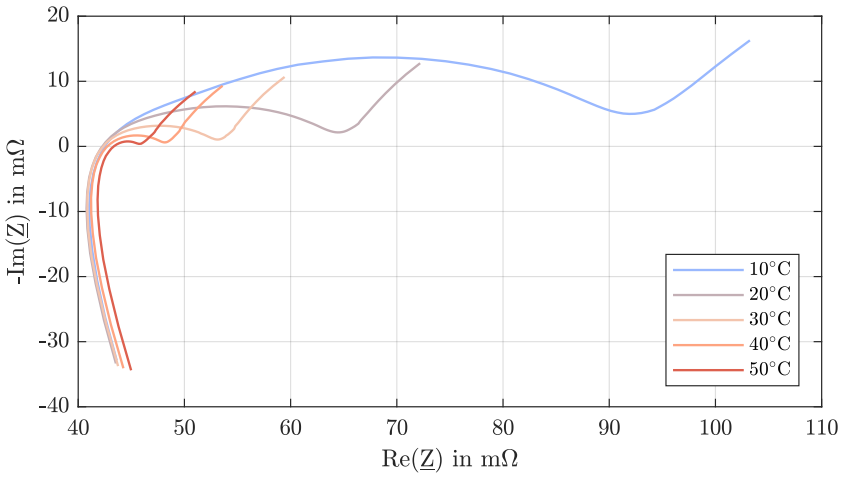

Figure 3.7: Impedance spectrum in a Nyquist plot of a Samsung ICR18650-26F cell with a nominal capacity of 2.6 Ah. The cell was tested at 100% SOC in a frequency range from 10 kHz to 10 mHz. The temperature varies from 10°C to 50°C.

3.3 Differential Voltage Analysis

In ageing studies, the degradation of LICs is usually shown by the development of the usable capacity. However, the usable capacity depends on the capacity of the two electrodes and the available lithium that can participate in the charging and discharging process. With help of DVA, a non-invasive electrical measuring method, information about the capacity of the electrodes and the amount of active lithium can be obtained.

When conducting a DVA, the investigated cell must be fully charged or discharged with a constant current. The resulting voltage curve must then be derived according to the charge ($\mathrm{d}U_{\mathrm{cell}}/\mathrm{d}Q$). The C-Rate for the measurement should be in the range of $\mathrm{C}/25$, in order to ensure that the reactions in the cell's porous electrode are as homogeneously distributed as possible [78]. If the current is too high, important information is lost, which affects the quality of the measurement. Due to the low measurement current, the derived curve is subject to strong noise. This noise is usually eliminated by mathematical filtering and smoothing [79]. In this way the characteristic peaks and areas of the differential voltage can be determined more clearly.

As already described in chapter 2.4.1 the cell voltage U_{cell} is a superposition of the cathode potential $\varphi_{\mathrm{cathode}}$ and the anode potential φ_{anode} (compare equation 2.6). According to equation 3.6 the derivative $\mathrm{d}U_{\mathrm{cell}}/\mathrm{d}Q$ therefore contains superimposed information of the derivatives of both electrodes [80, 81].

$$\left(\frac{\mathrm{d}U}{\mathrm{d}Q}\right)_{\mathrm{cell}} = \left(\frac{\mathrm{d}\varphi}{\mathrm{d}Q}\right)_{\mathrm{cathode}} - \left(\frac{\mathrm{d}\varphi}{\mathrm{d}Q}\right)_{\mathrm{anode}} \tag{3.6}$$

In Figure 3.8 the differential voltage curve of an NMC cathode and a graphite anode is shown as an example. The superposition of both curves according to equation 3.6 results in the differential voltage curve of the full cell.

Each electrode material has a characteristic shape and thus also a characteristic derivative, which can be used to evaluate the electrode ageing state. In the case of the electrode materials shown in Figure 3.8, graphite in particular stands out in the curve of the full cell. It exhibits a very distinct peak in the middle SOC and has another region at low SOC that includes several peaks. NMC, on the other hand, has hardly any characteristic shape, so that ageing-related changes can only be determined with difficulty and insufficient accuracy via DVA. Therefore, when analysing LICs with NMC as cathode material by means of DVA, the focus lies mostly on the changes

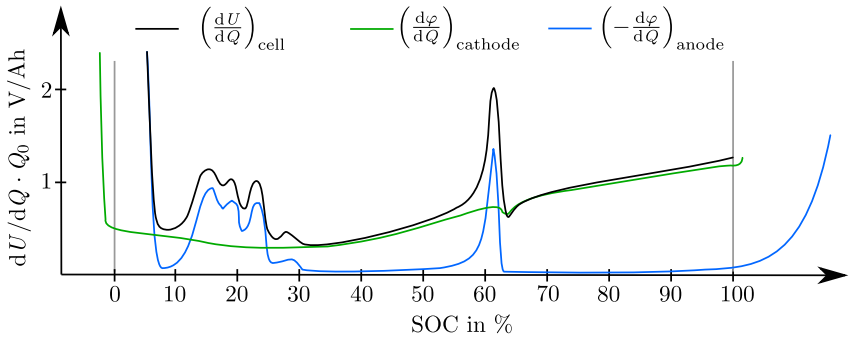

Figure 3.8: Differential voltage curves of a NMC cathode and a graphite anode, as well as their respective superposition are plotted qualitatively over the SOC area of a full cell. Both electrodes have a characteristic curve, which in some SOC areas allows a clear assignment to the respective electrode. Based on [82, 83].

in the graphite anode and the active lithium. [83]

The reason for the characteristic peaks in graphite originates from its layered structure and the intercalation of lithium-ions in it. In Figure 3.9, the voltage curve of a graphite anode versus Li/Li^+ is plotted across it's SOC. The names of the stages shown are given by the presence of lithium in every n-th interlayer. Stages marked with an L (liquid) show a random lithium intercalation. In stage 1L, therefore, each interlayer of the graphite anode is randomly and inhomogeneously lithiated (liquid like). In stages 1 and 2, on the other hand, the corresponding interlayers are fully and uniformly lithiated. In stage 2, for example, every second interlayer is completely and orderly lithiated, resulting in a SOC of the anode of 50%.

The phase transitions between the stages are classical 2-phase reactions, which lead to the potential plateaus of the graphite electrode [3, 84, 85]. These potential plateaus are transferred to the derivative of the anode voltage curve accordingly with a small value near 0 V/Ah, making the surrounding peaks stand out clearly. With NMC, on the other hand, the intercalation of lithium-ions takes place rather homogeneously over the entire process. Therefore, no potential plateaus are existing, which makes the evaluation via DVA extremely difficult [86].

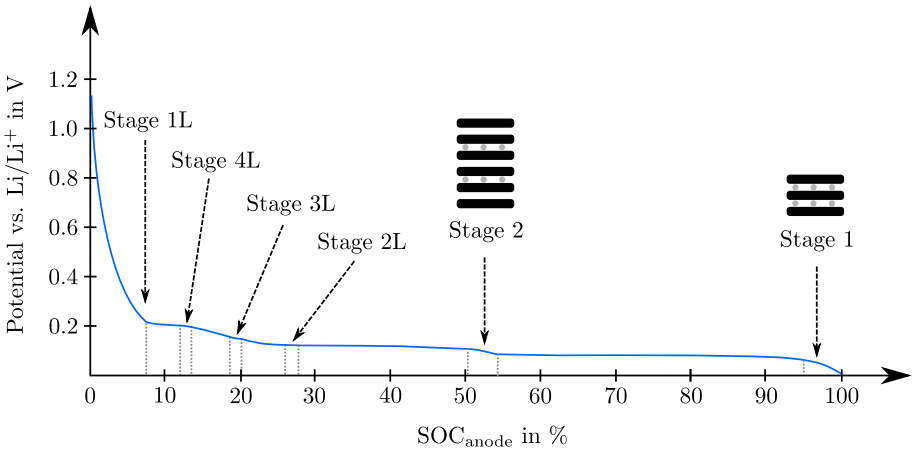

Figure 3.9: Voltage curve of a graphite anode as a function of its SOC. Different stages that occur during the intercalation of lithium are shown. Voltage plateaus exist between the stages which lead to the special characteristics of graphite. Based on [84].

3.3.1 Ageing-related Changes in the Electrode Behaviour

In order to better understand the ageing process of a LIC via DVA, possible changes in the electrode curves will first be theoretically discussed. As mentioned earlier, DVA for cells with NMC as cathode material focuses mainly on the changes in the graphite anode and the active lithium. To quantify these changes the anode potential curve is divided into two sections (Q_1 and Q_2). The boundary between Q_1 and Q_2 corresponds to stage 2 of graphite (see Figure 3.9). The outer limits of Q_1 and Q_2 are defined by the final charge and discharge voltage of the cell. The segmentation of the anode potential curve to evaluate changes can be found in various works [83, 87]. Changes in the cathode potential curve are not discussed in this chapter.

In Figure 3.10 the cathode and anode potential curves of a brand-new cell are qualitatively shown before formation. The magnitude of the End Of Charge (EOC) and EOD voltages of the entire cell U_{EOC} and U_{EOD} are visualized through the respective black bars and are given by the cell manufacturer's data sheet. The points corresponding to U_{EOD} and U_{EOC} are also drawn accordingly and mark the respective final charge and discharge potential at the cathode and the anode.

During the first charge of the cell, active lithium is transferred from the

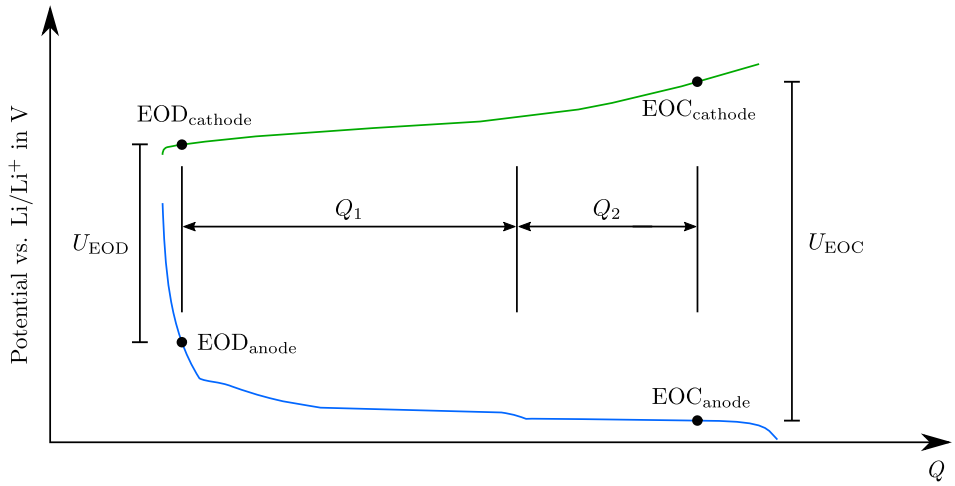

Figure 3.10: Cathode and anode potential curve of a brand-new cell before initial formation. The segmentation of the anode into the sections Q_1 and Q_2 is illustrated. Based on [85].

cathode to the anode. In addition to the intercalation of lithium in the graphite anode, active lithium is also consumed by the formation of the SEI. This Loss of Lithium Inventory (LLI) leads to an initial reduction in cell capacity, since the storage capacity of the electrodes can no longer be fully utilized. However, the storage capacity of both electrodes themselves remains unchanged. If the anode is again completely delithiated, the cathode can no longer be completely lithiated, assuming that the storage capacities are of the same size. This results in a compensating shift of the anode potential along the positive charge axis. This behaviour and the associated changes in the potential curves are shown in Figure 3.11 in more detail.

Due to the shifting of the anode potential curve, while keeping U_{EOD} and U_{EOC} unchanged, there is a shift of the EOD and EOC points on both electrodes too. In Figure 3.11 it is also visible that the capacity of cathode is utilized less after LLI when the anode is fully delithiated. In addition to the formation of SEI, other undesirable lithium-consuming side reactions lead to LLI, for example lithium plating. The shift of the anode potential curve also leads to changes in the previously defined sections Q_1 and Q_2. While Q_1 sees only a slight change after LLI, Q_2 shortens significantly as the EOC of the anode has shifted significantly towards the negative charge axis. Cell ageing which has manly taken place due to LLI can therefore be

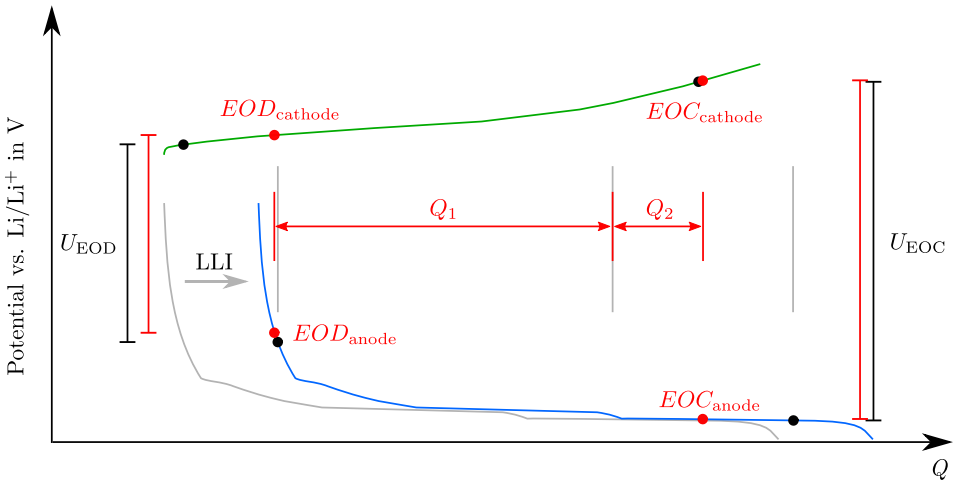

Figure 3.11: Cathode and anode potential curve of a cell solely aged by LLI. The height of U_{EOD} and U_{EOC} stays unchanged but the shifted anode curve leads to a shift of the corresponding potentials that are marked by red dots on the anode and cathode potential curve. Due to LLI Q_2 is significantly reduced. Based on [85].

well described by a reduction of Q_2.

Besides LLI, the Loss of Anode Active Material (LAAM) can also lead to a reduction in the capacity of an LIC. The causes for LAAM are manifold (see chapter 2.5.1.1). LAAM manifests itself in a compression of the anode potential curve along the charge axis. In Figure 3.12 LAAM in the delithiated state is depicted as an example. LAAM in the lithiated state would be equivalent to a combination of LAAM and LLI and is therefore not considered in this example. Here, too, the EOD and EOC points of the electrodes are adjusted accordingly. Only LAAM affects a compression of Q_1. A change due to LAAM can therefore be quantified well via the decrease in Q_1 (see Figure 3.12).

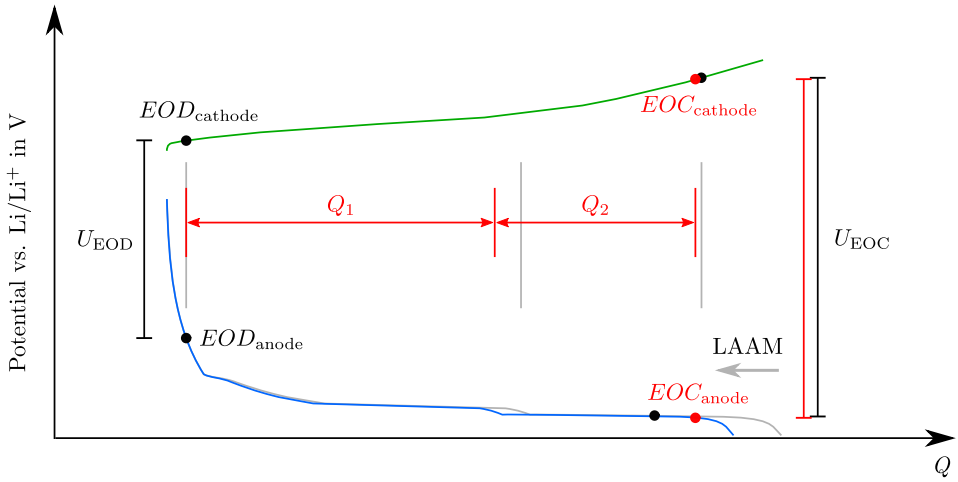

Figure 3.12: Cathode and anode potential curve of a cell solely aged by LAAM in delithiated state. The height of U_{EOD} and U_{EOC} stays unchanged but the compressed anode curve leads to a shift of the corresponding potentials that are marked by red dots on the anode and cathode potential curve. Due to LAAM Q_1 is significantly shortened. Based on [85].

In summary, the ageing-related changes in electrode behaviour can thus be described with a possible shift (so-called balancing) due to LLI and a compression due to LAAM. In reality, both effects overlap and vary depending on the ageing conditions. Figure 3.13 shows the introduced sections using the example of a brand-new Samsung ICR18650-26J LIC. In order to investigate the ageing behaviour of a LIC more precisely with the aid of DVA, changes in the marked sections Q_1 and Q_2 at BOT must be compared with later measurements in the ageing experiment.

In addition to the quantitative evaluation of Q_1 and Q_2, further statements can be made about ageing-related changes in the DVA curve shape. Lewerenz et al. [87] aged cylindrical cells with a graphite anode in their experiment. They found out that the homogeneity of the lithium distribution in the anode can be determined by the peak between Q_1 and Q_2. A decrease of the peak is associated with a decreased homogeneity of the lithium distribution, while an increase of the peak indicates a higher homogeneity. A local and thus inhomogeneous ageing of the anode is mentioned as a possible reason for the uneven distribution. Furthermore, the peaks located in section Q_1 in the lower SOC region also change. Here, an inhomogeneous distribution of lithium in the anode also becomes visible through a decrease and disappearance of the peaks.

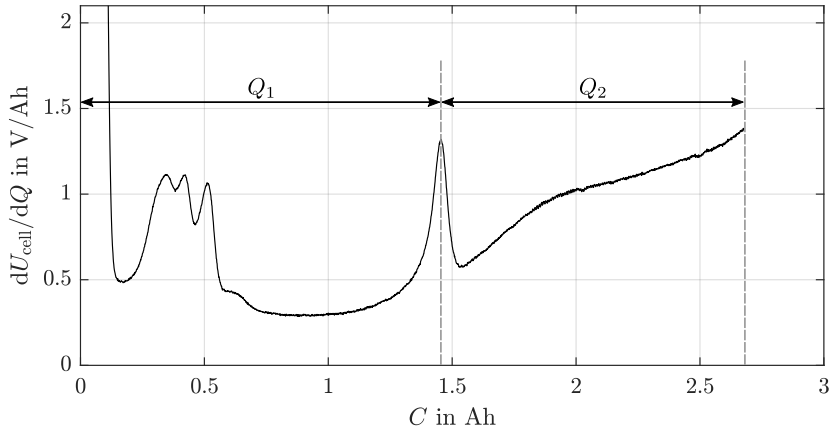

Figure 3.13: DVA of a brand-new Samsung ICR18650-26J with a nominal capacity of 2.6 Ah. The values Q_1 and Q_2 are depicted. The current during charging was set to C/20.

Chapter 4

Parameter Variation of New Lithium-Ion Cells

The production of LICs is a complex process. Due to materials and production tolerances, deviations among the cell parameters can occur. In this chapter, these production-related deviations will be investigated and quantified in more detail on 480 new cells. For this purpose, numerous characteristic parameters of the cells are recorded with the help of commonly used measuring methods. The results serve as the fundament of the work and are intended to reveal insights into the effects of production. Furthermore, the values from this post-production analysis will be used as comparative values for further experiments in the progress of the work.

Studies investigating the parameter variation of commercial brand-new LICs can already be found in the literature. Key findings are presented in the next section.

4.1 Insights from Literature

When examining brand-new LICs, it is important to have a sufficiently large number of samples. Accordingly, several 100 cells were used in most of the studies shown. This overview also includes studies that are not primarily concerned with the variation of brand-new cells, but include the measurement of new cells. These relevant studies are now briefly presented with their main focus. At the end of the section, a table presents the values that can be taken from the studies. In addition, a short paragraph discusses how comparable the results of the studies are and whether they can be used for further investigations.

- Dubarry et al. analysed 100 brand-new cells from one production lot to determine the intrinsic variations given by cell production. Both

statistical and electrochemical analyses were used to characterize and quantify the capacity variations between cells, along with other parameters that can be easily derived from the test results. A model was developed on the basis of the investigations which can predict the performance of the cells. Three critical factors were derived from this model, which lead to variation of the parameters. These are the amount of active material, the polarization resistance and localized kinetic factors. The investigated cells have a LCO cathode and a nominal capacity of 0.3 Ah. [88]

- Dubarry et al. also examined 10 new cells with a mixed cathode of $LiMn_{1/3}Ni_{1/3}Co_{1/3}O_2$ + $LiMn_2O_4$ and a graphite anode to determine the intrinsic variation of the cells. The weight and OCV of these cells were also measured again in the delivery condition. It was found that the cells are of high quality and show hardly any variation of the parameters. [89]
- In [90] Paul et al. presented the parameter variation of 20000 cells with a LFP cathode. The focus of the work was to investigate the inhomogeneous behaviour of the cells within a battery system. According to the authors, temperature variations in an actively cooled battery system have a great influence on the parameter variation. Therefore a battery module with 96 cells connected in series was aged and investigated. A model was used to validate the results.
- Rothgang et al. [60] have investigated the parameters of 700 new prismatic cells. The collected data such as weight, shipping OCV, capacity and internal resistance were checked for existing correlations. Based on the data from the work and previous experiments, the ageing behaviour of the cells was investigated at module level as a function of the selected cells, cell arrangement and temperature gradient. In a further work it is evaluated how the lifetime of current batteries can be extended by an improved interconnection of the cells (serial and parallel). The cells had a graphite anode, an NMC cathode and a nominal capacity of 5 Ah. [91, 92]
- Schuster et al. [93] examined 484 new and 1908 aged cells that were used for about 3 years in two identical vehicles (954 cells per vehicle). The capacity and internal resistance distributions of the cells were examined. It is reported that the distribution of the parameters changes from a symmetrical normal distribution in the new state to a skewed Weibull distribution in the aged state. The cells have a graphite anode

and an NMC cathode.

- In [94] An et al. perform a statistical analysis of 5473 cells from a single batch. First the capacity (determined at 0.2 C) is correlated with the weight of the cells. The data of weight and capacity of the cells follow a bimodal distribution. In the second part of the work 198 of the 5473 cells are randomly selected and the dependence of the parameter variation on the discharge current is determined. To get more information about the origin of the variation, 8 of the 198 cells are examined in detail by means of EIS. The cells have a mixed NCA/NMC cathode and a graphite anode with a nominal capacity of 5.3 Ah.
- Campestrini et al. [95] concentrate in their study on the ageing behaviour of battery modules. For this purpose they first measure 250 new cells consisting of an NCA cathode with a nominal capacity of 2.8 Ah. In further steps, the cells are used to build two modules that are aged. The ageing of the modules is then compared with the ageing of the individual cells.
- Rumpf et al. [59] are conducting an extensive statistical study of 1100 brand-new cells (3 Ah each) from two different production batches. The cells had a LFP Cathode and a graphite anode. The work concentrates on correlations among the cell parameters and evaluates 15 different parameters. Based on the results, parameters for the development and modelling of battery modules as well as for quality control of cell production are recommended.
- The study of Baumann et al. [58] deals with the parameter variation of cells connected in parallel. For the investigations 164 new cells and an aged battery pack consisting of a 96s2p configuration of a Mercedes Benz E-Cell Vito, which was driven about 30000 km, are used. It is shown that the aged cells show an increased spread compared to the new cells. If two modules of the aged battery pack continue to age, the variation of the entire module and especially the variation of the parallel connection increases. The new cells consist of an NCA cathode and a graphite anode and have a nominal capacity of 2.9 Ah.
- Devie et al. [57] study cells from one production batch to determine the initial variation in cell parameters and the variation caused by ageing. It was shown that even a small initial variation at BOT can lead to large variations during ageing of the cells. There was no correlation between the parameters of new and aged cells. The new cells consist of

a mixed NCA/NMC cathode and a graphite anode and have a nominal capacity of 2.8 Ah.

With the help of the studies listed, it becomes clear that extensive measurements on the parameter variation of new cells have already taken place. However, a closer look at Table 4.1 reveals that the investigated parameters of the cells as well as the conditions (e.g. discharge current, temperature, SOC range) under which the data were obtained vary significantly. In addition, there are different cell types with different electrode materials. A direct comparison of the parameter variation from the above mentioned studies is therefore only possible to a very limited extent. The measurements carried out in this chapter therefore serve on the one hand to expand the literature and on the other hand to determine the status quo of the cells used in this work. In order to be able to draw comparisons with the literature, individual cell parameters from the literature are included in the investigations of this thesis.

In the next section, the production process of LICs is briefly presented to show possible sources of variation in production, which can lead to varying cell parameters.

Author	Ref.	Number of cells	Parameters	COV (κ)
Dubarry	[88]	100	Weight	1.69%
			OCV	0.45%
			Capacity (C/2)	1.9%
			Capacity (C/5)	1.6%
			Pol. resistance	30%
Dubarry	[89]	10	Weight	0.13%
			OCV	0.02%
			Capacity (C/2)	0.2%
			Capacity (C/5)	0.2%
			Pol. resistance	5.7%
Paul	[90]	20000	Capacity	1.3%
			$R_{\mathrm{DC,Xs}}$	5.8%
Rothgang	[60]	700	Capacity (1C)	0.02%
			$R_{\mathrm{DC,10s}}$	0.03%
Schuster	[93]	484	Capacity (1C)	0.8%
			$R_{\mathrm{AC,1kHz}}$	1.94%
Campestrini	[95]	250	Capacity	0.16%
			$R_{\mathrm{AC,1kHz}}$	0.72%
Rumpf	[59]	1100	Weight B1	0.07%
		B1:600	Weight B2	0.12%
		B2:500	Capacity B1	0.41%
			Capacity B1	0.48%
			$R_{\mathrm{DC,10s}}$	1.43%
			$R_{\mathrm{DC,10s}}$	1.23%
Baumann	[58]	164	Capacity	0.35%
			$R_{\mathrm{DC,2s}}$	0.92%
Devie	[57]	51	Weight	0.2%
			OCV	4.8%
			Capacity (C/2)	0.3%
			Capacity (C/5)	0.4%
			$R_{\mathrm{DC,0s}}$	3.6%

Table 4.1: Research results concerning the parameter variation of brand new cells. In order to compare the variation of the different parameters, the results are given on the basis of the Coefficient Of Variation (COV).

4.2 Production Process of Lithium-Ion Cells

In this section, the production process of a LIC is presented using the example of a cylindrical cell, as used in this work. The manufacturing process is divided into three parts. First, the production of the electrodes is explained, second, the cell assembly and finally process of formation and ageing is described. Apart from cell assembly, the manufacturing process of other cell formats (prismatic cell, pouch cell) does not differ significantly [96]. Once the production process has been described, qualitative influences are summarized which can lead to a parameter variation among LIC.

4.2.1 Electrode Production

The first step in electrode production is the mixing (dry mixing) of the material components. In this process, active material, conductive additives and binder all in particulate form are mixed dry with each other using a rotating tool [10]. In a further step, wet mixing is carried out by adding a solvent [96]. The conductive additives create the electronic conduction between the rather poorly electrically conductive active material grains. The binder is an electrochemically inactive material, which stabilizes the mixture. It is used for contacting to the current collector [3]. This mix is called electrode slurry [10, 96]. This process must ensure that the components are evenly mixed, since local inhomogeneities can lead to irregular ageing [97].

In the next step, the electrode slurry is applied to the current collector (copper or aluminium foil) either continuously or intermittently in several separate lanes using an application tool (see Figure 4.1). The amount of material applied is referred to as Areal Mass Loading (AML). The coating of the underside of the carrier foil is done the same way or carried out after drying the upper side [96]. The current collector with the applied material is then cut to size at the gaps without active material [3].

The coated current collector needs to go through a drying process afterwards. The drying process is carried out by air jets or infrared radiation. During this process, the solvent evaporates and the active mass solidifies on the current collector [3,10]. The set temperature profile during drying is essential for the adhesion of the material to the current collector and the binder distribution over the layer thickness [3]. After the drying process, the current collector is cooled down to room temperature and wound up [96].

The dried roll then is subsequently fed to the calender. Here, the density

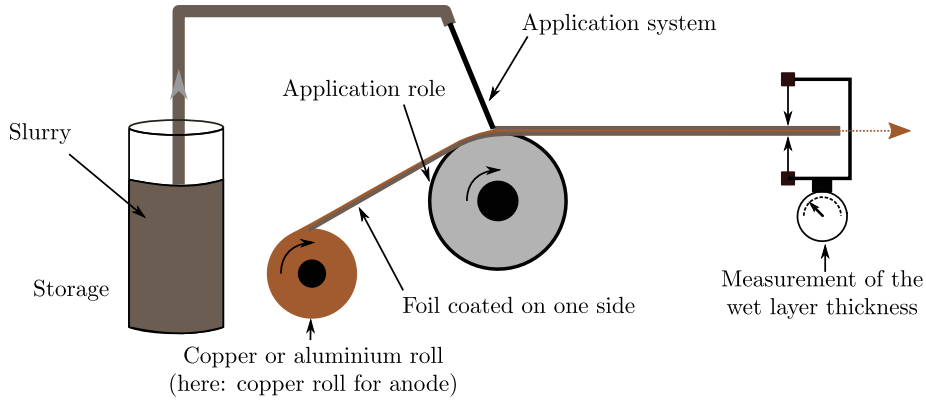

Figure 4.1: Coating process of the anode (continuously). Based on [96].

of the applied active material is increased in several steps by rotating top and bottom rolls (see Figure 4.2) [3]. The electrode foil is statically discharged and cleaned to reduce impurities to a minimum. Then the electrode is pressed to the desired thickness between the top and bottom roller. A constant pressure of the rollers is an important quality indicator. During the process the porosity of the material is reduced to about 50% or less (down to 20%). At the end of this process the electrode foil is rewound to a roll (so called mother roll) [96]. The aim of calendering is to increase the conductivity both within the electrode and between the active material coating and the current collector [10].

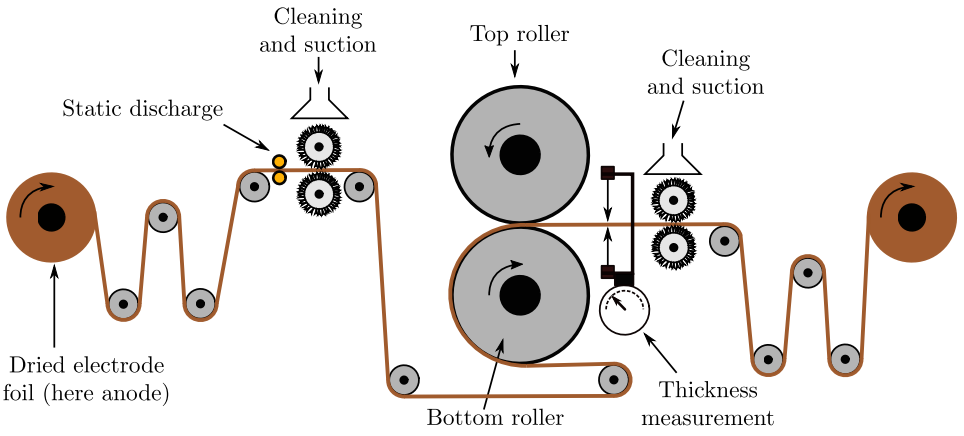

Figure 4.2: Calendering process of the anode. Based on [96].

In the subsequent process step, called slitting, the mother rolls are cut into smaller rolls, depending on the cell type, and rewound into so called daughter rolls (see Figure 4.3). Rolling knives are usually used for slitting. An important feature in this step is the cutting quality of the electrode edges [96]. In addition to rolling knives, lasers can also be used for cutting the mother rolls [3, 10, 96].

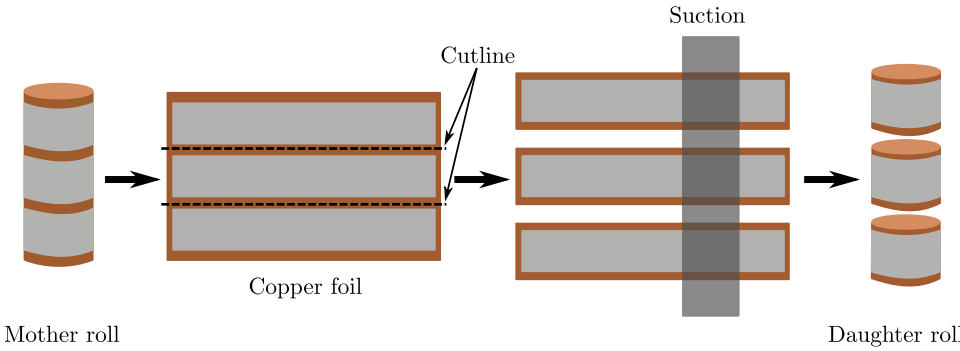

Figure 4.3: Slitting process used for cylindrical cells. Based on [96].

Moisture and solvent residues are once again removed from the daughter rolls to the maximum extent possible. For this purpose they are dried in a vacuum oven for about 12 h to 30 h before they are further processed [96]. If the materials are not dried sufficiently, the life of the future LIC suffers enormously (compare to chapter 2.5.3).

4.2.2 Cell Assembly

During so called winding, the dried daughter rolls (cathode and anode) are wound around a pin together with two separator sheets in the sequence cathode-separator-anode-separator. The coils are wound in such a way that the separator extends beyond the coated areas of the anode and cathode to prevent short circuits. The coating area on the anode is also slightly wider than on the cathode, so that the total anode area is larger than the cathode area (over dimensioning of the anode). The finished coil is fixed with an adhesive strip and called jelly roll [3]. Compared to stacking, winding results in significantly shorter production times, which enables a higher production output [96]. Figure 4.4 shows the steps during the winding process.

To protect the jelly roll from a short circuit, a bottom insulator is inserted

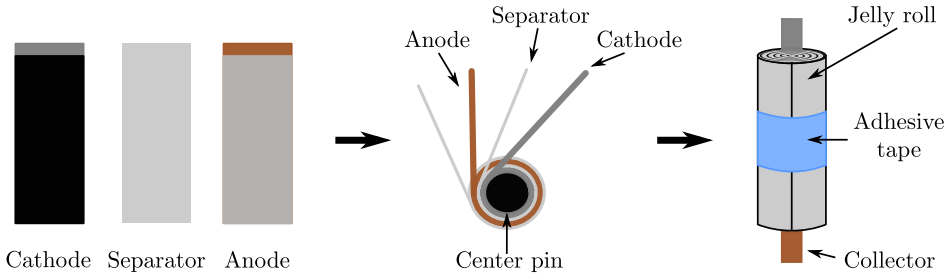

Figure 4.4: Winding process of a cylindrical cell. Based on [96].

into the cylindrical metal housing (e.g. aluminium). The housing provides the function of a water vapour barrier, otherwise moisture can get into the cell interior and lead to severe ageing (compare to chapter 2.5.3) [3]. In the following step, the cathode and anode are welded to the bottom of the housing and to the housing cover. During welding excessive heat getting into the cell components must be avoided otherwise there is a risk of damage. Finally, an insulation ring is inserted between the jelly roll and the housing cover [96].

In the final step of the assembly the cell is filled with the electrolyte. It is important that the electrolyte enters all structures as deeply as possible. This is ensured by a vacuum which activates the capillary action in the cell. Otherwise irreversible damage during use will occur [3]. The housing of the cylindrical cell is then sealed by crimping or flanging [96].

4.2.3 Forming and Ageing

After production the LIC is completed in an uncharged state. Formation therefore represents the first charging process, during which the important first forming of the SEI takes place (see chapter 2.5.1.1). Formation can be carried out in different ways. One possibility is combining the forming process with a subsequent quality control. For this purpose two complete charge/discharge cycles take place. The first cycle forms the SEI, the second cycle is used to record the cell parameters. Another possibility, often used for consumer cells, involves only one charge cycle up to a voltage at which the SEI begins to form. This option requires a high level of safety throughout the entire process, as there is no possibility of additional control [3].

The final production step is the ageing process. It is used for quality assurance and can take up to 3 weeks, depending on the chemistry and manufacturer. In this step, the cells stored at defined temperatures are checked at regular intervals. The test includes mainly the monitoring of the OCV, which can be used to determine the self-discharge rate of the LICs. Slight changes of the parameters during this time indicate a good quality [3, 96]. Significant voltage drops during storage indicate internal cell short circuits and thus a poor quality. In this case the production line or the material used must be checked for impurities.

Before leaving the factory the cells are discharged to a SOC suitable for shipping and storage. Finally, the cells are sorted into different classes by determining the internal resistance and the capacity [96]. Due to distribution of material process parameters cells have different parameters at the end of production. Sorting is therefore useful for the end customer in order to get cells with similar characteristics.

4.2.4 Production Variations and their Effects on the Cell

After the production process has been discussed, possible consequences from production variations are shown in this subsection. As already described the production process of a LIC consists of a number of production steps and many materials. A production line cannot be assembled by a single manufacturer or machine builder, since the enormous number of different machines requires a lot of expertise. The cell manufacturer is finally responsible for combining all process steps with different machines from different manufacturers to form a coordinated production process. Therefore the production of cells is generally subject to a qualitative spread. If the process is for example divided into 15 successive production stages with a yield of 99% each, the total yield at the end is just 86% (0.99^{15}). In order to monitor the manufacturing process, cell manufacturers need retain samples, as long-term effects of changes in production cannot be detected immediately. [3]

The following Table 4.2 summarizes some production variations and their effects. Since production variations are characterized by a large number of effects, including interlinked effects, the table does not cover all the possibilities but provides an insight.

Cause	Effect
Electrode production:	
Inhomogeneous slurry	Material inhomogeneities lead to irregularities in the current density distribution and thus to faster ageing [97].
Impurities in slurry	Impurities such as traces of water lead to faster degradation of the electrolyte.
	Impurities are germ cells for lithium plating. [3]
Coating defects	Capacity reduction of the electrode.
	Unbalanced electrode pairs when assembling the anode and cathode.
Different AML	Uneven energy density of the electrodes.
	Uneven distribution of current density leads to lithium plating.
	Unbalanced electrode pairs when assembling the anode and cathode.
Varying pressure during calendering	Compression too low, almost independent of conductive carbon black or the AML, leads to a higher standard deviation of the electrode capacity. [98]
	Increase in cell impedance due to poorer connectivity of active material particles and the active material with current collector. [98]
Impurities during electrode cutting	Impurities are germ cells for lithium plating. [3]
Cell assembly:	
Poor area coverage (e.g. due to angular offset when rolling up the Jelly Roll)	Disturbed capacity ratio of anode to cathode.
	Inhomogeneous current density distribution resulting in lithium plating.

Unbalanced electrode pairs	Potential of the anode drifts into the negative compared to Li/Li^+ and leads to lithium plating [99].
Uneven electrolyte filling	If not all areas of the cell are filled with electrolyte, lithium plating will occur during formation and later use. [3]
General factors:	
Several production lines or different maintenance levels of the machines	Several lines can lead to variations in the cell parameters even in the same batch of material. (Slightly different lines, different abrasion of tools, change of material, etc.).
Different work shifts (human factor)	More errors tend to happen at night than during the day, different work care.

Table 4.2: Possible sources for cell variations from the production process of LICs.

4.3 Objectives

The aim of this chapter is to reveal the effects of production on the variation of cell parameters for brand-new cells. Furthermore, dependencies of the observed cell parameters in the form of correlations and reference values for DVA and EIS are determined. Reference values play an important role in the further thesis. The following tasks are carried out for this purpose:

- Determination of various relevant cell parameters to check the quality and status quo of the 480 new cells.
- Calculation of the parameter variations of the new cells.
- Find correlations among the different parameters to identify dependencies between the parameters.
- Obtain reference values for DVA and EIS of new cells for comparison with the later planned ageing studies.

4.4 Design of Study

To achieve the described aim, 480 new cells are available. The parameters to be determined are selected based on the literature. The selected cell with its specifications is presented in the next subsection. The test procedure is then described in chapter 4.4.2.

4.4.1 Examined Cell

The LIC selected for the experiment is a commercial cylindrical cell in 18650 format from the manufacturer Samsung SDI. The cell is a high-energy cell with the designation ICR18650-26J. It has an NMC cathode and a graphite anode. All available cells come from the same production batch. Table 4.3 summarises characteristic values of the cell.

According to the manufacturer, the cells have a SOC of 30% in delivery state and are ranked in category B. Category B cells have a lower capacity than category A cells, but a higher capacity than category C cells. The production of the cells took place in January 2018. Thus, the cells have an age of 20 months at the time of delivery and start of the experiment. The cells are delivered in four packs with 100 cells and one pack with 80 cells. Parametric grouping can thus also be compared with the cell position in the packs.

Manufacturer	Samsung SDI Co.,Ltd
Designation	ICR18650-26J
Batch number	NRIA07J12A05
Nominal capacity	2.6 Ah (min. 2.55 Ah)
Weight	45.0 g (max.)
Cathode material	NMC ($LiNiCoMnO_2$)
Anode material	Graphite
Maximal voltage	4.20 V
Nominal voltage	3.63 V
Minimal voltage	2.75 V
Standard charge	1.3 A (0.5C)
Rapid charge	2.6 A (1.0C)
Maximum continuous discharge	5.2 A (2.0C)
Charging temperature (surface)	0°C to 45°C
Discharging temperature (surface)	-10°C to 60°C

Table 4.3: Characteristic properties of the investigated cell.

4.4.2 Test Procedure

This subsection describes the entire test procedure. Figure 4.5 shows an overview of the most important steps and their sequence.

After arrival the cells are stored at room temperature for about 3 weeks. In the next step, the weight of the cells is recorded. The measurement is carried out in a draft-free environment at 25°C with gloves to avoid transferring fat and sweat to the cells. A precision scale from Kern (TGD 50-3C) is used to measure the weight. The resolution is 1 mg with an accuracy of 3 mg in the specified measuring range of 0 g to 50 g.

After recording the weight, the cells are labelled according to the packaging (1 to 480). In this way, any groupings can be traced back to the packaging units.

Before starting the data collection, the voltage of the cells is checked with a multimeter (Fluke 175) in order to be able to determine any differences in the delivery condition. Cells with a significantly lower voltage may have

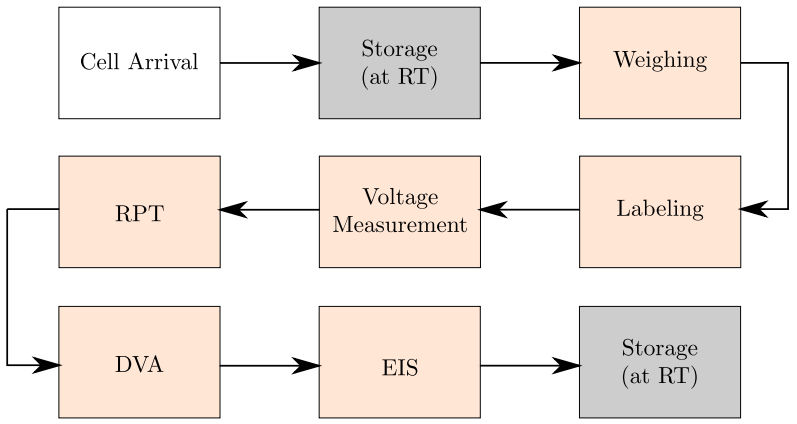

Figure 4.5: Test procedure for the new cells.

internal damages such as e.g. short circuits.

To record the electrical cell parameters, a Reference Parameter Test (RPT) is carried out for each cell. This test combines the measurement methods described in chapters 3.1 and 3.2.1 and thus serves to determine the capacity and the internal resistance in the time domain.

In the first part of the RPT, the discharge capacities C_{DCH} and $C_{\mathrm{DCH,CV}}$ are determined, then the internal resistance at 7 different SOCs is calculated. A detailed description of the RPT follows in the next paragraphs.

The cells are first fully discharged with a current of 0.52 A (0.2 C) followed by a CV phase at 2.75 V. The CV phase is terminated when the current falls below 20 mA. After a pause of 10 minutes, full charging of the cells to 4.2 V begins. The applied current in the CC phase during charging is set to 1.3 A (0.5C). In the CV phase starting at 4.2 V, the current is lowered to a value of 20 mA. After another 10 minutes, the discharge process starts and thus the determination of the values C_{DCH} and $C_{\mathrm{DCH,CV}}$. Thereby the discharge takes place again with 0.52 A (0.2C) in the CC phase followed by a CV phase at 2.75 V terminated at 20 mA. Both capacity values are determined via Ah-counting.

After another charge to 4.2 V with the same conditions, the internal resistance ($R_{\mathrm{DC,t_p}}$) is determined at different SOCs. For this purpose, the cells

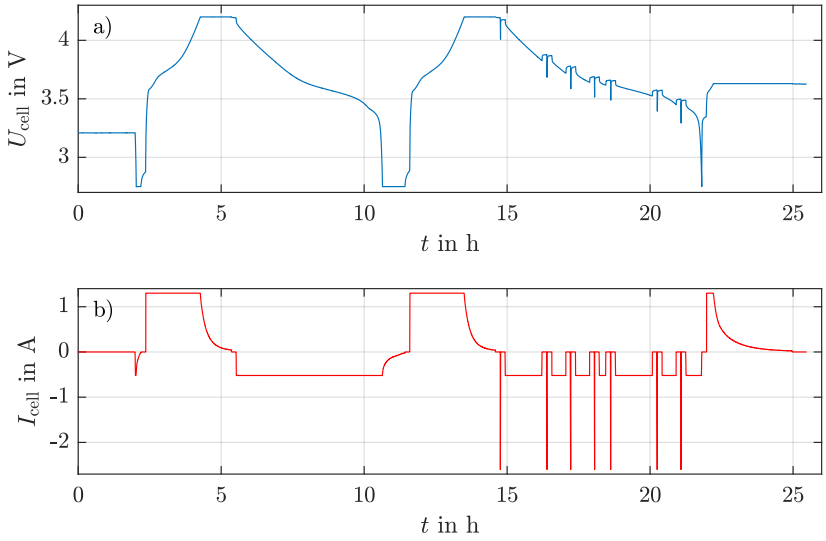

Figure 4.6: RPT used to investigate the 480 new cells. a) resulting voltage, b) applied current profile.

are loaded at 100%, 75%, 65%, 55%, 50%, 25% and 15% SOC with a 2.6 A (1C) current pulse for t_p=30 s. Thus, R_{DC,t_p} can be calculated in a period between 1 s and 30 s. To set the different SOC levels, a discharge with 0.52 A (0.2C) to the next SOC level takes place after the end of each pulse. The entire sequence of the RPT is shown in Figure 4.6.

The RPT is carried out at an ambient temperature of 25°C, in a temperature chamber from Memmert (IPP55). The automated acquisition of the measured values and the execution of the RPT takes place with a BaSyTec Cell Test System (CTS). Important characteristics about the temperature chamber and the CTS can be taken from Table 4.4.

Device	Variable	Accuracy	Range
BaSyTec CTS	Voltage	±1 mV	[0 V, 6 V]
	Current	±1 mA	]0.3 A, 5.0 A]
		±50 μA	]15 mA, 300 mA]
Memmert IPP55	Temperature	±0.1°C	[0°C, 70°C]

Table 4.4: Accuracy of the used equipment for the RPT.

For DVA, the identical equipment is used as for the RPT. The ambient temperature during the measurement is also 25°C. At the beginning of the DVA routine, the cells are fully charged. The cells are then fully discharged to 2.75 V with 130 mA (0.05C). After a pause of 10 minutes, the cells are recharged with 130 mA (0.05C) to 4.2 V. DVA can be conducted both during charge and discharge. The DVA is only performed on a sample of 16 of the 480 cells.

The EIS is performed at 25°C using a Reference 3000 from Gamry. For this purpose, 24 randomly selected cells are tested in a frequency range from 10 mHz to 10 kHz in hybrid mode at 100% SOC (see chapter 3.2.2). Again, the primary purpose is to determine the characteristic shape of EIS of the new cells. The results are not used to calculate a variation. With the selected excitation amplitude of $\hat{U}$=10 mV and the chosen frequency range, the acquired impedance results in a maximum error of 1% according to the data sheet.

4.4.3 Measured Cell Parameters

This subsection provides a summary of all cell parameters that are recorded in this chapter, although not all recorded values are presented in the subsequent results.

Capacity

With the help of the presented RPT, the values C_{DCH} and $C_{\mathrm{DCH,CV}}$ are recorded. They include the discharge capacity during the CC discharge and an additional CV discharge.

Internal Resistance

Also during the RPT, the internal resistance of the cells is determined with the help of the current step response presented in chapter 3.2.1 at different times and different SOC levels ($R_{\mathrm{DC,t_p}}$). In addition, the characteristic values R_{Im0} and R_{CT} are taken from the EIS.

Differential Voltage Analysis

In order to obtain information about the state of the electrodes and their balancing, the variables Q_1 and Q_2 are recorded by means of DVA as described in chapter 3.3.1.

Further measured parameters

At the beginning of the test procedure, the cell voltage U_{cell} of all cells from the delivery state, as well as the weight m_{cell} are recorded.

4.4.4 Statistics

In order to quantify the variation and correlation of the measured cell parameters, statistical methods are used, which are briefly presented in this subsection.

Parameter Variation

The Coefficient Of Variation (COV) κ_x is a relative value and is used to make the variation of different parameters comparable. In contrast to the standard deviation σ_x, the COV κ_x is a unit-free percentage value. The COV is calculated with the help of the standard deviation σ_x and the mean value μ_x through

$$\kappa_x = \frac{\sigma_x}{\mu_x}. \tag{4.1}$$

The mean value μ_x of the considered variable is given by

$$\mu_x = \frac{1}{n} \cdot \sum_{i=1}^{n} x_i \tag{4.2}$$

where n is the number of cells. The standard deviation σ_x is calculated by

$$\sigma_x = \sqrt{\frac{1}{n} \cdot \sum_{i=1}^{n} (x_i - \mu_x)^2}. \tag{4.3}$$

Parameter Correlation

With the help of the correlation coefficient $\rho_{x,y}$ according to Karl Pearson, the strength and direction of a linear correlation between two measured variables x and y can be expressed. This is calculated as follows

$$\rho_{x,y} = \frac{\sum_{i=1}^{n} (x_i - \mu_x)(y_i - \mu_y)}{\sqrt{\sum_{i=1}^{n} (x_i - \mu_x)^2 \cdot \sum_{i=1}^{n} (y_i - \mu_y)^2}} \tag{4.4}$$

where μ_x and μ_y is the mean value of the two considered variables. The correlation coefficient $\rho_{x,y}$ can reach values between -1 and 1. If $\rho = 1$ or $\rho = -1$ is given, a perfect positive or negative linear correlation exists between the measured variables x and y. If $\rho = 0$ is given, there is no linear relationship between the two variables. However, it should be noted that non-linear correlations cannot be detected or can only be detected insufficiently. According to [100], values for ρ are classified as follows:

weak correlation $|\rho| < 0.5$,

moderate correlation $0.5 \leq |\rho| < 0.8$,

strong correlation $|\rho| \geq 0.8$.

Depending on the literature source and the sample size, the limits given may vary slightly.

4.5 Results and Discussion

In the following subsections, the results of the parameter variation and the parameter correlation of the 480 investigated cells are presented. Finally, reference values are created for DVA and EIS, which serve as initial comparison values in the further progress of this thesis.

4.5.1 Parameter Variation

In this subsection, relevant parameters for all 480 cells are displayed graphically and the values for σ_x, μ_x and κ_x are calculated. The values determined from the new cells serve as reference values in the later ageing studies.

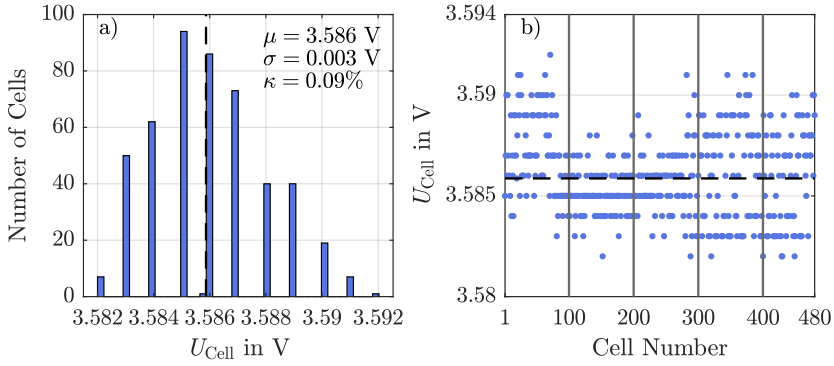

Figure 4.7: a) histogram and b) scatter plot for U_{cell} in delivery state.

Cell Voltage in Delivery State

In Figure 4.7 a) and b) U_{cell} of the 480 cells in the delivery state is shown in a histogram and a scatter plot. The voltage measurement is used to check the status quo of the cells before determining the capacity and internal resistance. If there would be any significant differences in U_{cell} in the delivery state, this may indicate that the concerned cells are damaged.

The cells have an average voltage of 3.586 V and are almost normally distributed (see Figure 4.7 a)). Among the 480 cells, one cell was found with 3.528 V, which is about 58 mV below the mean value and thus clearly stands out (cell 19 of 480). It is possible that this cell was short-circuited or that there is a higher self-discharge than in the other cells (see chapter 4.2.3). Cell 19 is therefore excluded from the planned experiments and not included in the plots of Figure 4.7.

In Figure 4.7 b) U_{cell} is plotted over the respective cell number in a scatter plot. The vertical grey lines visualise the beginning of a new packaging unit in which the cells were delivered (e.g. cell 100 to 199). In this way, possible groupings with regard to the voltage in the delivery state can be traced back to the packaging units. However, when observing the scatter plot, no significant clusters can be detected. The visible grouping of U_{cell} (stripe pattern) is due to the maximum resolution of the multimeter used. The voltages of some cells only differ at values <1 mV, what cannot be detected with the 1 mV resolution of the multimeter.

When comparing the voltage variation in delivery state with Table 4.1, the 480 cells in this thesis perform comparatively well with κ=0.09%. In the literature listed, values from 0.02% to 4.8% were found.

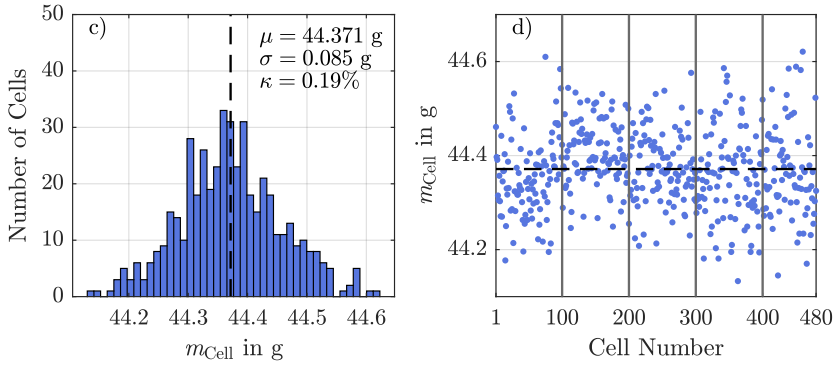

Figure 4.8: a) histogram and b) scatter plot for m_{cell}.

Cell Mass

Figure 4.8 a) and b) show the mass of the 480 cells in a histogram and a scatter plot. On average, m_{cell} results to 44.371 g with a minimum and maximum value of 44.133 g and 44.621 g, respectively (see Figure 4.8 a)). Furthermore, the values are approximately normally distributed and show a variation of $\kappa = 0.19\%$. In the literature listed in Table 4.1 values ranging from 0.07% to 1.69% were found. In contrast to U_{cell} in delivery state, no outliers are found for m_{cell}.

The production-related background of m_{cell} and its distribution is difficult to interpret, as each cell component contributes to the cell mass. Some studies have demonstrated a high positive correlation ($\rho > 0.9$) between cell mass and cell capacity, which has been attributed to AML [60, 94]. The more active material is applied to the current collector in production, the heavier the cell and the higher the cell capacity become. This potential correlation will be investigated later in this thesis.

Figure 4.8 b) shows m_{cell} with the corresponding cell number in a scatter plot to make groupings and drifts along the cell number visible. Here, too, there is no apparent relationship between m_{cell} and the packaging units.

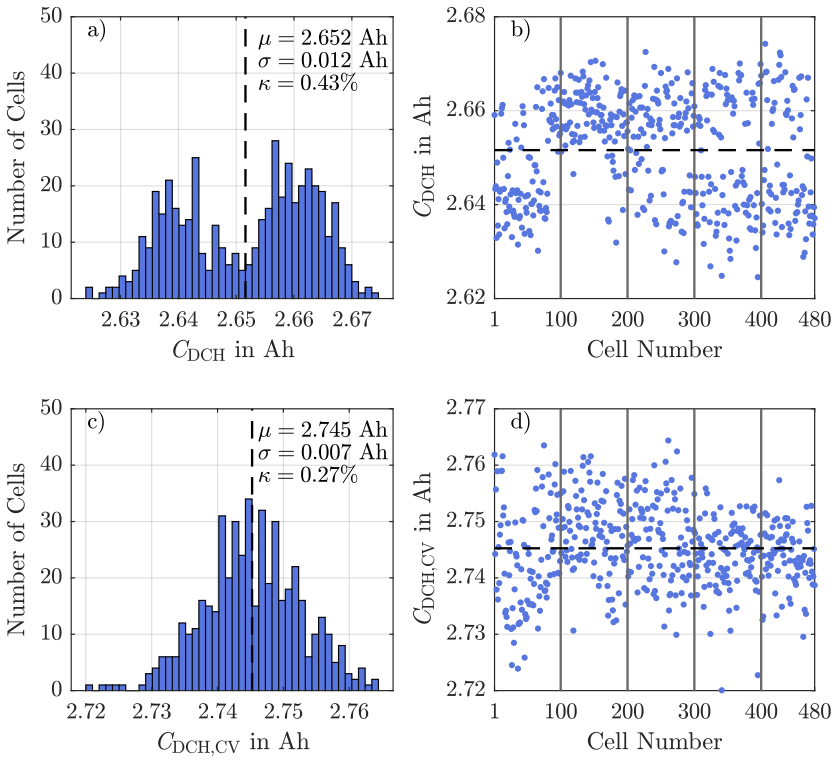

Figure 4.9: A histogram and a scatter plot are shown for C_{DCH} in a) and b), and for $C_{\mathrm{DCH,CV}}$ in c) and d).

Discharge Capacity

Figure 4.9 shows the result for the values C_{DCH} and $C_{\mathrm{DCH,CV}}$ which represent the capacity of a normal CC discharge and the capacity of a CC-CV discharge. When observing the histogram for C_{DCH}, it is noticeable that the distribution of values is bimodal and consists of two overlapping normal distributions (see Figure 4.9 a)). Multimodal distributions usually occur when data are collected from parallel processes. In this case, the bimodal distribution could possibly result from the cell production on two different production lines. Variances between the production lines can be caused by various factors, such as slight material differences, ongoing adjustment of process parameters or the different abrasion of the tools [59]. Bimodal distributions for the cell capacity have already been demonstrated in the

literature [60, 92, 94, 101]. In some publications, the bimodal distribution was observed for capacity values with additional CV phase, in others again for capacity values without additional CV phase. In [94], it was additionally demonstrated that the bimodal distribution of the discharge capacity also persists at different discharge currents.

Regardless of the distribution, the cells of this work have a mean value (C_{DCH}) of 2.652 Ah with minimum and maximum values of 2.625 Ah and 2.674 Ah, respectively. A variation of $\kappa = 0.43\%$ results, which is also comparable with the values from the literature (see Table 4.1). No outliers are found in the measurement of C_{DCH}. Cell 19, which had a significantly lower voltage already in the delivery state, is shown at the left edge of the data set with a capacity of 2.638 Ah. However, the given deviation in the delivery voltage is not reflected to the same extent in C_{DCH}.

Observing C_{DCH} in the scatter plot (Figure 4.9 b)), the two normally distributed groups are clearly visible. While C_{DCH} of the cells of the first packing unit (cell 1 to 99) is generally below the mean value, the majority of the cells in the second packing unit (cell 100 to 199) is above the mean value. The cells of the remaining packing units are evenly distributed around the mean value.

Figure 4.9 c) shows the result for $C_{\mathrm{DCH,CV}}$. Due to the additional CV phase in the discharge process, the bimodal distribution of the values is no longer present. Since the influence of the internal resistance of the cells is eliminated with the help of the additional CV phase, it is reasonable to assume that the bimodal distribution of C_{DCH} results from the distribution of the internal resistance values. This fact is checked later when observing the internal resistance values. For the values of $C_{\mathrm{DCH,CV}}$ a mean value of 2.745 Ah with minimum and maximum values of 2.720 Ah and 2.764 Ah, respectively, is obtained. A variation of $\kappa = 0.27\%$ can be determined, which is clearly below the variation of C_{DCH}. The explanation for the lower variation of $C_{\mathrm{DCH,CV}}$ is the decoupling from the internal resistance as already mentioned. Also from literature the variation value of the capacity significantly decreases with an additional CV phase. Again, the values of the 480 cells do not form clusters nor drifts (see Figure 4.9 d)).

Internal Resistance

The internal resistance of the cells can theoretically be evaluated at any SOC and at any time. In this work, the value at 100% SOC is used to evaluate the internal resistance. The pulse duration t_p for the determination of the internal resistance in the performed RPT amounts to 30 s and thus enables the evaluation between 1 s and 30 s. Figure 4.10 shows the results for the values $R_\mathrm{DC,1s}$, $R_\mathrm{DC,10s}$ and $R_\mathrm{DC,30s}$ extracted at 1 s, 10 s and 30 s after starting the discharge pulse.

The histograms in Figure 4.10 a), c) and e) show approximately normally distributed data sets for the three values shown. The assumed bimodal distribution of the resistance values with respect to C_DCH (Figure 4.9 a)) can not be detected in the data sets shown.

The later the evaluation time the higher the mean value of $R_\mathrm{DC,t_p}$. Mean values from 45.5 mΩ ($R_\mathrm{DC,1s}$) to 71.1 mΩ ($R_\mathrm{DC,30s}$) are recorded. With longer pulse durations, slower ohmic cell processes are increasingly captured, which increase the total measured value (compare to EIS measurement in Figure 3.3). In return, the variation of the measured resistance value decreases from $\kappa = 1.70\%$ ($R_\mathrm{DC,1s}$) to $\kappa = 1.21\%$ ($R_\mathrm{DC,30s}$) at later evaluation times. Values from 30% to 0.03% were recorded in Table 4.1. Here, too, the variation in internal resistance was always higher than for the capacity values.

No outliers can be found when measuring the internal resistances. The scatter plots in Figure 4.10 b), d) and f) show no groupings nor drifts along the cell number.

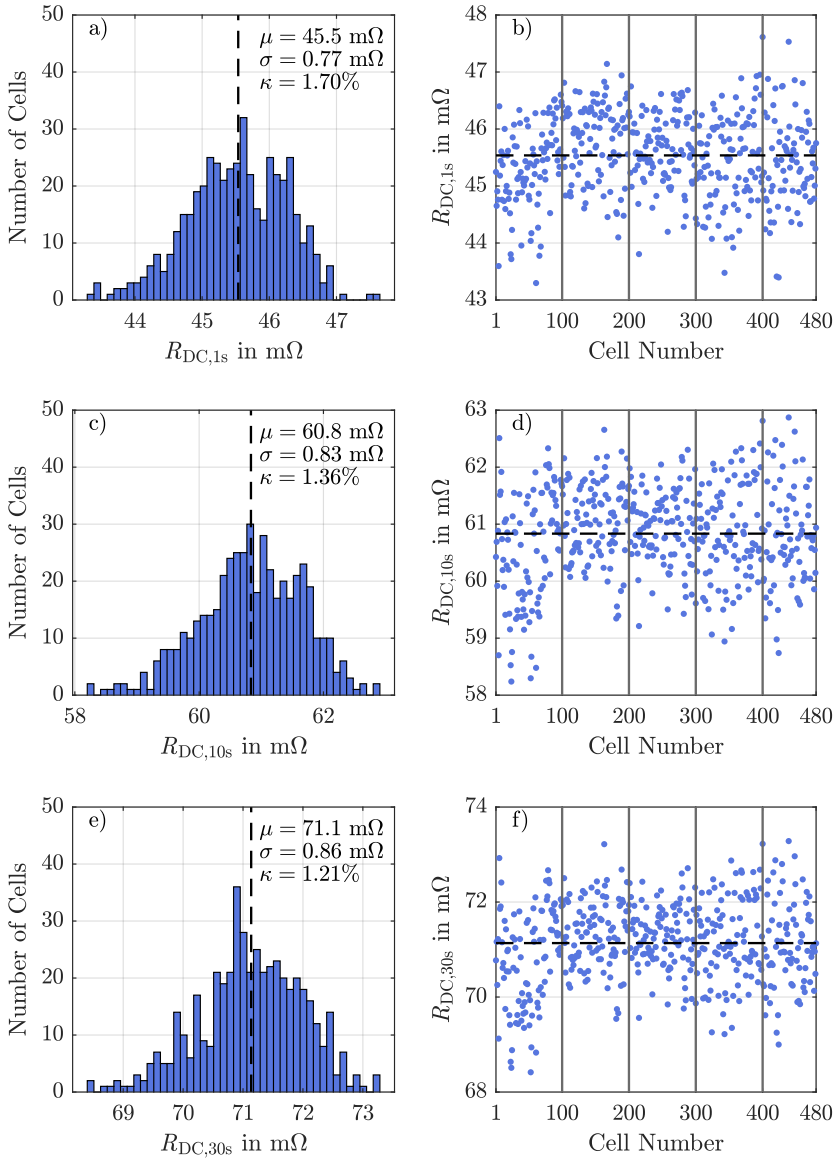

Figure 4.10: Histograms and scatter plots for $R_{\mathrm{DC,1s}}$ in a) and b), for $R_{\mathrm{DC,10s}}$ in c) and d), and for $R_{\mathrm{DC,30s}}$ in e) and f) at 100% SOC.

4.5.2 Parameter Correlation

For the parameters presented in the last subsection, correlations are now analysed that can indicate existing dependencies among the respective parameters. The result is summarised in a correlation matrix.

The correlation matrix in Figure 4.11 contains the 7 parameters presented. By comparing all 7 parameters pairwise, this results in a 7x7 matrix with a total of 49 possible correlations. The main diagonal of the correlation matrix corresponds to the correlation of the observed parameter with itself and always results in $\rho_{xx} = 1$. Therefore, the main diagonal is used instead to write in the respective parameter name. For a better visualisation of the correlation strength, the matrix is coloured.

By definition a correlation matrix is a symmetric matrix with identical entries above and below the main diagonal. This symmetry occurs due to the fact that each parameter combination is tested in both directions (ρ_{xy} and ρ_{yx}).

When observing Figure 4.11 only a few parameter pairs show a strong correlation ($|\rho| \geq 0.8$). Here, the correlations among $R_{\mathrm{DC,1s}}$, $R_{\mathrm{DC,10s}}$ and $R_{\mathrm{DC,30s}}$, as well as C_{DCH} and $C_{\mathrm{DCH,CV}}$ stand out in particular. This fact is simple to explain, as the respective values are directly linked to each other. For example, $R_{\mathrm{DC,1s}}$ is completely contained in $R_{\mathrm{DC,10s}}$ and $R_{\mathrm{DC,30s}}$, respectively, and also represents a large part of the total value. The same situation occurs with C_{DCH} and $C_{\mathrm{DCH,CV}}$. The value of C_{DCH} is fully contained in $C_{\mathrm{DCH,CV}}$ and makes up the major part of the value. The same behaviour was also demonstrated in [101].

For other parameter pairs, the correlation coefficient decreases significantly. For example, there is still a moderate correlation between the cell mass m_{cell} and C_{DCH} with $\rho = 0.48$, which according to the literature can be attributed to the AML of the current collectors. It was expected that the correlation of m_{cell} with $C_{\mathrm{DCH,CV}}$ is even more pronounced in this thesis due to the decoupling of the capacity from the internal resistance, but the correlation decreases to $\rho = 0.28$.

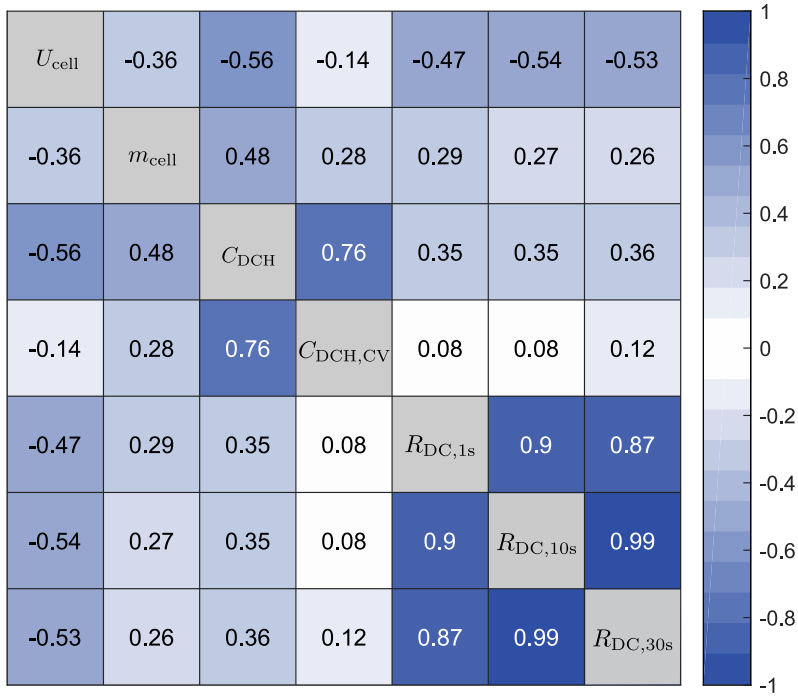

Figure 4.11: Symmetrical correlation matrix of the 7 presented cell parameters. The values in the boxes correspond to the respective correlation coefficient ρ between two parameters.

Further moderate correlations ($|\rho| \approx 0.5$) result from the correlation between U_{cell} and C_{DCH}, as well as U_{cell} and the resistance values $R_{\text{DC,1s}}$, $R_{\text{DC,10s}}$ and $R_{\text{DC,30s}}$. One reason for the correlation between U_{cell} and C_{DCH} could be the 20-month calendar ageing between the production date and the start of the measurements. A higher voltage leads to higher capacity loss during calendar ageing [83, 102]. The capacity loss due to calendar ageing simultaneously leads to formation of the SEI and thus to an increase in the internal resistance. However, this assumption is contrary to the correlation of U_{cell} and the resistance values $R_{\text{DC,1s}}$, $R_{\text{DC,10s}}$ and $R_{\text{DC,30s}}$. The internal resistance tends to be lower at higher storage voltage. No suitable explanation for the existing relationship can be found in the literature.

The weakest correlations ($0.08 \leq \rho \leq 0.12$) are obtained between the discharge capacity $C_{\text{DCH,CV}}$ and the internal resistances ($R_{\text{DC,1s}}$, $R_{\text{DC,10s}}$ and $R_{\text{DC,30s}}$). These correlations confirm the almost complete independence of the value $C_{\text{DCH,CV}}$ from the internal resistance, which is achieved by an additional CV phase during discharge.

All parameter combinations are also visually checked for non-linear correlations with the help of a scatter plot, as these are not captured by the correlation coefficient (e.g. exponential or quadratic correlations). However, no further non-linear correlations can be found among the parameters.

4.5.3 Reference Values for DVA and EIS

Due to limited measurement equipment and the time required to reliably and correctly carry out DVA and EIS, these measurements are only carried out randomly on 16 (DVA) and 24 (EIS) of the 480 new cells in order to record the characteristic curve shape and important parameters of the respective measurement method. Due to the smaller sample size, no statistical calculations are made here. The data obtained serve as comparative values for the further work, since the evaluation of DVA and EIS is primarily based on the changes in important parameters (e.g. R_{CT}) during the ageing process.

Figure 4.12 a) and b) show 16 DVA curves and the extracted values for Q_1 and Q_2. The curves show that the variance among the 16 measured cells is very small. The mean values for Q_1 and Q_2 result in 1.45 Ah and 1.26 Ah, respectively. In relation to the SOC of the cells, the significant peak corresponding to graphite stage 2 between Q_1 and Q_2 is on average at 53.46%. This value will be used as the initial comparison value for all future DVA measurements.

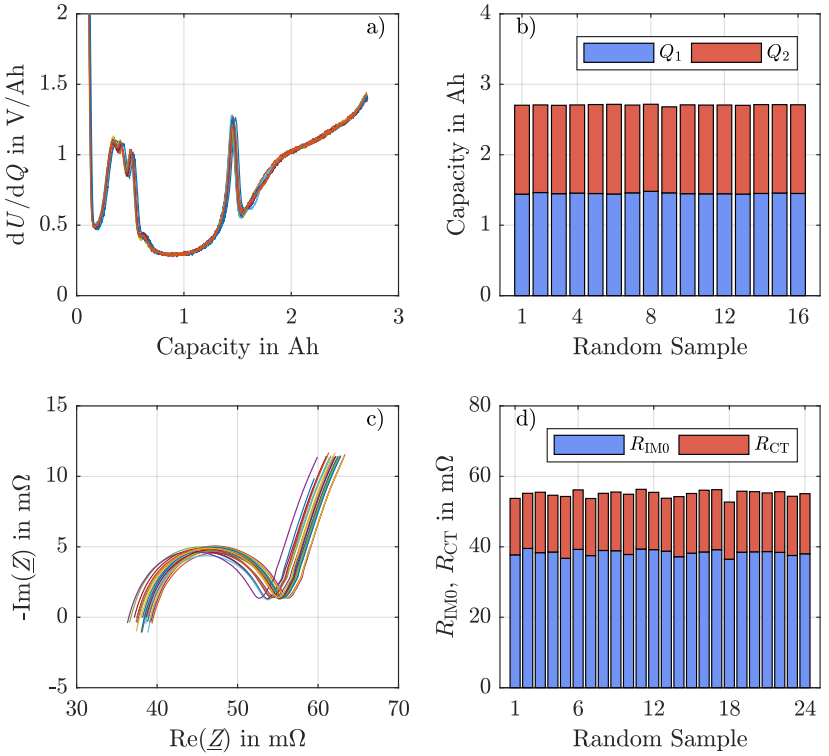

Figure 4.12: a) DVA curves of 16 cells, b) Q_1 and Q_2 extracted from the DVA curves, c) EIS curves (capacitive part) of 24 cells at 100% SOC, d) R_{Im0} and R_{CT} extracted from the EIS curves.

Figure 4.12 c) and d) show mainly the capacitive part of the EIS curves, as well as the extracted values for R_{Im0} and R_{CT} of all 24 measured cells at 100% SOC. The variation among the curves is clearly more pronounced here than for the curves of the DVA. This may be due to the greater production-related variation of the cell resistance itself compared to the capacity, but also to varying measurement conditions. The SOC of the cells and the relaxation time since the last SOC change have a great influence on the result of the EIS (see chapter 3.2.2). On average, R_{Im0} and R_{CT} result in values of 38.3 mΩ and 16.7 mΩ, respectively. These values will be used as initial comparison values for all future EIS measurements.

4.5.4 Summary

With help of this chapter, the effects of the production on the cell parameters are shown. For this purpose, various relevant cell parameters, their variation and their correlations with each other were examined in accordance with the literature. While expanding the literature knowledge regarding the parameter variation and parameter correlation of new cells, the current state of the 480 cells could also be checked. The state of the cells plays a major role in the planned ageing tests. A quantity of cells that varies too much or contains many outliers would be unsuitable for the further ageing studies. Furthermore, reference values for the time-consuming measurement methods DVA and EIS were created during the measurements. In general, no abnormalities were found. The values determined were always in line with the existing values from the literature. It can be concluded that 479 out of 480 cells are well suited to conduct the ageing tests and analysis since they form a homogeneous group of new cells.

Chapter 5

Parameter Variation of Aged Lithium-Ion Cells

With help of the measurements in the previous chapter, the initial production-related differences of non-aged cells were investigated. In order to obtain further information on the parameter variation of LICs, the influence of ageing on the parameter variation is investigated in this chapter.

In real-world applications, LICs are usually used in various serial and parallel connections to achieve the necessary requirements of a battery module such as voltage and capacity. However, the ageing of individual cells is influenced by this interconnection. Electrical and thermal interactions among the cells will have a significant impact on the individual cell ageing. These cell-extrinsic influences make it impossible to capture the underlying intrinsic cell-to-cell variation during ageing.

In order to fundamentally investigate the parameter variation of cells without interactions, in this chapter only groups of unconnected single cells are therefore aged under identical conditions. Extrinsic effects that could influence cell ageing and thus the resulting parameter variation are prevented as far as possible by creating uniform operating conditions. Only under such conditions is it possible to measure the progressive development of intrinsic and thus cell-given parameter variation. The parameters for the individual cells determined from such a study will therefore provide a new and valuable insight into the process of cell-to-cell variation during ageing.

First studies have already been carried out in the literature on this topic, which are described in more detail in the following section.

5.1 Insights from Literature

The literature listed deals with the parameter variation of single cells obtained from ageing experiments. It should be noted that significantly less research is done in this area than on the study of the variation of new cells. Also, the number of cells investigated in literature studies is significantly small due to high measurement effort long test times and the equipment required. The following relevant studies were found:

- In the study by Devie et al. [57], 15 of 51 brand-new LICs were exposed to 1000 cycles to determine the resulting parameter variation. The cells were charged with C/2 and discharged with 1.5C between 4.3 V and 3.0 V. Every 100 cycles the ageing was briefly interrupted for an RPT to obtain further data. Afterwards the ageing of the cells was continued. No correlation could be found between the initial and final parameters of the 15 cells.
- In the study by Baumhöfer et al. [73] 48 brand-new LICs were aged under identical operating conditions. Cyclic ageing was performed at 25°C ambient temperature in a range of 3.9 V to 3.5 V (SOC: approx. 80% to 20%). The current during charging and discharging was limited to 4 A (approximately 2C). At fixed intervals the cyclic ageing was interrupted to perform a RPT. Using a data mining algorithm, correlations between the initial performance and the performance at EOT were investigated. According to the authors a model based on this algorithm is able to estimate the lifetime of the cells and can help to classify the cells better before module assembly. The investigated cells consist of an NMC cathode and a graphite anode and have a nominal capacity of 2.05 Ah. However, cells of category C were used for the experiment. They have a capacity of 1.85 Ah only.
- Harris et al. [103] deal with the failure probability of commercial LICs. For this purpose 24 cells were aged at room temperature (approx. 25°C) in a range from 4.35 V to 3 V. The cells were charged with 1C and discharged with 10C to accelerate the ageing process. To document the ageing process, the capacity and impedance of the cells were measured after each cycle. This study shows that parameters of the cells at the beginning of cyclic ageing say little about future ageing. The cells investigated consist of an LCO cathode and a graphite anode and have a nominal capacity of 4.4 Ah.
- Eom et al. [104] focus on the prediction of life time and the reliability

of LICs. For this purpose, 12 identical cells were aged at an ambient temperature of 23°C in a range from 4.2 V to 2.7 V until the remaining capacity was 80% of its initial value. Charge and discharge current were 0.5C each. The cells used have a nominal capacity of 1.0 Ah.

- Severson et al. [105] focused exclusively on predicting the lifetime of LICs using machine learning. To generate a data set as diverse as possible, 124 cells were aged at an ambient temperature of 30°C with 72 different rapid charging profiles from 3.6C to 6C. The cells were all discharged at 4C in a range from 3.6 V to 2.0 V. Only a very weak correlation was found between the initial capacity and the final lifetime of the cells. The authors claim that by including the entire discharge curve, temperature and internal resistance over several discharge cycles, the prediction improves significantly. The investigated cells consist of a LFP cathode and a graphite anode and have a nominal capacity of 1.1 Ah.

The overview of the studies shows that the investigations are primarily concerned with predicting the lifetime of single cells. Here, prediction models are generated with help of the measured data from previously aged single cells. Furthermore, parameters from new cells are compared with those in the later ageing process. Different parameters such as capacity and internal resistance were used for the observations. All the studies mentioned conclude that there is only a very small correlation between the initial parameters and the further ageing progress of the cells. In the studies [73, 103, 106] it could be determined that the transition from linear ageing during the first section of the lifetime to non-linear ageing during the second section of the lifetime hast a strong influence on the parameter variation of the cells. Therefore, special attention is paid to the transition between the ageing sections in this work.

In the existing literature there is no general quantification nor qualification of the parameter variation of aged single cells for different operating conditions (e.g. temperature, load current).

The studies shown give a first insight into the topic of parameter variation of aged single cells. However, different operating conditions of the cells among the studies lead to limited comparability. Neither SOC range, charging and discharging currents nor temperature are identical. This results in a variety of different ageing mechanisms for the aged cells in the studies, which does not allow an overall evaluation of the parameter variation. In addition, the use of different cell types such as NMC, NCA etc. makes it even more

difficult to compare the results. The author is not aware of any studies that have comprehensively investigated the parameter variation behaviour of a cell under different operating conditions, including temperatures above and below room temperature.

5.2 Objectives and Tasks

The objective of this chapter is to investigate the influence of different operating conditions on the parameter variation of ageing single cells. Another objective is to find out whether operating conditions can be identified that particularly promote the development of a parameter variation. To achieve these objectives the following tasks are carried out:

- Ageing of identical cell groups under different temperature and load conditions.
- Analyse the influence of temperature and load on the parameter variation in each cell group.
- Investigate the relationship between initial cell parameters and subsequent cell ageing.
- Interpretation of the results for real-world application. Derivation of operating strategies.

5.3 Design of Study

In order to be able to examine the ageing process and determine the associated parameter variation of the LICs, they are aged under defined operating conditions. Since the number of possible test conditions is almost infinite and the available measurement equipment limited, a few test conditions with different ageing mechanisms are selected. For each test condition, 8 identical cells are aged.

5.3.1 Test Conditions

To carry out the investigations, a total of 10 operating conditions are selected (see Figure 5.1). Here, the temperature and the charging/discharging current are varied. The selected operating conditions are described in more detail in the following paragraphs. Due to the selected conditions the influ-

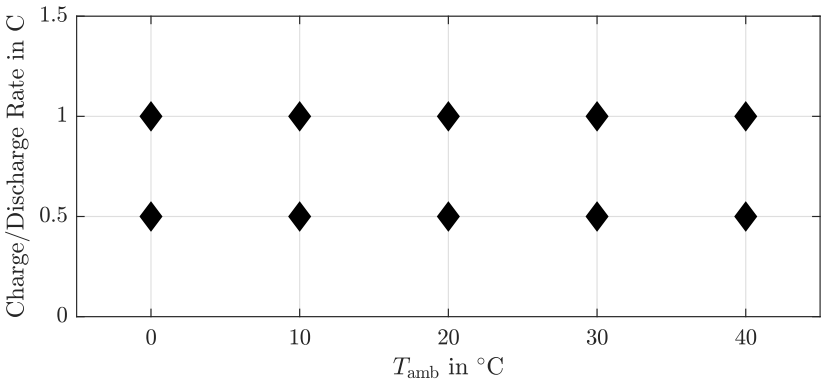

Figure 5.1: Test matrix of the performed cycle ageing tests. Each test is carried out with 8 identical cells.

ences of different ageing mechanisms on cell ageing and parameter variation can thus be observed in a differentiated manner.

Voltage Range

The voltage limits have a huge impact on the ageing process and therefore also on the lifetime of the cells. There are numerous studies in literature that demonstrate these influences [102, 107]. The fastest ageing is achieved by fully utilising the voltage limits. For short test times the cells in this thesis are operated between 2.75 V and 4.175 V. This corresponds approximately to the maximum possible voltage range from the data sheet. The maximum voltage of 4.175 V (instead of 4.2 V) is chosen to ensure comparability with the module tests in chapter 6.

Load Profile

The current, has a significant impact on the lifetime of LICs as well [63, 108, 109]. Since there are no comparable studies of this kind, the load or charging current is selected according to the data sheet of the investigated cell. It defines a value of 1.3 A (0.5C) as the standard charging current. The maximum current for charging is 2.6 A (1.0C). The discharge current is set to the same values. During ageing the charging process is terminated in the CV phase as soon as the current falls below a threshold of 130 mA (0.05C). Variable load cycles are not used in this study.

Temperature Range

The temperature range is selected on the basis of the data sheet, too. Exceeding these limits is rejected for safety reasons. Although the cell can be discharged at temperatures in the range from -10°C to 60°C, the temperature range during charging is limited between 0°C to 45°C. The temperature is not changed between charging and discharging and the temperature range is finally set to values from 0°C to 40°C.

With help of the relaxation measurement presented in chapter 2.5.1.2, an insight into the expected ageing is now provided at the selected temperatures and currents. If, under these conditions, lithium plating can already be detected after the fist charging process (at BOT), a shortened lifetime can be expected.

Figure 5.2 shows 12 relaxation measurements and their derivatives for different temperatures at C-rates of 0.5C (a), b)) and 1.0C (c), d)). The charging is carried out according to the test conditions presented above. In addition to Figure 5.1, a relaxation measurement is carried out at 5°C for both charging currents. Only new cells are used for the measurements. Thus, the measurements provide an insight at BOT of the cyclic ageing.

At a charging rate of 0.5C (a), b)), lithium plating occurs at temperatures of 0°C and 5°C. The extremum is at about 1.6 h and 0.75 h respectively. Thus, the amount of plated lithium approximately doubles when the temperature is reduced from 5°C to 0°C. At temperatures between 20°C and 40°C, there is definitely no significant voltage drop or inflection point during relaxation. Thus no lithium plating is expected at BOT. At 10°C, there seems to be a transition point between plating an non-plating. The voltage at this operating condition drops significantly lower in a) than at 20°C, 30°C and 40°C. Also, the derivative of the voltage already stands out slightly. Thus, it is expected that lithium plating with low intensity may already take place at this operating condition at BOT.

When the charging rate is increased to 1.0C (see Figure 5.2 c) and d)), lithium plating now definitely takes place at 10°C. The clearly measurable extremum is at approximately 0.5 h. At 5°C and 0°C, plating takes place as well. With maximum values at 1.6 h for 5°C and 3 h for 0°C, it can be concluded that the plating intensity is much higher with 1.0C compared to 0.5C.

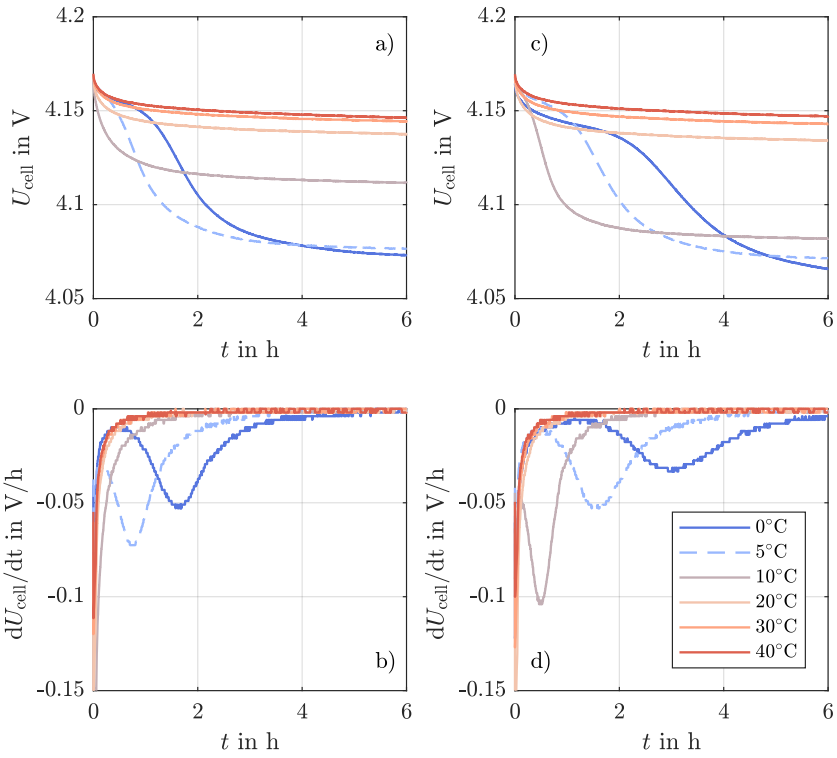

Figure 5.2: Relaxation measurement of new cells to determine the lithium plating behaviour under defined operating conditions after the first charging process. The voltages during relaxation are shown, as well as their derivatives for 0.5C (a),b)) and 1.0C (c),d)).

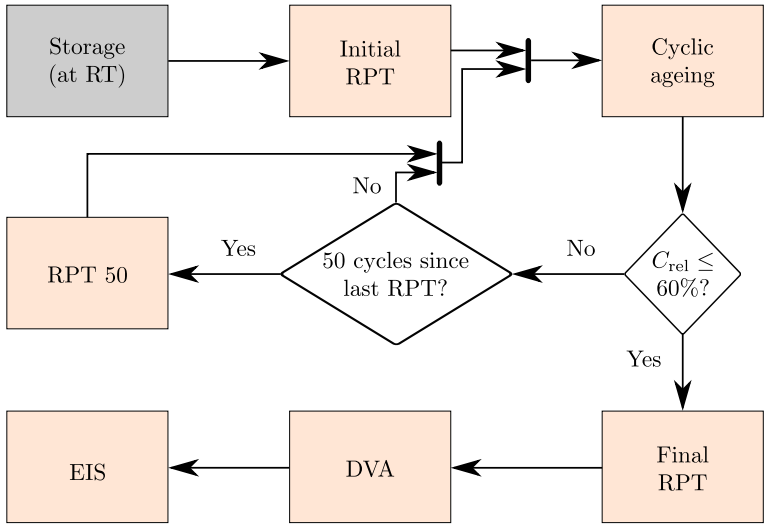

Figure 5.3: Test procedure applied to 80 cells in 10 groups of 8 cells each.

5.3.2 Test Procedure

To carry out the investigations, the procedure shown in Figure 5.3 is run through once for each cell group.

First, the 8 cells per operating condition, previously stored at a voltage of 3.6 V, run through an initial RPT again before BOT in order to create a uniform basis for comparison. This is necessary because the time span between the first RPT from chapter 4 and the start of the ageing experiment can vary by several months due to a limited test capacity.

Cyclic ageing starts after a pause of 10 minutes with a CC discharge of the cells with either 0.5C or 1.0C to a final discharge voltage of 2.75 V. In comparison to the RPT, there is no additional CV phase after reaching 2.75 V. After another 10-minute pause, the cells are charged with 0.5C or 1.0C. As soon as the cells reach a voltage of 4.175 V, a CV phase follows, which is terminated when the charging rate falls below 0.05C. Then the cycle starts again. Figure 5.4 shows the complete cycle.

After each completed cycle, it is checked whether the cells have reached the termination criteria $C_{rel} \leq 60\%$. Here, C_{rel} is calculated based on the first full cycle. C_{rel} is chosen below 70% or 80% that are usually assumed as EOL criteria. Thus it can be investigated how the cells behave beyond these

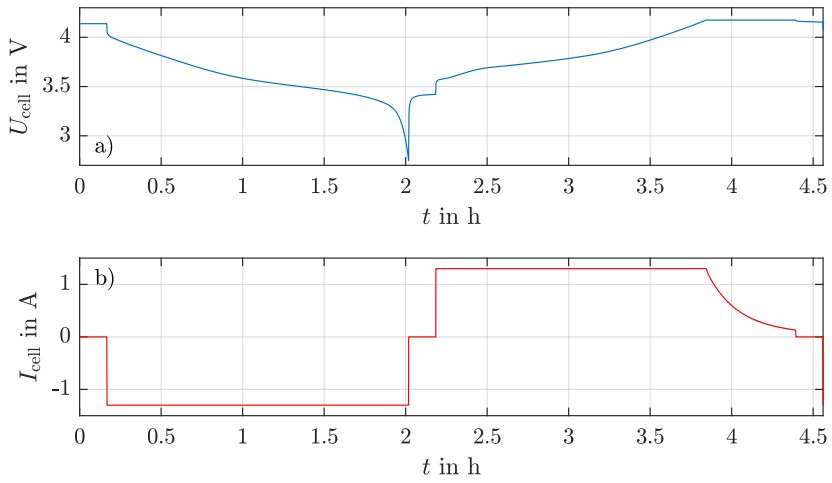

Figure 5.4: Ageing cycle of the single cells. The example shows the test condition 0.5C/20°C. a) shows the resulting cell voltage U_{cell}, b) shows the applied current I_{cell}.

limits. Such low values for C_{rel} play an important role, especially with regard to second-life applications.

Since ten cell groups are aged at different currents and temperatures, an additional RPT (RPT 50) takes place after every 50 completed cycles. This allows the cells to be measured independently of their assigned test condition. The dependence of the cell parameters on T_{amb} and the different currents is thus eliminated. Thus, the results regarding ageing and parameter variation can be examined under common conditions. If the cells reach $C_{\text{rel}} \leq 60\%$, ageing is terminated with a final RPT. Subsequently, DVA and EIS provide additional insights into the status quo of the aged cells.

RPTs, DVA and EIS are carried out identically to the measurement of the new cells in chapter 4 in order to maintain comparability among the tests. All measurements take place in IPP55 temperature chambers from Memmert. With the exception of cyclic ageing, all measurements are also carried out at 25°C. Several CTS devices are used to carry out the ageing cycle, the RPTs as well as DVA. EIS is carried out again with a Reference 3000 from Gamry.

5.3.3 Measured Cell Parameters

During all measurements carried out, various cell parameters are recorded for the evaluation of the ageing process. They are summarised in a brief overview.

Capacity

To measure the capacity of the cells, different values are recorded, which come both directly from the cyclic ageing and from the RPT. During cyclic ageing, the discharge capacity is recorded in each cycle when the cut-off voltage is reached. The respective recorded value is then set in relation to the first complete discharge capacity of the cell (C_{rel}). It should be noted that C_{rel} depends on the temperature and the selected current of the test condition. For evaluation under uniform conditions, C_{DCH} and $C_{\mathrm{DCH,CV}}$ are recorded every 50 cycles with an RPT at 25°C. With help of C_{DCH}, the SOH of the respective cell can be calculated.

Internal Resistance

As with the capacity, the internal resistance of the cells is recorded both during cyclic ageing and during RPT. In cyclic ageing, at the beginning of each discharge process (approximately 100% SOC), the applied discharge current is used as a pulse and is evaluated after 1 s. Just as with C_{rel}, the resistance value calculated from this pulse test is set in relation to the resistance value from the first discharge process (R_{rel}). Also with the RPT, the evaluation takes place at 100% SOC and 1 s ($R_{\mathrm{DC,1s}}$). Additionally the impedance in the frequency domain is also recorded by means of EIS at EOT. Here, the characteristic values R_{Im0} and R_{CT} are determined.

Differential Voltage Analysis

To obtain information about the current state of the electrodes and their balancing at EOT, the sections Q_1 and Q_2 are captured by means of DVA as described in chapter 3.3.1.

5.4 Results and Discussion

The progressive development of parameter variation among identical cells is basically the result of individual ageing rates. In order to understand the origin of the parameter variation, the ageing behaviour of the cells used is therefore extensively examined first. Afterwards results concerning the pa-

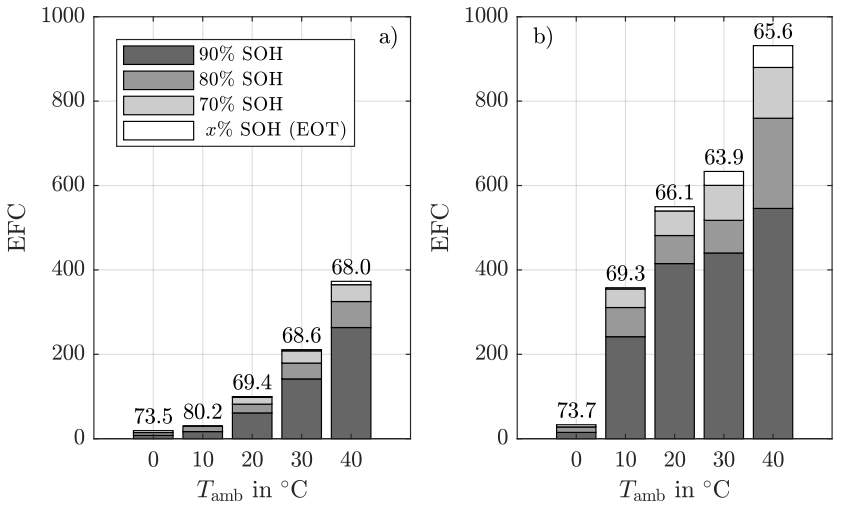

Figure 5.5: Mean achieved lifetime of the 10 groups with 8 cells each under test conditions from Figure 5.1. The SOH values are determined with the help of the RPT data and can be compared among the groups. In a) the results for 1.0C are shown, in b) for 0.5C.

rameter variation are presented. In addition to cyclic ageing, the influence of storage on cell ageing (calendar ageing) and parameter variation is examined as well.

Finally, with the help of the measurement results, test conditions can be determined under which the parameter variation of the cells is as low as possible.

For the investigations, a total of 80 cells are aged over a period of 2 years at 2 different loads and 5 different temperatures according to the specified test procedure.

5.4.1 Results from Ageing Data

In Figure 5.5 the mean achieved lifetime of each cell group based on the RPT data is shown. By observing the mean lifetime for each test condition, the lifetime variation in the cell groups is initially eliminated for a first observation of the results.

Since the EOT of the cells is determined during cyclic ageing down to 60% C_{rel}, the RPT provides a higher end value for the SOH in Figure 5.5.

The achieved lifetime strongly depends on T_{amb} and the C-rate (see Figure 5.5). The lifetime of the cells at 1.0C/0°C is 20 EFC only, while the cells have a maximum lifetime of 942 EFC at 0.5C/40°C.

For cells operated at 1C (Figure 5.5 a)), a 10°C increase in T_{amb} almost doubles the mean lifetime for each test condition. However, this correlation does not exist for cells operated at 0.5C. Here, an increase in T_{amb} is characterised by a varying increase in lifetime. The reason for the different behaviour will be explained later using the ageing curves and the different ageing mechanisms.

The difference in the lifetime of the cells operated at 0.5C between 0°C and 10°C is particularly impressive (Figure 5.5 b)). Here, an increase in T_{amb} by 10°C leads to a tenfold increase in lifetime on average. This fact can be explained with help of the relaxation measurement. While no pronounced lithium plating could be detected at 0.5C/10°C, this was the case for 0.5C/0°C. Thus, a significantly shortened lifetime was expected for 0.5C/0°C. Overall, the lifetime of the cells aged with a C-Rate of 0.5C is significantly higher than that aged with 1.0C at all ambient temperatures.

For the visual representation of the ageing curves on the next pages, the cyclic data are used instead of the RPT data due to a higher measurement resolution. Especially for test conditions with a short lifetime, only one RPT could be recorded after the initial RPT and before EOT. The detailed ageing process under these test conditions can therefore not be monitored by the RPT values. The ageing curves from the RPT are shown in appendix A.1.

5.4.1.1 Ageing Sections of Lithium-Ion Cells

The ageing process of a LIC can be split into different ageing sections, which will briefly be explained before presenting the results. The ageing curve of a LIC can be divided into a increasing, a linear and a non-linear section (see Figure 5.6). While there are many studies on the linear and non-linear section, there are considerably less studies on the increasing section at the beginning of cell ageing. The causes for the individual ageing sections are explained in more detail below.

Increasing Section

In [111] and [110] the increasing section is explained with the passive electrode effect due to geometric influences of the electrodes.

When manufacturing a LIC, the anode is oversized by a factor of approxi-

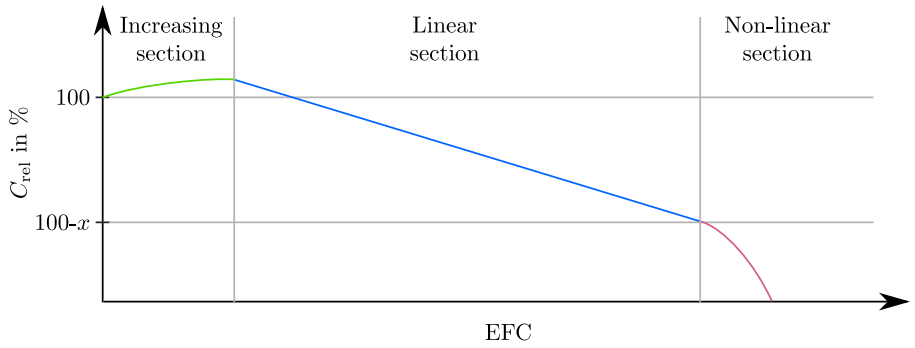

Figure 5.6: Simplified schematic illustration of different ageing sections of a LIC. Based on [110].

mately 1.2 compared to the cathode in order to prevent lithium deposition, especially at the edges, as well as for production reasons [111]. Thus, when the two electrodes are merged together, the anode is not completely covered by the cathode in every area. These uncovered areas are located at the edge of the anode and called passive electrode. This passive part of the anode cannot be charged or discharged directly due to the missing cathode material on the opposite side. Figure 5.7 shows a schematic illustration.

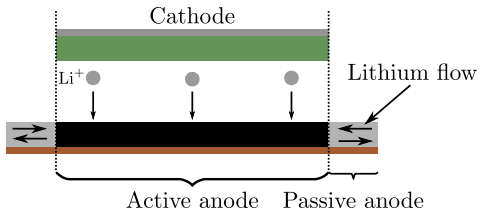

Figure 5.7: Schematic illustration of passive and active anode.

Immediately after production, there is no lithium in the anode. When the cell is charged for the first time during initial formation, lithium is stored in it for the first time. Through a subsequent storage of the cell, a balancing process takes place between the active and the passive anode, whereby a part of the stored lithium shifts into the passive anode through diffusion. This process has different effects on the removable cell capacity. Depending on the average SOC of the active anode during subsequent storage, additional lithium can be gained from the passive electrode in the next capacity check-up test, which results in an increasing capacity and thus in values above

100% C_{rel}. For cyclic ageing, the evaluation of the passive electrode effect is more complex. Here, the average potential of the anode during cyclic ageing plays the decisive role. How long the passive electrode effect lasts at the beginning of cell ageing depends strongly on the selected test conditions. Under certain conditions, an increase in C_{rel} is not or only hardly noticeable, as rapid cell ageing can completely overshadow a slight gain of lithium. If the average SOC of the active anode is higher than that of the passive anode during operation, there may even be a compensatory migration of lithium into the passive anode, which additionally reduces the capacity of the cell.

Linear Section, Non-linear Section

The linear and non-linear section are also directly affected by the anode.

In the literature, the linear section is attributed to the formation of the SEI [21, 109, 110]. The formation of the SEI leads to both a continuous, linear decrease in capacity and a continuously growing internal resistance. Factors that influence the growth rate of the SEI and thus the slope of the linear section have already been investigated in the literature. For example, high temperatures as well as a wide SOC range lead to an accelerated growth of the SEI due to high volume changes in the graphite (see chapter 2.5.1.1) [28, 112].

The non-linear section is initiated by the onset of lithium plating. In addition to the ongoing growth of the SEI, the cell significantly looses lithium, due to lithium plating during the charging process. In this process, lithium deposits on the anode surface instead of being intercalated into the anode (compare with chapter 2.5.1.2).

The change between the linear and the non-linear ageing section can be explained with help of the anode potential during charging (see Figure 5.8). In general, the anode potential shows a dependence on the temperature and the charging current. Higher temperatures, as well as lower charging currents result in a higher potential vs. $\mathrm{Li/Li^+}$ (lower $|\eta_{\mathrm{anode}}|$), compared to lower temperatures and higher charging currents (higher $|\eta_{\mathrm{anode}}|$) (see Figure 5.8 a)).

Due to structural changes of the anode during ageing (e.g. growth of the SEI), the anode porosity and thus the accessibility for lithium ions into to the anode material worsens (increasing $|\eta_{\mathrm{anode}}|$) [109]. As soon as the anode potential of the cell gets below 0 V vs. $\mathrm{Li/Li^+}$ during charging (see Figure 5.8 b)), lithium plating occurs and the cell enters the non-linear ageing section.

Thus, lithium plating can occur during ageing, although no plating took

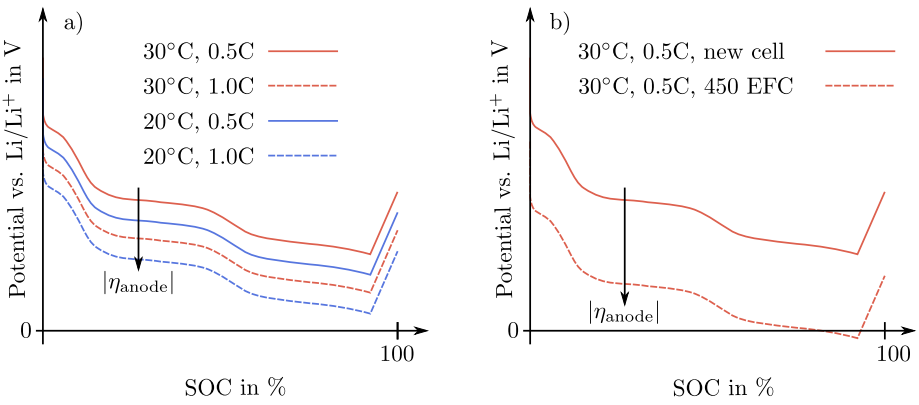

Figure 5.8: Qualitative illustration of the anode potential as a function of the operating temperature and the charging current in a), as well as a comparison of the anode potential of a new cell and an aged cell with reduced anode porosity in b). Based on [109].

place under the same conditions at BOT. The ageing rate from lithium plating is generally higher than that from SEI formation, which explains the much steeper non-linear ageing curve [109, 112].

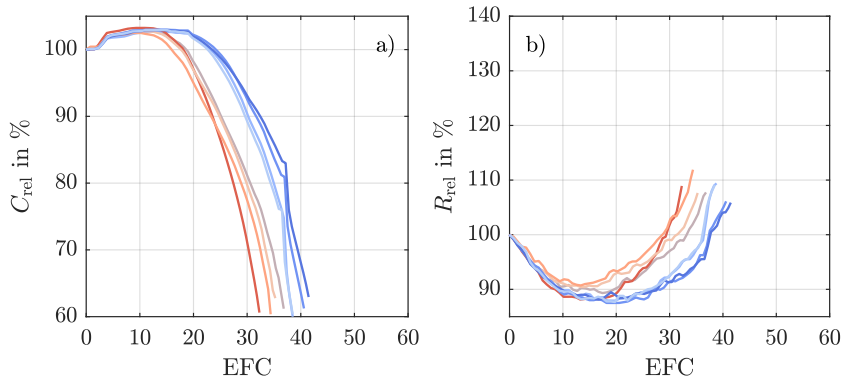

Figure 5.9: a) relative capacity and b) relative internal resistance of all 8 cells at test condition 0.5C/0°C. The colouring of the curves from red to blue is based on the lifetime within the test condition.

5.4.1.2 Development of Cell Parameters

After clarifying the causes for the different ageing sections, the ageing behaviour of the examined cells is now presented. For this purpose, the results are grouped according to the test conditions. Finally, the results of the DVA at EOT provide further insight into the current state of the electrodes and their balancing. The effects of the pure calendar ageing of 137 cells after the test period of approximately 2 years are also presented.

Results from 0.5C/0°C

The ageing at 0.5C/0°C leads to a low lifetime. After a short increase of C_{rel} for all cells, the non-linear ageing section follows directly (see Figure 5.9 a)). This indicates that the ageing is strongly driven by lithium plating, which was already suggested by the relaxation measurement in chapter 2.5.1.2. However, the difference in lifetime of the cells is rather small. The minimum and maximum lifetime of the cells amount to 32 EFC and 42 EFC. The corresponding SOH end value determined is approximately 74% on average. There are no premature cell failures during the test.

Figure 5.9 b) shows the corresponding resistance curves. Initially, a clear decrease of R_{rel} can be seen, which returns to its original value after 33 EFC. A decrease of the internal resistance was also observed in [63, 113, 114] and was attributed to the impedance of the anode. The calculated value of R_{rel} does not only include the pure ohmic part. The evaluation time after 1 s

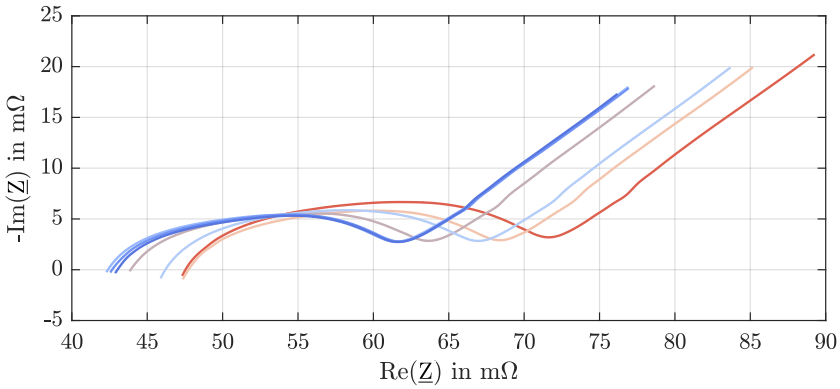

Figure 5.10: EIS data of all 7 measurable cells from the test with 0.5C/0°C at EOT. One cell can not be measured due to a triggered Current Interrupt Device (CID). The colouring of the curves matches that of the cyclic data plots.

also includes the lower frequency range of the impedance of the anode and SEI. The decrease of R_{rel} is therefore not due to an improved conductivity of the electrolyte, but to a reduction of the anode impedance. The final value of R_{rel} is on average about 107%.

Additional insight into the internal resistance of the cells is provided by EIS after completion of the cyclic ageing in Figure 5.10. The measured EIS curves have not changed significantly compared to the initial measurement (compare to chapter 4.5.3). No further semicircle is present that would indicate a significant growth of the SEI. This is also confirmed by the average value of the charge transfer resistance R_{CT}, which has grown only slightly from 16.7 mΩ to 20.3 mΩ. In addition, there is a shift in R_{Im0} from 38.3 mΩ to 44.8 mΩ on average, which also shows a slight increase in the ohmic losses of the cells. Although a capacity loss of 26% SOH can be measured for the cells, R_{CT} hardly increases. This suggests that most of the capacity in test condition 0.5C/0°C is lost due to the formation of dead lithium. In addition to capacity reduction, the isolation of the lithium leads to a measurable deterioration of the conductivity of the electrolyte, which can be observed in the change of R_{Im0}.

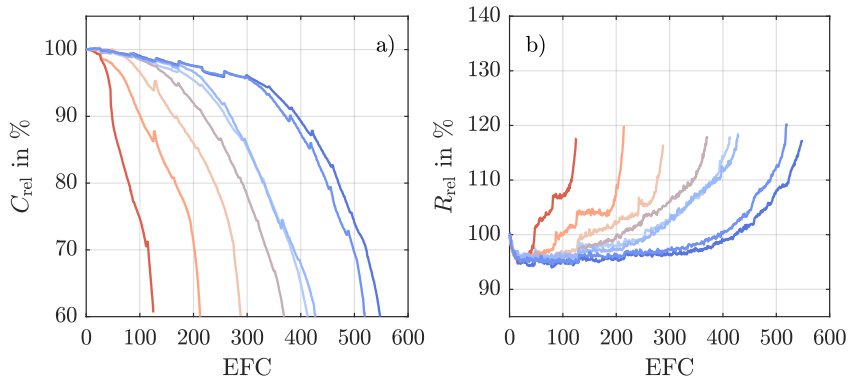

Figure 5.11: a) relative capacity and b) relative internal resistance of all 8 cells at test condition 0.5C/10°C. The colouring of the curves from red to blue is based on the lifetime within the test condition.

Results from 0.5C/10°C

Figure 5.11 a) shows the results for 0.5C/10°C. At BOT, C_{rel} of the cells hardly increases. The passive electrode effect therefore does not occur or only with low intensity. The ageing behaviour of the cells is basically very different, which becomes apparent in a distinct lifetime range from 125 EFC to 548 EFC. The detection of ageing sections is difficult. While some cells run directly into the non-linear section, there are some cells that seem to show a linear section (see Figure 5.11 a)). Under this test condition it is assumed that slight differences in cell production and small temperature differences in the temperature chamber determine the immediate or later onset of lithium plating, which results in high differences in lifetime for test condition 0.5C/10°C. This topic will be examined in more detail later. From RPT, a final average value of approximately 69% SOH is obtained.

Similar to 0.5C/0°C, there is also an initial reduction of R_{rel}, which evolves to a final value of about 120% after a different number of EFC at EOT(see Figure 5.11 b)).

Through EIS at EOT in Figure 5.12 further insights can be obtained. However, one cell can not be measured due to a triggered internal safety mechanism (triggered CID) (2-*nd* worst cell with 212 EFC). In the EIS, values of 46.2 mΩ to 48.4 mΩ are obtained for R_{Im0} (initial value 38.3 mΩ), which hardly differ considering the large difference in lifetime of 423 EFC. At the

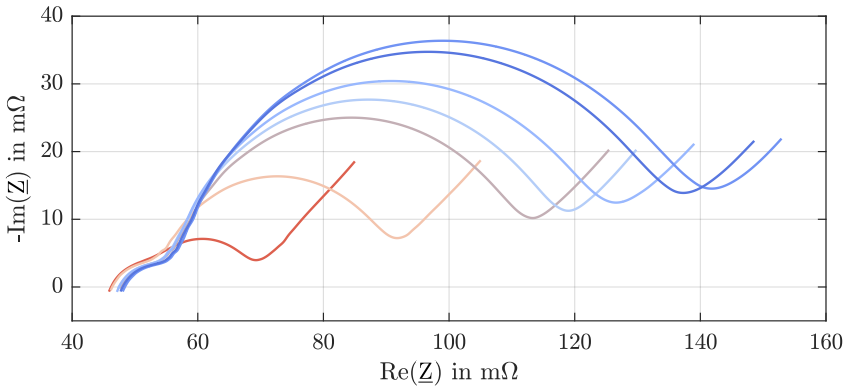

Figure 5.12: EIS data of all 7 measurable cells from the test with 0.5C/10°C at EOT. One cell can not be measured due to a triggered CID. The colouring of the curves matches that of the cyclic data plots.

same time, however, a dependence on the lifetime can be observed in the measured EIS values. The more EFC are achieved, the stronger the second semicircle develops and thus also R_{CT} (see Figure 5.12). The minimum, average and maximum values for R_{CT} result in 23.1 mΩ, 66.8 mΩ and 93.4 mΩ (initial value 16.7 mΩ). R_{CT} contains information about the charge transfer resistance of both electrodes. According to [63] and [114], a deterioration of the charge transfer of the cathode leads to a strong increase of the second semicircle during the ageing of NCA/graphite cells. In [115] and [116], the same behaviour was also demonstrated for NMC cells. From the literature [40, 116] the reasons for the increasing impedance of the cathode are the formation of surface films on the cathode (similar to SEI), but above all, changes in the layer structure during ageing. They become visible in the EIS. When the layer structure changes, the impedance increases due to the blocking of the diffusion channels in the cathode. This can also explain the dependence of R_{CT} on the lifetime. Although the 8 cells have almost the same SOH at EOT, cells with a longer lifetime experience significantly more charge/discharge cycles, which correspondingly can cause more structural damage in the cathode. The increasing internal resistance of the entire cell is therefore mainly caused by the cathode. In addition, a significant growth of the SEI can be observed in all cells, which is noticeable in a change of the EIS curves by the formation of the associated first semicircle.

Results from 0.5C/20°C, 30°C, 40°C

Figure 5.13 shows the results from the test with 0.5C/20°C, 30°C, 40°C. An increase in lifetime can be observed with increasing T_{amb}. While the increase in T_{amb} from 20°C to 30°C results in an average increase of about 82 EFC, there is a significant increase at 40°C with an average increase of 307 EFC compared to 30°C. Although it was initially assumed in the literature that a higher temperature would lead to a shorter lifetime due to a faster growing SEI, other literature sources have identified significantly longer lifetimes at higher ambient temperatures [117–120].

In Figure 5.13 a) the red coloured curve shows an abnormal cell behaviour. Despite similar initial cell parameters, a faster ageing of this cell can be observed, which, however, seems to stabilise after a while. At about 470 EFC, the cell finally fails due to a triggered CID. In Figure 5.13 d) this behaviour is reflected in a sudden increase in R_{rel}. Due to the abnormal behaviour, this cell is declared as an outlier for the later progress of this thesis and is not included in the calculation of the parameter variation. However, it demonstrates that abnormal cells cannot easily be detected after production and may cause unexpected battery failures.

With minimum and maximum values of 515 EFC to 582 EFC at 20°C (with no failed cell), 609 EFC to 666 EFC at 30°C and 884 EFC to 1025 EFC at 40°C, the 8 cells of each group achieve similar lifetimes within the respective test conditions. Final values of respectively 66% SOH, 63% SOH and 65% SOH on average are obtained.

Due to the already mentioned correlation between SOH and internal resistance, the curves in Figure 5.13 d) to f) behave similarly to the curves of C_{rel} in a) to c). A faster decrease of C_{rel} is accompanied by a steeper increase in R_{rel}.

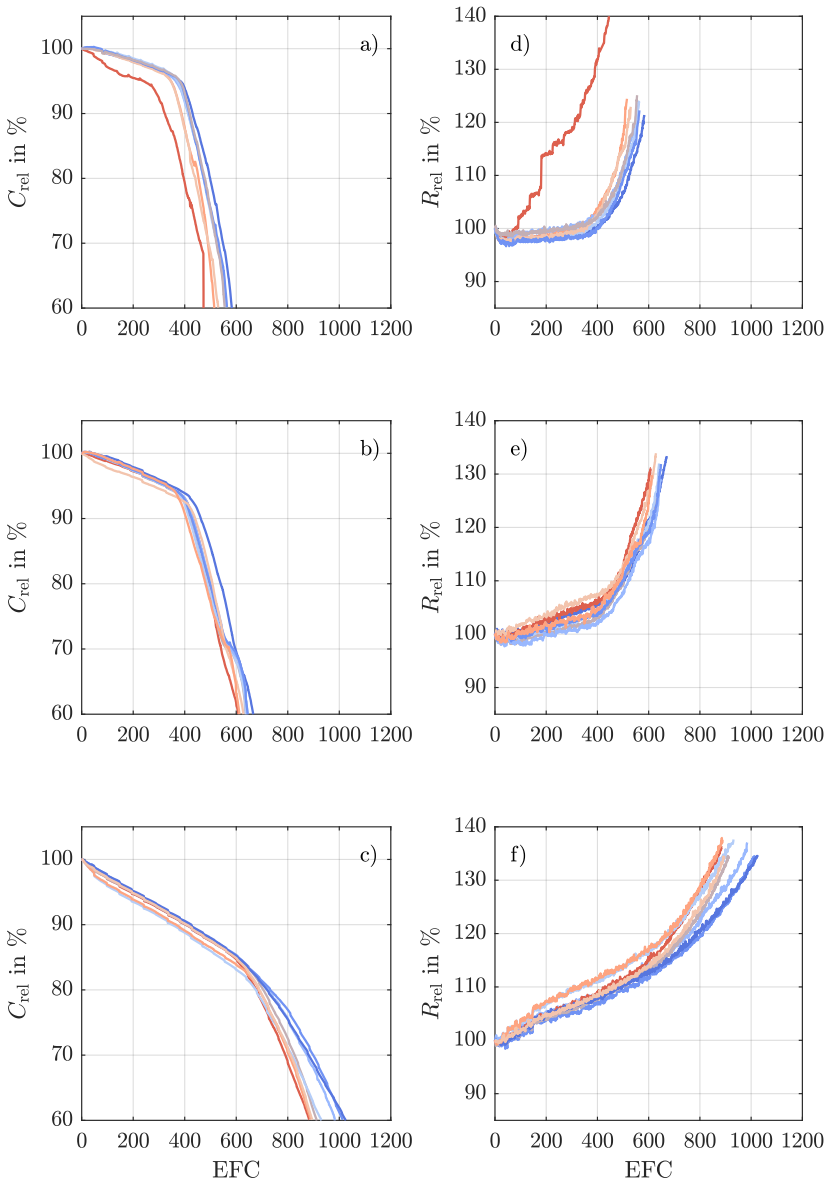

Figure 5.13: Plots a) to c) show C_{rel} for the test conditions 0.5C/20°C, 30°C, 40°C, respectively. Plots d) to f) show the corresponding curves of R_{rel}. The colouring of the curves from red to blue is based on the lifetime within the respective test condition.

R_{Im0} again shows very similar values within the test conditions. The measurement results from the EIS in Figure 5.14 clearly show a significant increase of R_{CT} under all three test conditions, which is generally again dependent on the achieved lifetime. In Figure 5.14 a), b) and c) average values for R_{CT} at EOT are determined at 130.6 mΩ, 171.8 mΩ and 181.2 mΩ (initial value 16.7 mΩ). These values are thus clearly different from 0.5C/0°C and 0.5C/10°C, with an average R_{CT} of 20.3 mΩ and 66.8 mΩ respectively. The pure ohmic values R_{Im0} in Figure 5.14 a), b) and c) are on average 50.5 mΩ, 51.9 mΩ and 51.5 mΩ (initial value 38.9 mΩ). Again these are very similar in view of the significant differences in lifetime between the test conditions.

Under all three test conditions, the first semicircle is clearly visible next to the second, which indicates a pronounced growth of the SEI (see Figure 5.14). The second semicircle causes the biggest increase in internal cell resistance, which, according to literature, can again be attributed to an increased impedance of the cathode.

The selected minimum frequency of the EIS of 10 mHz is no longer able to record the diffusion section in Figure 5.14 completely. For example, the corresponding frequency of R_{CT} for 0.5C/40°C shifts on average from an initial frequency of 0.67 Hz to 0.018 Hz in aged state. This shift can be explained by the progressive internal structural changes of the cells. As a result, the chemical reactions are much slower than at BOT. Due to a triggered CID, a cell from test condition 0.5C/20°C can not be measured any more (worst cell with 470 EFC).

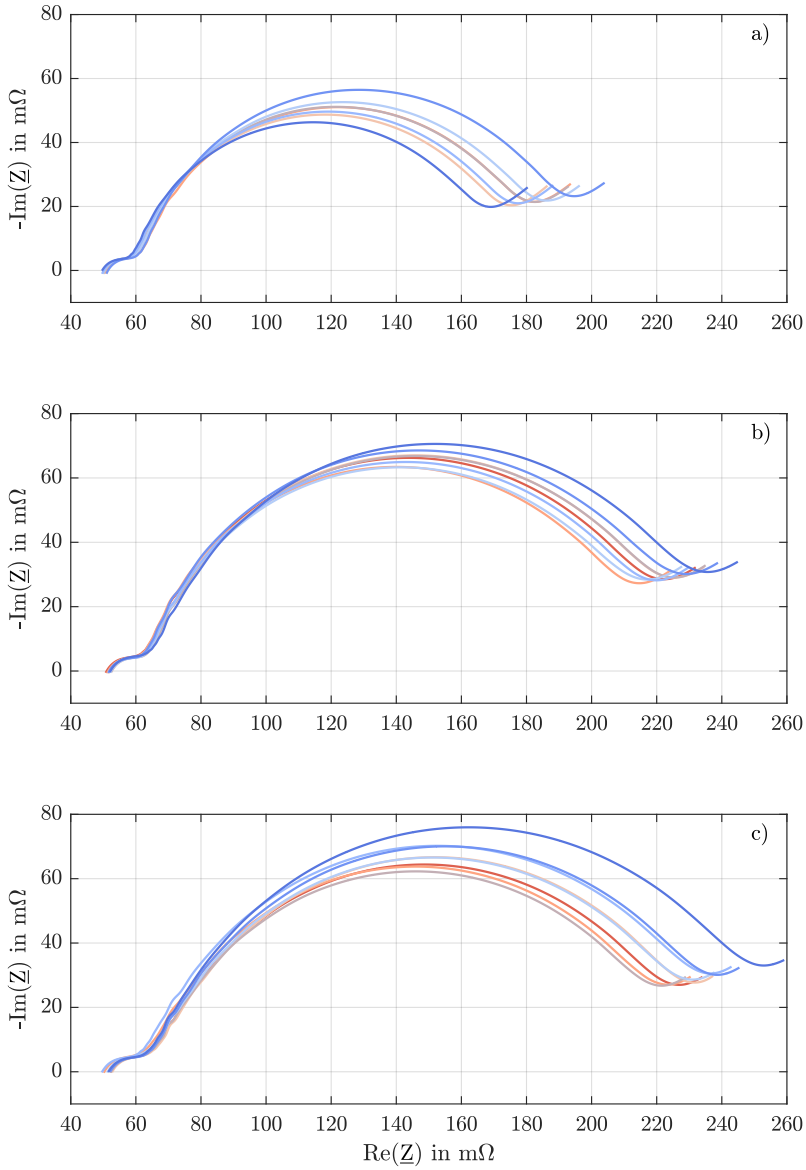

Figure 5.14: EIS data from all 23 measurable cells aged under the test conditions 0.5C/20°C, 30°C, 40°C in a), b) and c) at EOT. One cell in a) could not be measured due to a triggered CID. The colouring of the curves matches that of the cyclic data plots.

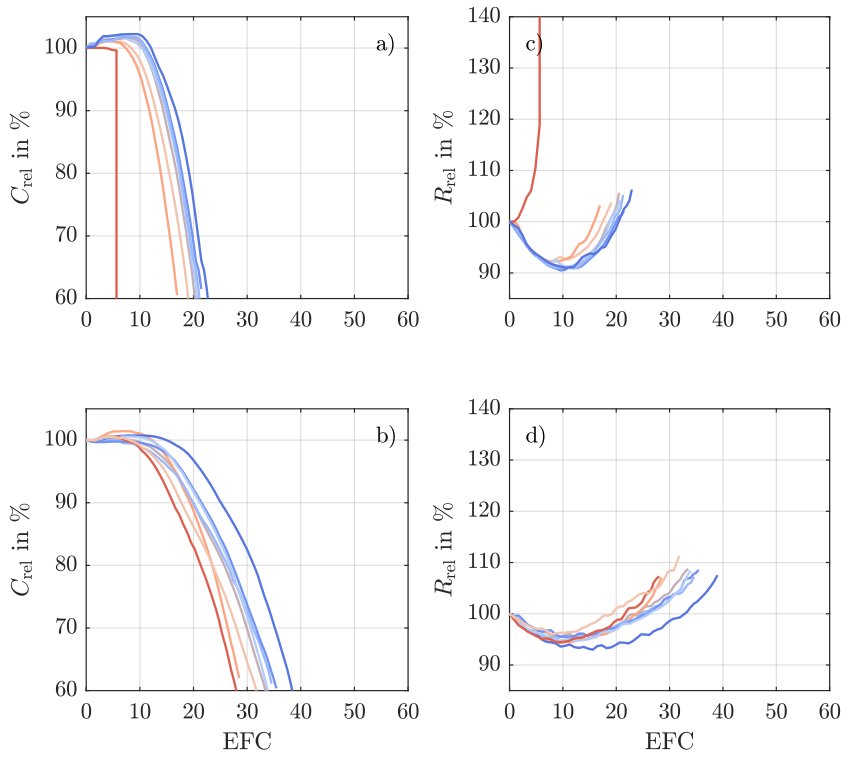

Figure 5.15: Plots a) and b) show C_{rel} of the test conditions 1.0C/0°C, 10°C respectively. Plots c) and d) show the corresponding curves of R_{rel}. The colouring of the curves from red to blue is based on the lifetime within the respective test condition.

Results from 1.0C/0°C, 10°C

In Figure 5.15 the test results under the conditions 1.0C/0°C and 1.0C/10°C are shown. Both test conditions show a rapid degradation of the cells, with a short increase in C_{rel} followed directly by a non-linear ageing section. This behaviour is consistent with the previously performed relaxation measurement, that predicted immediate lithium plating for both test conditions. Due to the high load in combination with 0°C, one cell (red coloured curve) already fails after 6 EFC. This again reflects a rapid increase of R_{rel} (see Figure 5.15 a) and c)). The abnormal behaviour of this cell can already be detected during the first cycles by R_{rel}. At test condition 1.0C/0°C, 17 EFC

to 22 EFC (without the the red coloured cell) and at 1.0C/10°C 28 EFC to 38 EFC are achieved, resulting in similar lifetimes within groups of same test conditions.

After a short reduction of R_{rel}, the cells of both test conditions develop to uniform values of approximately 104% at 0°C and 108% at 10°C. The final RPT at EOT results in values of 74% SOH (0°C) and 80% SOH (10°C) on average.

Figure 5.16 shows the results of the EIS measurement at EOT for both ambient temperatures. Due to a triggered CID, only 7 of 8 cells from 1.0C/0°C and only 2 cells from 1.0C/10°C can be measured. The EIS measurement results obtained under this test conditions show a similar behaviour, which can also be compared with that of 0.5C/0°C, where strong lithium plating takes place as well.

The shape of the EIS curves has not changed significantly. No semicircle has formed indicating SEI growth. The average values of R_{Im0} are 42.3 mΩ in a) and 43.4 mΩ in b) (initial value 38.3 mΩ). R_{CT} mean values are 17.0 mΩ in a) and 13.8 mΩ in b) (initial value 16.7 mΩ). Since R_{CT} has hardly changed under both test conditions, it can be assumed that the investigated cells lose their capacity due to dead isolated lithium as a result of strong lithium plating. A very similar ageing process for NMC cells with 1C load at 0°C ambient temperature was also found in [121]. Through subsequent cell opening and spectroscopic measurement of the extracted material, the accumulation of metallic lithium at the anode could be determined as the main reason for the rapid ageing.

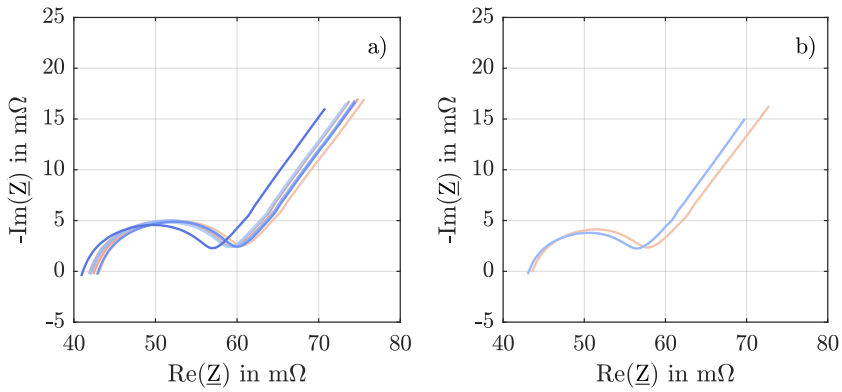

Figure 5.16: EIS data from all 9 measurable cells under the test conditions 1.0C/0°C, 10°C in a) and b) at EOT. 7 cells could not be measured any more due to a triggered CID. The colouring of the curves matches that of the cyclic data plots.

Results from 1.0C/20°C, 30°C, 40°C

Figure 5.17 shows the results obtained under the last test conditions 1.0C/20°C, 30°C, 40°C. Despite the higher test current, no cells failed during cyclic ageing. The capacity curves shown in Figure 5.17 a) to c) not only differ strongly in their achieved lifetime, but also in their shape. At 1.0C/20°C and 1.0C/30°C, only short linear ageing sections can be seen, which quickly change into non-linear sections. At 1.0C/40°C, linear sections can be seen, which differ significantly in their slope.

Like the cells operated with 0.5C, the lifetime can be significantly increased by raising T_{amb} from 20°C to 40°C. Overall, the cells achieve lifetimes of 68 EFC to 153 EFC at 1.0C/20°C, 121 EFC to 293 EFC at 1.0C/30°C and 262 EFC to 517 EFC at 1.0C/40°C, which thus show high differences even within groups of the same test conditions. With regard to the SOH, final values of 69.4%, 68.6% and 68.0% respectively are determined at EOT.

As with all other test conditions, R_{rel} develops similarly to C_{rel} at all three temperatures (see Figure 5.17 d) to f)). All cells reach similar end values within groups of the same test conditions.

Figure 5.18 shows the corresponding EIS measurement results. They show several parallels to the results of the test conditions 0.5C/20°C, 30°C ,40°C. In all curves, the first semicircle has clearly formed, indicating significant growth of the SEI. In addition, the same dependence of R_{CT} on the achieved lifetime can also be seen. In general, the more EFC are reached, the greater the increase of R_{CT}, which is again predominantly caused by the growth of the second semicircle. The average values of R_{CT} for 1.0C/20°C, 30°C, 40°C result in 30.5 mΩ, 43.7 mΩ and 57.6 mΩ respectively (initial value 16.7 mΩ). For R_{Im0} average values of 46.0 mΩ in a), 47.4 mΩ in b) and 48.6 mΩ in c) are obtained (initial value 38.3 mΩ).

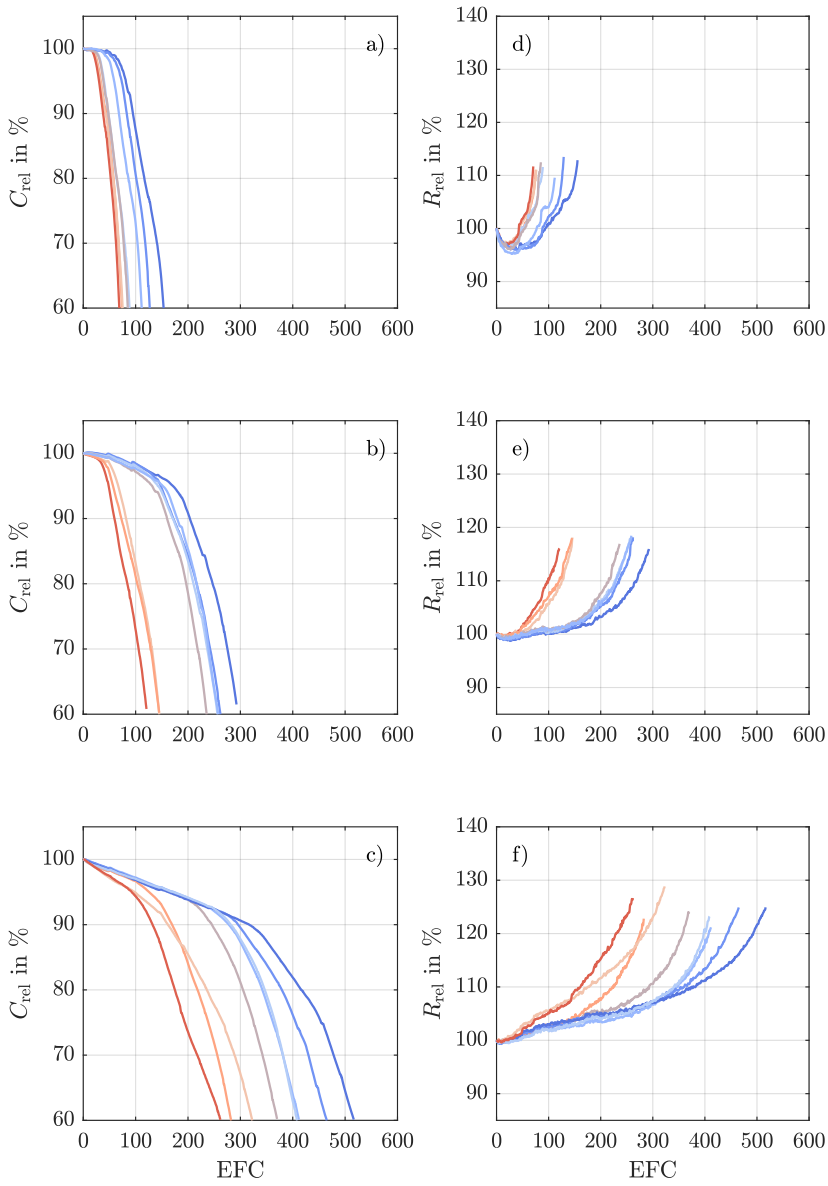

Figure 5.17: Plots a) to c) show C_{rel} of the cells under test conditions 1.0C/20°C, 30°C, 40°C, respectively. Plots d) to f) show the corresponding curves of R_{rel}. The colouring of the curves from red to blue is based on the lifetime within the respective test condition.

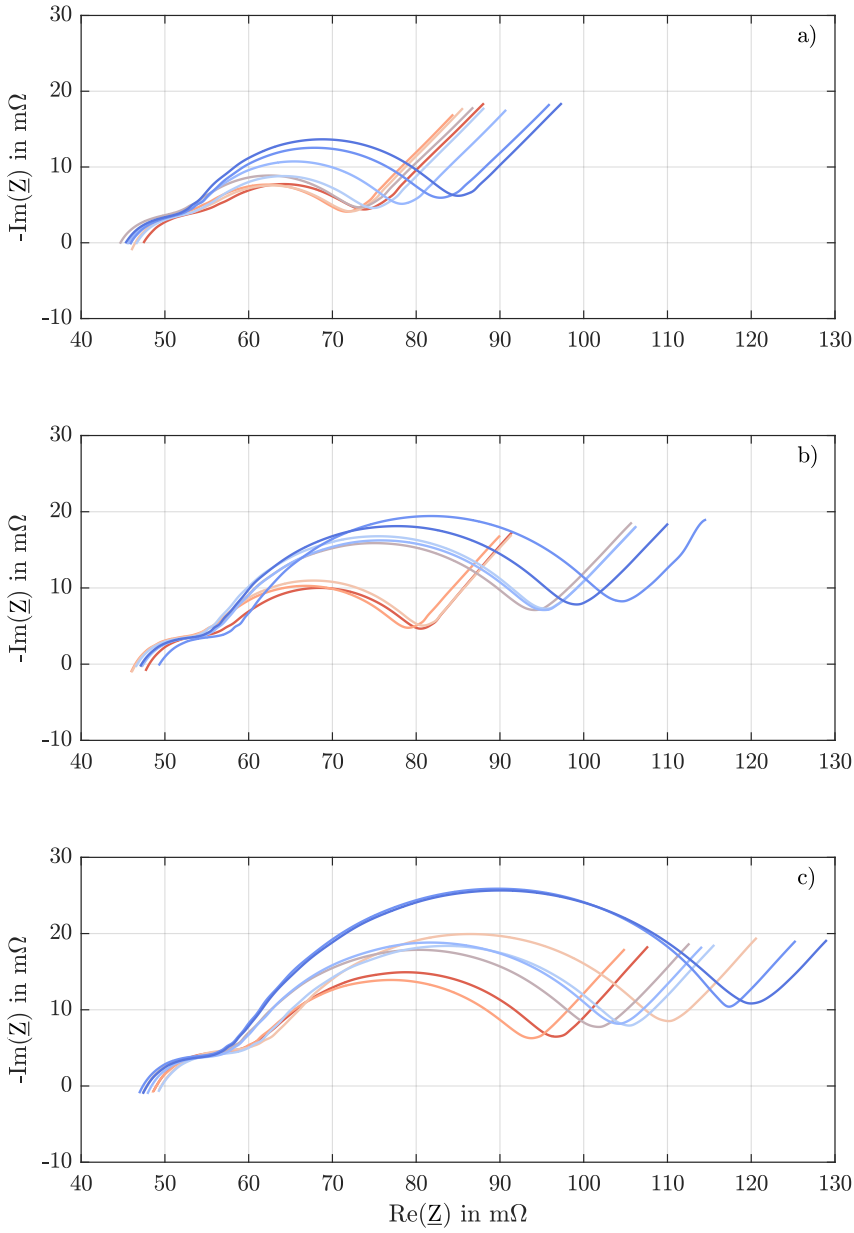

Figure 5.18: EIS data of all cells obtained under the test conditions 1.0C/20°C, 30°C, 40°C in a), b) and c) at EOT. The colouring of the curves matches that of the cyclic data plots.

Comparison of EIS Results

Figure 5.19 summarises the average EIS data for 1.0C in a) and for 0.5C in b). For comparison of the aged cells with the initial state, a solid line shows the initial value of R_{Im0} and a dashed line $R_{\mathrm{Im0}}+R_{\mathrm{CT}}$ in the initial state.

Despite the low SOH achieved at EOT, R_{Im0} increases only slightly compared to the initial value (see Figure 5.19). The conductivity of the electrolyte, as well as the other components with a pure ohmic part, therefore contribute only insignificantly to the ageing-related performance loss of the cells. Instead, based on the measurements of R_{CT} and the literature, it is concluded that the measurable increase in resistance of the aged cells is predominantly triggered by a deterioration of the charge transfer, which results mainly from irreversible changes in the cathode material. In addition, a dependence of the measured values R_{Im0} and R_{CT} on the lifetime of the cells can be recognised. Both show a high Pearson correlation coefficient of $\rho = 0.92$ (R_{Im0}) and $\rho = 0.96$ (R_{CT}) with the completed EFC. They also show a high Pearson correlation coefficient of $\rho = -0.89$ (R_{Im0}) and $\rho = -0.79$ (R_{CT}) with the achieved SOH at EOT.

When observing the results, it becomes clear that the individual parts of the impedance should be analysed in more detail in order to obtain information about the ageing state of the cells. Here, test condition 1.0C/10°C is explicitly mentioned, where the sum of R_{Im0} and R_{CT} hardly changes compared to the initial value. Only the evaluation of R_{Im0} gives information about a possible ageing of the cells from 1.0C/10°C. Especially the described current step response method to determine $R_{\mathrm{DC,t_p}}$ reaches its limits here. With this method, it is not possible to record the purely ohmic part with sufficient accuracy. The main reason is the sampling interval of the measuring device which usually can't be chosen small enough.

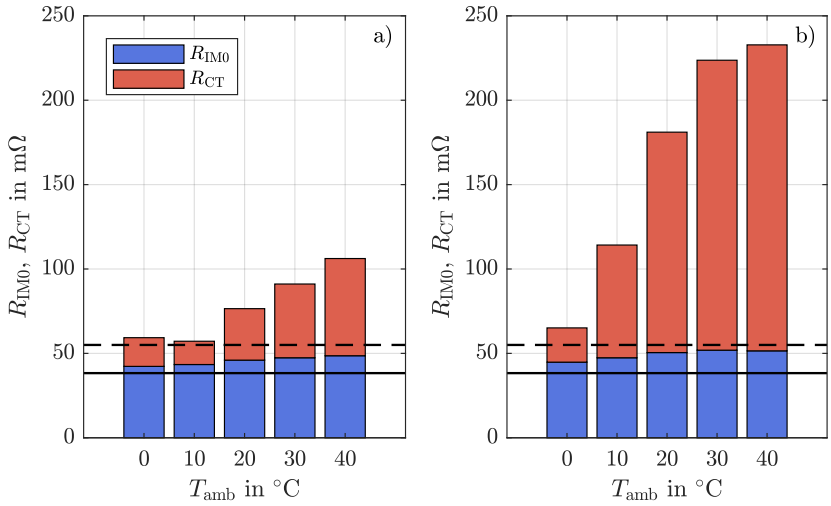

Figure 5.19: Summary of characteristic EIS values. In a) the values from the 1.0C test, in b) those of the 0.5C test are shown. For comparison, the average initial values of R_{Im0} and R_{Im0}+R_{CT} are shown as solid and dashed lines in both plots.

Test condition	Linear section	Non-linear section
0.5C/20°C	0.33	4.35
0.5C/30°C	0.41	4.02
0.5C/40°C	0.47	2.81
1.0C/20°C	—	11.3
1.0C/30°C	—	9.5
1.0C/40°C	0.56	6.9

Table 5.1: Average ageing rates in the linear and non-linear section in mAh/EFC in the range from 20°C to 40°C. The values are calculated on the basis of the comparable RPT data.

Comparison of Ageing Behavior

After comparing the EIS results, the ageing behaviour is now compared across the test conditions. The ageing behaviour of the cells under the test conditions 1.0C/0°C, 1.0C/10°C and 0.5C/0°C have already been sufficiently explained with help of the relaxation measurement. Due to the direct onset of lithium plating at BOT, a rapid non-linear ageing with a short lifetime results in each condition. Under the other test conditions, different ageing sections can be seen which differ in their slope. For comparison, Table 5.1 shows the approximate average ageing rates of the linear and non-linear sections based on the RPT data in mAh/EFC.

Table 5.1 reveals that the average ageing rate of the linear section increases with increasing T_{amb}. Increasing the current to 1.0C leads to a further increase in the ageing rate of the linear section due to a stronger internal heating of the cells (e.g. 1.0C/40°C). In the literature, this relationship was also proven by measurements [110, 112].

For other test conditions (0.5C/10°C and 1.0C/20°C, 30°C), it is initially not clear whether the ageing takes place in the linear section or whether lithium plating already contributes at BOT. The two best cells with regard to the achieved lifetime in test condition 0.5C/10°C seem to start ageing in the linear section for several hundred EFC (see Figure 5.11 a)). When calculating the ageing rate, however, it becomes clear that lithium plating already contributes to the ageing, as an average ageing rate of 0.57 mAh/EFC results. For the linear section at 0.5C/10°C, however, a value would be expected below the ageing rate of 0.5C/20°C with 0.33 mAh/EFC. It can be concluded

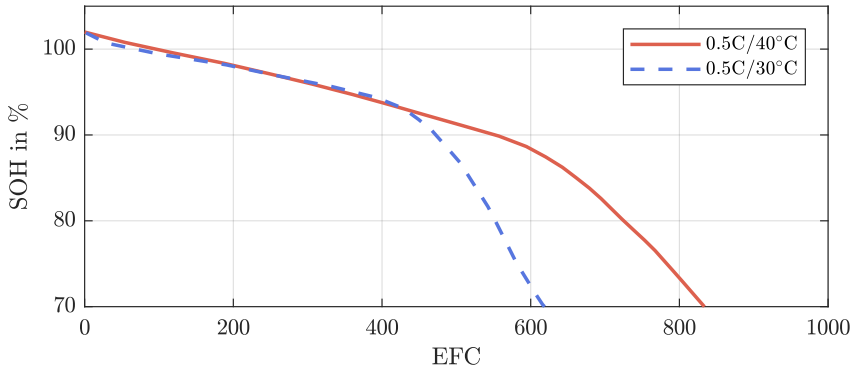

Figure 5.20: The ageing rate of the non-linear sections of both cells show a dependence of SOH. The lower the SOH at the start of lithium plating, the lower the resulting ageing rate in the non-linear section.

that the two cells observed at 0.5C/10°C have already completed a large part of their lifetime with a slow onset of lithium plating. The same is valid for the test conditions 1.0C/20°C and 1.0C/30°C (see Figure 5.17). Lithium plating in the presumed linear ageing section already takes place since the calculated ageing rates lead to higher values than at 1.0C/40°C.

While the ageing rate in the linear section increases with increasing T_{amb}, the ageing rate of the non-linear section decreases over temperature. Furthermore, the ageing rate in the non-linear section is generally lower at 0.5C than at 1.0C. This behaviour can be explained with the anode potential, which is responsible for the onset of lithium plating and thus for the change into the non-linear section.

As already described, the anode potential depends on the temperature. A higher temperature leads to a lower $|\eta_{\mathrm{anode}}|$ and thus to a higher anode potential vs. $\mathrm{Li/Li^+}$ at BOT (compare to Figure 5.8 a)). Due to the higher anode potential, more cycles can be completed before the lithium plating criterion $\varphi_{\mathrm{anode}} \leq 0\ V$ is reached, although the ageing rate in the linear section is somewhat higher at higher temperatures. Figure 5.20 demonstrates this effect with an example of two cells aged at 0.5C/30°C and 0.5C/40°C. At the onset of lithium plating, the cell aged at 0.5C/40°C already has a lower SOH or in case of dominating LLI less available lithium. The amount of available lithium in the cells when lithium plating starts, however, is decisive for the ageing rate in the non-linear section. The lower the SOH at

the start of lithium plating, the lower the resulting ageing rate in the non-linear section. This fact will play an important role in the evaluation of the parameter variation.

Based on the curves shown and the calculated ageing rates, it can also be explained why the lifetime of the 1.0C tests conditions almost doubles for every 10°C increase in T_{amb}. The investigations show that the ageing of all cells operated with 1.0C predominantly takes place with lithium plating. According to the literature, within this plating-driven ageing section, a correlation of the ageing rate with T_{amb} exists [24]. On the other hand, at test conditions operated with 0.5C, ageing takes place through the formation of the SEI and through lithium plating. Here, the different ageing mechanisms overlap. There is no such temperature-related correlation as under the 1.0C test conditions.

Another difference in the ageing behaviour under the test conditions is given by the initial increasing section. This section is only found at 1.0C/0°C, 1.0C/10°C and 0.5C/0°C. The direct onset of lithium plating under these test conditions may be responsible for triggering the passive electrode effect. The lithium originating from the cathode is not completely stored in the anode during the charging of these cells, as parts of it accumulate on the anode surface due to lithium plating. Accordingly, the anode is not lithiated to the same extent as the cathode is delithiated. As a result, the SOC of the anode is progressively reduced, possibly leading to an average SOC where the passive electrode effect comes into play and additional lithium is extracted from the passive anode.

5.4.1.3 Further Insights from DVA

EIS allows the cause of the performance loss to be specified more precisely. Similarly, DVA allows a more detailed analysis of the capacity loss. For this purpose, Figure 5.21 and Figure 5.22 show the DVA of all aged cells at EOT. The representation via SOC simplifies the visual evaluation of the electrode balancing. The values Q_1 and Q_2 are noted in each plot if the values can be determined. For comparison with the initial state at BOT, each plot contains a grey dashed line. An absolute representation of the DVA plotted over Ah can be found in appendix A.2.

Observing all curves reveals that the shape of the derivatives changes significantly compared to BOT. Under all test conditions, the characteristic peaks of the anode are clearly flattened. In some cases they completely dis-

appeared. The reason for this can be assumed to be the almost complete utilisation of the voltage range of the cells during cyclic ageing. Especially the selected discharge voltage of 2.75 V leads to mechanical stress in the anode material and progressive degradation due to a high volumetric expansion at such low voltages. This phenomenon was also observed in [63]. Due to an inhomogeneous ageing of the anode at high stress conditions and the resulting poorer accessibility of some anode areas for lithium, an inhomogeneous distribution of lithium finally occurs, which can no longer reflect the typical characteristics of the anode potential curve [87, 122].

None of the cells aged under the test conditions features a middle anode peak below 50% SOC. Thus it can be concluded that the anode has no limiting and thus capacity-determining effect at any of the test conditions. Nevertheless, the mean values of Q_1 show that the anode suffers a significant capacity loss. When new, the anode was 50% lithiated (stage 2) at an average Q_1 of 1.45 Ah. After completion of the ageing test, the value decreases to an average value of about 1.0 Ah.

DVA cannot provide any solid values for the NMC cathode. However, it can be concluded from the literature that the cathode also experiences a loss of its capacity during cyclic ageing, but has a capacity-limiting effect only in rare cases [114]. Assuming that also the cathode would not limit the cells capacity, LLI only would determine the resulting capacity of the cells investigated in this thesis and thus also the occurring capacity variation.

Furthermore, the measurements reveal a dependence of the electrode balancing on the selected test condition. Both in Figure 5.21, as well as Figure 5.22, a shift of the middle anode peak towards a higher SOC can be seen with increasing T_{amb} and thus also increasing lifetime. A longer lifetime or higher operating temperature thus leads to relatively more LLI and less LAAM. The same could also be observed in [114]. This behaviour can be explained by the fact that the degradation of the anode is more pronounced at the begin of ageing and decreases with increasing number of cycles in relation to LLI. This is also confirmed by the average values of Q_1. Despite the longest lifetime, $\overline{Q}_1$ at 0.5C/40°C has the highest storage capacity of the anode with 1.13 Ah, while at the same time $\overline{Q}_2$ has the highest LLI resulting in 0.62 Ah. In the 1.0C test conditions (see Figure 5.22), the described shift of the middle anode peak with increasing T_{amb} and lifetime can also be seen. However, compared to the 0.5C test conditions, the middle anode peak is generally located at lower SOC values, so that a higher degradation of the anode material can be observed under these test conditions. In [63], this behaviour was also shown on NCA/graphite cells. The reason for this is the

significantly higher stress on the anode material due to higher currents.

Another finding from the DVA is that the large differences in the cell-lifetime of several 100 EFC within same test conditions (e.g. 0.5C/10°C) are reflected in a very similar electrode balancing. The ratio of Q_1 and Q_2 of the cells differs only insignificantly within the test conditions, although the ageing shows clearly different courses. Further tests must be carried out to clarify this observation.

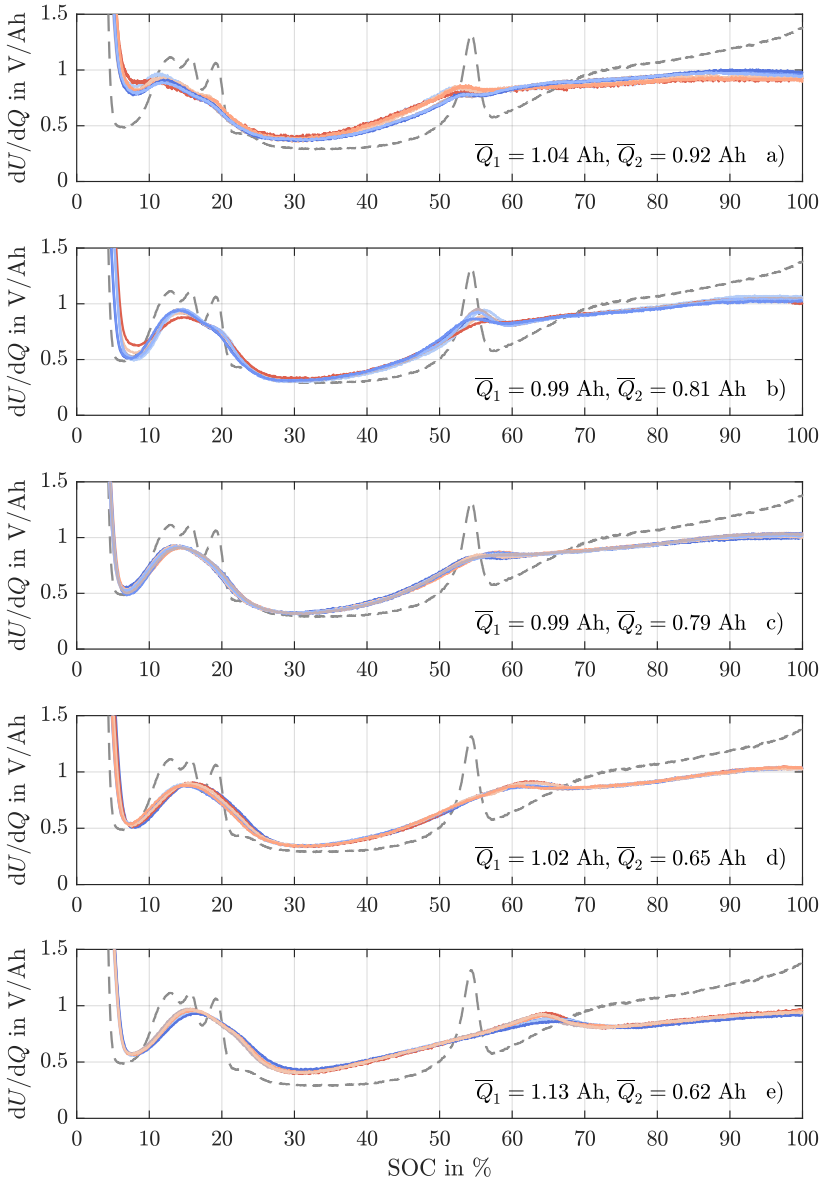

Figure 5.21: DVA of cells aged with 0.5C. In a) to e), the temperatures from 0°C to 40°C are shown in steps of 10°C in ascending order. The colouring of the curves again matches that of the cyclic data plots and represents the achieved lifetime. The average values of $\overline{Q}_1$ and $\overline{Q}_2$ are shown in each subplot.

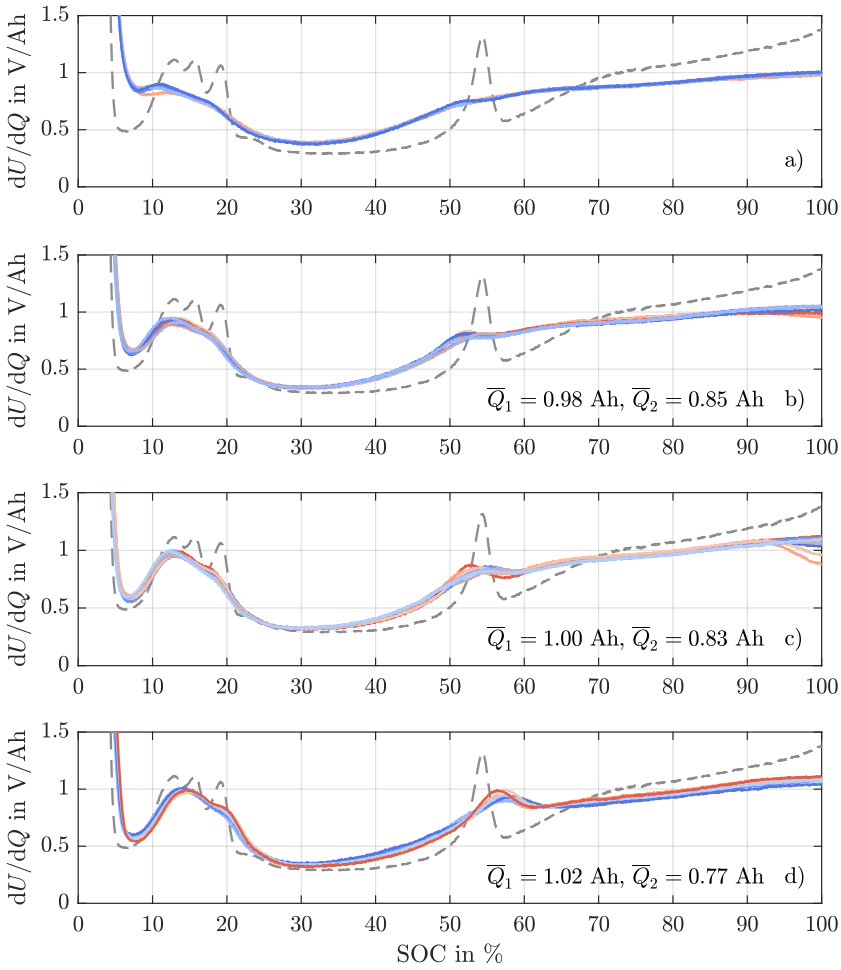

Figure 5.22: DVA of cells aged with 1.0C. In a) the cells aged at 0°C are shown in b) to d) the cells from 20°C to 40°C in steps of 10°C are shown in ascending order. DVA for 1.0C/10°C is not possible due to triggered CIDs. The colouring of the curves again matches that of the cyclic data plots and represents the achieved lifetime. The average values of $\overline{Q}_1$ and $\overline{Q}_2$ are shown in each plot if the evaluation is possible.

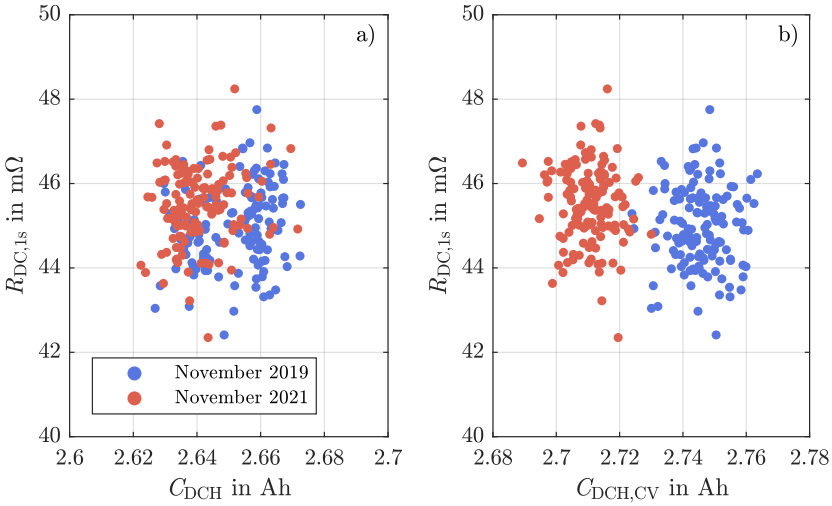

Figure 5.23: Measurement of 137 stored cells after two years. The SOC during storage was about 30%, the temperature about 20°C. C_{DCH}, $C_{DCH,CV}$ and $R_{DC,1s}$ are shown.

5.4.1.4 Influence of Storage on Cell Ageing

After extensive investigations on cyclic ageing, the calendar ageing of the stored cells is also investigated. For this purpose, 137 cells from the original batch stored for 2 years are still available at EOT. The voltage during storage was set to 3.63 V, which corresponds to a SOC of about 30%. Figure 5.23 shows the result for the parameters C_{DCH} and $C_{DCH,CV}$ compared to $R_{DC,1s}$. The change of the measured parameters within the 2 years is very small. C_{DCH} decreases on average from 2.65 Ah to 2.64 Ah and $C_{DCH,CV}$ decreases on average from 2.74 Ah to 2.71 Ah. $R_{DC,1s}$ increases on average from 45.0 mΩ to 45.5 mΩ.

The overall small change in the cell parameters is in accordance with the literature. With a SOC of 30% and T_{amb} of approximately 20°C, hardly any calendar ageing is expected [83, 123].

In the DVA of the stored cells, the characteristic peaks of the anode are less distinct compared to 2019, indicating a decrease in homogeneity with respect to lithium distribution. The electrode balancing, however, does not change.

5.4.1.5 Summary

Numerous observations on cell ageing have been made on the last few pages. For better clarity, all findings are now summarised in bullet points.

Capacity Loss/Lifetime

- The achieved lifetime is strongly dependent on the C-Rate and T_{amb}. Lower C-Rates, as well as a higher T_{amb}, enable the longest lifetimes (see Figure 5.5).
- Since the value of 60% C_{rel} in each test condition is achieved with lithium plating, in particular the selected charging current plays a major role in the ageing process and thus achieved lifetimes. Lower charging currents could significantly increase the lifetime of the cells.
- At test conditions 1.0C/0°C, 1.0C/10°C and 0.5C/0°C, lithium plating occurs immediately at BOT and thus results in a greatly reduced lifetime. This could be reliably predicted with help of the relaxation measurement (see Figure 5.2). At all other test conditions, lithium plating only occurs in the progress of ageing, due to a growing anode overpotential.
- The ageing processes differ in the individual ageing sections in terms of duration and slope. High temperatures cause slightly faster ageing rates in the linear section, but lead to flatter non-linear sections. The combination of duration and ageing rate of the sections finally results in the lifetime of a cell (see Table 5.1).
- The lower the SOH of the cells at the onset of lithium plating, the lower the ageing rate in the non-linear section (see Figure 5.20).
- An increase in capacity due to the passive electrode effect can only be observed in cells that already suffer from lithium plating at BOT. The reason for this is assumed to be a reduced SOC of the anode due to lithium plating (see Figure 5.9 and Figure 5.15).
- The stored cells at 30% SOC and 20°C show hardly any ageing (see Figure 5.23).

Performance Loss

- The biggest part of the performance loss of the cells originates from an increasing charge transfer resistance R_{CT} (see Figure 5.19).
- Based on the literature and the measurements, the increase in R_{CT} is

mainly triggered by a deteriorating charge transfer of the cathode.

- To reliably assess the cell condition, both R_{Im0} and R_{CT} should be determined to better assign their shares in performance loss.
- R_{Im0} and R_{CT} both show a high Pearson correlation coefficient of $\rho = 0.92$ (R_{Im0}) and $\rho = 0.96$ (R_{CT}) with the completed EFC. They also show a high Pearson correlation coefficient of $\rho = -0.89$ (R_{Im0}) and $\rho = -0.79$ (R_{CT}) with the achieved SOH at EOT.

DVA

- The anode deteriorates significantly under all operating conditions. The characteristic anode peaks are hardly visible any more (see Figure 5.21 and 5.22). The reason for this is the high volumetric stress when the voltage limits are fully utilised.
- The anode does not limit the capacity of any cell. Assuming that the cathode does not limit the cell capacity either, LLI alone is responsible for the ageing shown and therefore the resulting capacity variation.
- With increasing temperature and lifetime, the electrode balancing changes towards more LLI and less LAAM (see Figure 5.21 and 5.22).
- Despite high differences in lifetime within the same test conditions, the cells show hardly any differences in DVA (see Figure 5.21 and 5.22).

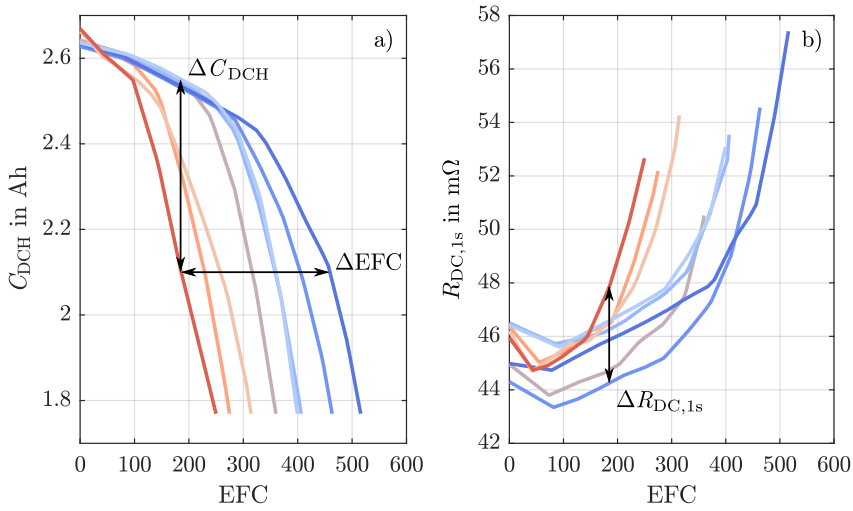

Figure 5.24: Examples for capacity variation (ΔC_{DCH}) and lifetime variation (ΔEFC) in plot a), as well as internal resistance variation ($\Delta R_{\mathrm{DC,1s}}$) in plot b), evaluated at 2.08 Ah (80% SOH of worst cell) and 190 EFC respectively.

5.4.2 Results from Parameter Variation

After extensive investigations of the cell-ageing behaviour, the resulting variation behaviour within in and between the test groups is now quantified and evaluated. The term variation is very broad and can theoretically refer to all determined cell parameters. It will therefore be clarified in more detail which variation values are investigated in this section and how they are determined.

From the ageing curves shown in chapter 5.4.1, variation obviously appears as shown in Figure 5.24. The values ΔC_{DCH} and $\Delta R_{\mathrm{DC,1s}}$ result from cell parameters C_{DCH} and $R_{\mathrm{DC,1s}}$ measured directly, while ΔEFC is calculated indirectly from the cell parameters via the different lifetime. In this section all three variation quantities are investigated.

ΔC_{DCH} is the capacity difference between the currently best and worst cell in a certain test condition at the same EFC value. Similarly, $\Delta R_{\mathrm{DC,1s}}$ is the difference between the resistances of the currently best and worst cell at the same EFC value. Both values are taken at the same EFC value of the cell with the lowest lifetime (red coloured curve).

ΔEFC, on the other hand, is the difference in lifetime between the best and worst cell at the same capacity value (e.g. 80% SOH). Since the lifetime of the cells under different test conditions varies significantly, only the relative variation value κ_{EFC} (based on COV) is used instead of the absolute value ΔEFC.

In addition to the variation from cyclic ageing, the effect of pure calendar ageing on the parameter variation of cells stored for 2 years is also investigated towards the end of this subsection.

5.4.2.1 Results from Cyclic Ageing

In the following sections, the capacity variation ΔC_{DCH} and the internal resistance variation $\Delta R_{\mathrm{DC,1s}}$ are evaluated for all investigated test conditions. The EFC value is taken when the worst cell reaches a value of 2.08 Ah (80% SOH) within the test conditions, often assumed as EOL. The results for the test conditions operated at 0.5C and 1.0C are shown separately in Figure 5.25 and Figure 5.27. Since the parameter variation (ΔC_{DCH}, $\Delta R_{\mathrm{DC,1s}}$) at BOT can vary in each test condition, the difference between the final value and the initial value is given as well.

Results from 0.5C/0°C, 10°C

Under the test conditions 0.5C/0°C, 10°C the cells show a rapid development of the parameter variation within a few EFC for both the capacity and the internal resistance (see Figure 5.25). When the SOH of the worst cell reaches 80%, ΔC_{DCH} results in 0.31 Ah (+0.28 Ah) at 0°C and 0.5 Ah (+0.48 Ah) at 10°C. For $\Delta R_{\mathrm{DC,1s}}$ values of 6.1 mΩ (+4.0 mΩ) and 3.5 mΩ (+2.4 mΩ) are obtained for 0°C and 10°C, respectively (see Figure 5.25 a) and b)).

ΔC_{DCH} at 0.5C/10°C reaches the highest value among the 0.5C tests due to the lithium plating behaviour under this test condition. The relaxation measurement revealed that there is already a starting tendency for lithium plating at BOT. While lithium plating of high intensity occurs directly in some cells, other cells of the same group age much more slowly with lithium plating of lower intensity or in the linear section. The coexistence of these fundamentally different ageing rates leads to the pronounced variation behaviour at test condition 0.5C/10°C.

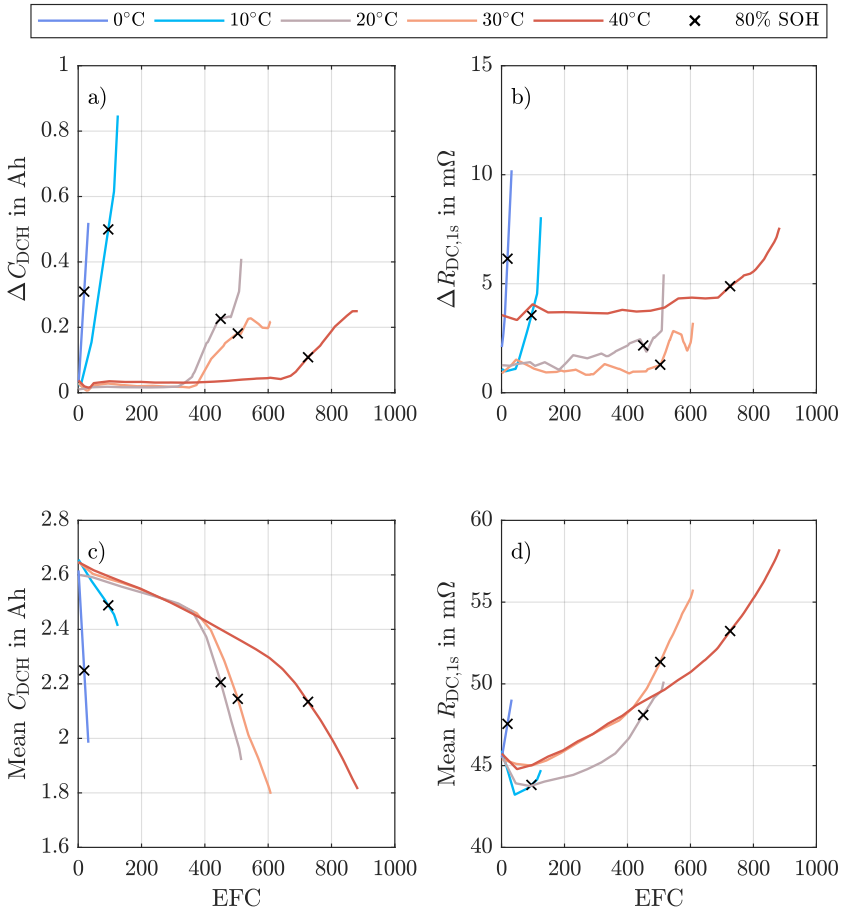

Figure 5.25: Variation behaviour of all cell groups operated at 0.5C. The variations regarding capacity and internal resistance are shown in a) and b); the corresponding average values of all 8 cells in c) and d). The point at which the worst cell in each group reaches 80% SOH is marked with an x.

Due to the immediate proximity to the plating boundary ($\varphi_{\text{anode}} \leq 0\ V$), it is assumed that small production-related variations in cell parameters and small thermal variations inside the temperature chamber can determine whether cells initially age in the linear or already in the non-linear section. The temperature distribution of the cells without load in the chamber shows a maximum difference of approximately 0.5°C.

ΔC_{DCH} at 0.5C/0°C is also high compared to the other test conditions at 0.5C, but since the same ageing mechanisms are active in all cells from BOT (with strong lithium plating), there are no such large differences in the ageing rate within the 8 cells compared to 0.5C/10°C. The capacity variation ΔC_{DCH} at 0.5C/0°C is mainly caused by different lithium plating intensities, but the difference in ageing rates here is smaller than that of fundamentally different ageing mechanisms. However, this supposed advantage over 0.5C/10°C with regard to ΔC_{DCH} is relativised by a significantly shorter lifetime.

$\Delta R_{\text{DC,1s}}$ behaves very similarly to ΔC_{DCH} with a sudden increase after few cycles. Although $\Delta R_{\text{DC,1s}}$ at 0.5C/0°C has a higher absolute value at 80% SOH than at 0.5C/10°C, it can be seen from the graph that the variation at 0.5C/0°C is higher from the beginning and thus the two test conditions can be evaluated similarly. For 0.5C/0°C and 0.5C/10°C values at 80% SOH of 6.1 mΩ (+4.0 mΩ) and 3.6 mΩ (+2.5 mΩ) result respectively.

Results from 0.5C/20°C, 30°C, 40°C

The transition from the linear to the non-linear section of the ageing curve is clearly visible in a sudden increase of ΔC_{DCH} at all three test conditions (0.5C/20°C, 30°C, 40°C). Since the lithium plating intensities of the 8 cells in each group are not identical, ΔC_{DCH} continues to increase. In the linear ageing section, the curves of ΔC_{DCH} run almost horizontally, which indicates that the already existing capacity variation hardly changes (see Figure 5.25 a)). The explanation for the stagnation of ΔC_{DCH} in the three test conditions can be found in very similar ageing rates within the linear section. The slight differences in the ageing rates among the 8 cells cannot lead to a significantly larger ΔC_{DCH} within a few hundred EFC.

The steep increase of ΔC_{DCH} is not due to lithium plating per se, but to the different entry time of the respective cell into the non-linear section. If all cell parameters as well as the ageing rates of the 8 cells are identical, they would enter simultaneously into the plating section, whereupon the ageing rate of all cells would increase strongly, but ΔC_{DCH} would not change. Under the three test conditions, however, the different onset times of lithium plating

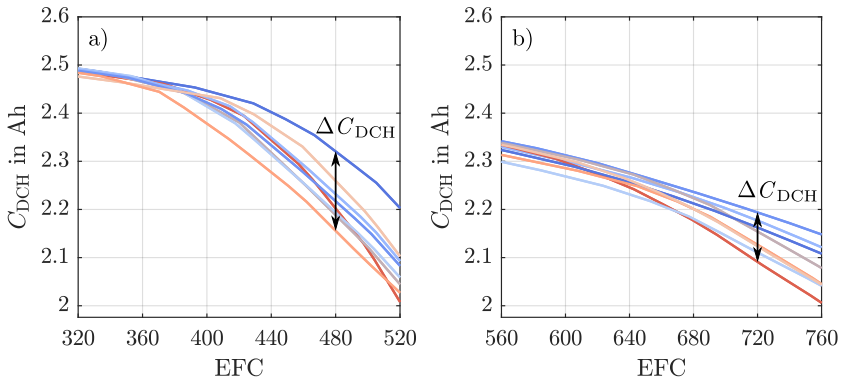

Figure 5.26: a) begin of non-linear ageing section for test condition 0.5C/30°C, b) for 0.5C/40°C. Due to the lower slope in b), the different onset times of lithium plating result in a significantly lower ΔC_{DCH} after the same number of EFC compared to a) (e.g. 160 EFC).

within the cell groups obviously lead to a sudden increase in ΔC_{DCH}. This behaviour was also observed in [73]. Whether or not the point at which the cells enter the non-linear section is linked to the initial parameters of the cells will be discussed in a separate section.

ΔC_{DCH} at 80% SOH decreases with increasing T_{amb} due to the ageing behaviour of the cells (see chapter 5.4.1). Since the onset of lithium plating is shifted to higher EFC values at higher T_{amb}, these cells have undergone significantly less cycles with lithium plating. Therefore a lower ΔC_{DCH} results. A higher T_{amb} results in a further advantage. Lithium plating at lower SOH results in a slower ageing rate in the non-linear section (compare with Table 5.1). Thus with slower ageing rates, the different entry times of lithium plating among the 8 cells have a less pronounced effect on ΔC_{DCH}. This circumstance is illustrated in Figure 5.26.

A higher value than T_{amb}= 40°C was not tested due to the recommended data sheet limits. However, it is assumed that the positive effect of delaying the onset of lithium plating and lowering the ageing rate of the non-linear section by a higher T_{amb} is outweighed by too rapid ageing in the linear ageing section at a specific temperature.

The variation behaviour of the capacity is only reflected to a limited extent in the variation behaviour of the internal resistance. In contrast to the ca-

pacity variation ΔC_{DCH}, the internal resistance variation $\Delta R_{\mathrm{DC,1s}}$ does not develop abruptly and only reaches slightly higher values towards the EOT. From Figure 5.25 c) and d) it can be seen that the previously determined correlation between C_{DCH} and $R_{\mathrm{DC,1s}}$ is given, but $\Delta R_{\mathrm{DC,1s}}$ seems to be decoupled from ΔC_{DCH}.

Despite a similar mean value of $R_{\mathrm{DC,1s}}$ at BOT at 0.5C/40°C compared to other operating conditions, there is a relatively high $\Delta R_{\mathrm{DC,1s}}$ from the beginning in Figure 5.25 b) and d). A high initial $\Delta R_{\mathrm{DC,1s}}$ does not necessarily lead to a stronger development of the parameter variation. The absolute increase of $\Delta R_{\mathrm{DC,1s}}$ at 0.5C/40°C during the ageing process is comparable to those of 0.5C/20°C and 0.5C/30°C.

When the SOH of the worst cell reaches 80%, ΔC_{DCH} at 0.5C/20°C and 0.5C/30°C results in 0.23 Ah (+0.22 Ah) and 0.18 Ah (+0.15 Ah), respectively. The minimum ΔC_{DCH} can be determined at 0.5C/40°C with 0.11 Ah (+0.07 Ah). For $\Delta R_{\mathrm{DC,1s}}$ values of 2.17 mΩ (+0.91 mΩ), 1.3mΩ (+0.42 mΩ) and 4.88mΩ (+1.32 mΩ) are determined respectively.

Results from 1.0C/0°C, 10°C

Just as for 0.5C/0°C, there is a rapid development of ΔC_{DCH} at 1.0C/0°C, 10°C (see Figure 5.27). When the worst cell reaches an SOH of 80%, ΔC_{DCH} results in 0.18 Ah (+0.16 Ah) at 1.0C/0°C and 0.13 Ah (+0.10 Ah) at 1.0C/10°C. These relatively low values are again the result of uniform ageing mechanisms. With the relaxation measurement and the cyclic ageing data, the direct onset of high-intensive lithium plating at BOT could be identified for these test conditions. Thus, there are only identical ageing mechanisms that can not cause large differences in ageing speed between the cells. Although the variation is at an even lower level than for 0.5C/20°C, 30°C no advantage can be gained due to the extremely short lifetime.

$\Delta R_{\mathrm{DC,1s}}$ has hardly changed within the short lifetime. Only at 1.0C/0°C a slight increase can be determined. For 1.0C/0°C and 1.0C/10°C $\Delta R_{\mathrm{DC,1s}}$ is 3.7 mΩ (+2 mΩ) and 1.8 mΩ (-0.1 mΩ).

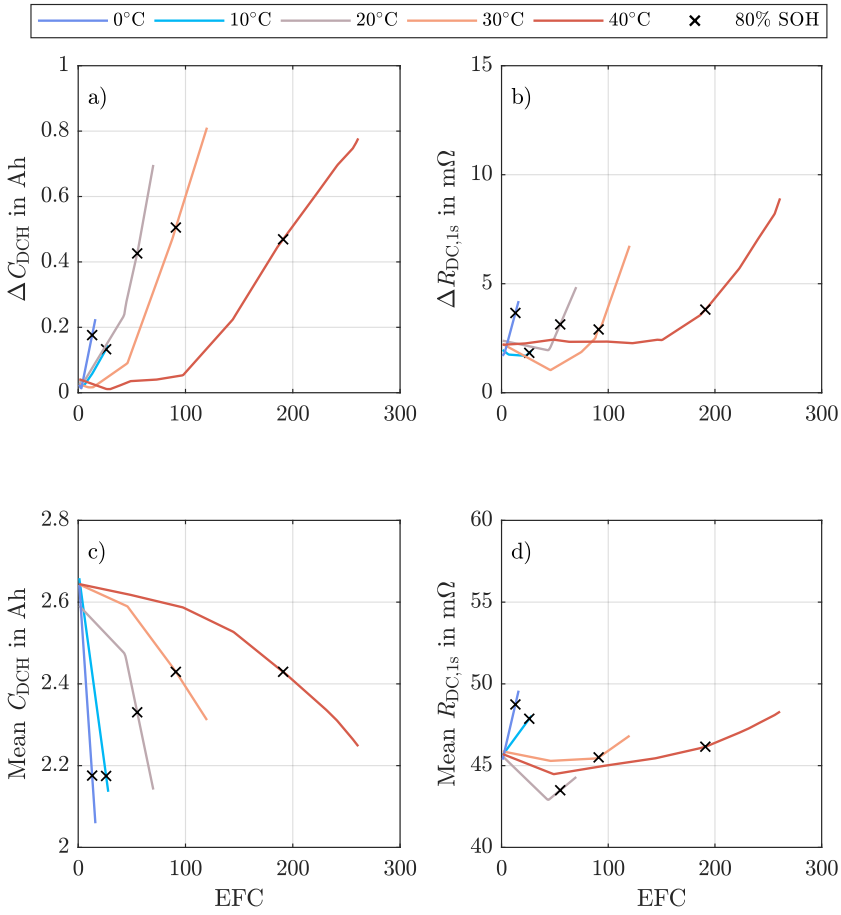

Figure 5.27: Variation behaviour of all cells aged with 1.0C. The variation regarding capacity and internal resistance are shown in a) and b); the corresponding average values of the 8 cells in each group in c) and d). The point at which the worst cell in each group reaches 80% SOH is marked with an x.

Results from 1.0C/20°C, 30°C, 40°C

The ageing behaviour and thus also the variation behaviour under these three test conditions is very similar to 0.5C/10°C (see Figure 5.27). At BOT some cells switch to the fast non-linear ageing section after a few cycles already, while other cells still remain in the slower linear ageing section. This again results in a large ΔC_{DCH} due to a large difference in the ageing rates. By increasing T_{amb} from 20°C to 40°C, the linear ageing section can only be slightly extended. However, this hardly influences ΔC_{DCH} at 80% SOH, since during the majority of completed EFC lithium plating happened.

For $\Delta R_{\mathrm{DC,1s}}$ the behaviour is similar to the test conditions 0.5C/20°C, 30°C, 40°C. Down to 80% SOH of the worst cell, there are only minor changes in $\Delta R_{\mathrm{DC,1s}}$, which, moreover, develop considerably later than ΔC_{DCH}. At 1.0C/20°C and 1.0C/30°C, there is even a reduction of $\Delta R_{\mathrm{DC,1s}}$ despite a strongly increasing ΔC_{DCH}.

Again, it seems that $\Delta R_{\mathrm{DC,1s}}$ is largely decoupled from ΔC_{DCH}, or significantly delayed in time, so that further unknown reasons for $\Delta R_{\mathrm{DC,1s}}$ can be assumed (see Figure 5.27 b)). Ageing mechanisms that are decoupled from the capacity, such as the delamination of active materials from the current collectors are possible here. However, the data collected cannot clarify this question which could be investigated in more detail in future works.

When the worst cell reaches a SOH of 80%, ΔC_{DCH} for 1.0C/20°C, 30°C, 40°C results in 0.43 Ah (+0.40 Ah), 0.51 Ah (+0.48 Ah) and 0.47 Ah (+0.43 Ah), respectively. For $\Delta R_{\mathrm{DC,1s}}$ at 1.0C/20°C, 30°C, 40°C respective values of 3.1 mΩ (+0.7 mΩ), 2.9 mΩ (+0.7 mΩ) and 3.8 mΩ (+1.6 mΩ) are obtained.

Summary of Paramter Variation Based on COV

Figure 5.28 finally summarises all results regarding capacity variation and internal resistance variation and compares them for different SOH values. Again, the SOH values refer to the current state of the worst cell in each test group with 8 cells. For comparison with BOT and to include all 8 cells in the calculation, the COV $\kappa_{C_{\mathrm{DCH}}}$ and $\kappa_{R_{\mathrm{DC,1s}}}$ are used instead of ΔC_{DCH} and $\Delta R_{\mathrm{DC,1s}}$ for this summary. The COV is calculated as introduced in chapter 4.4.4.

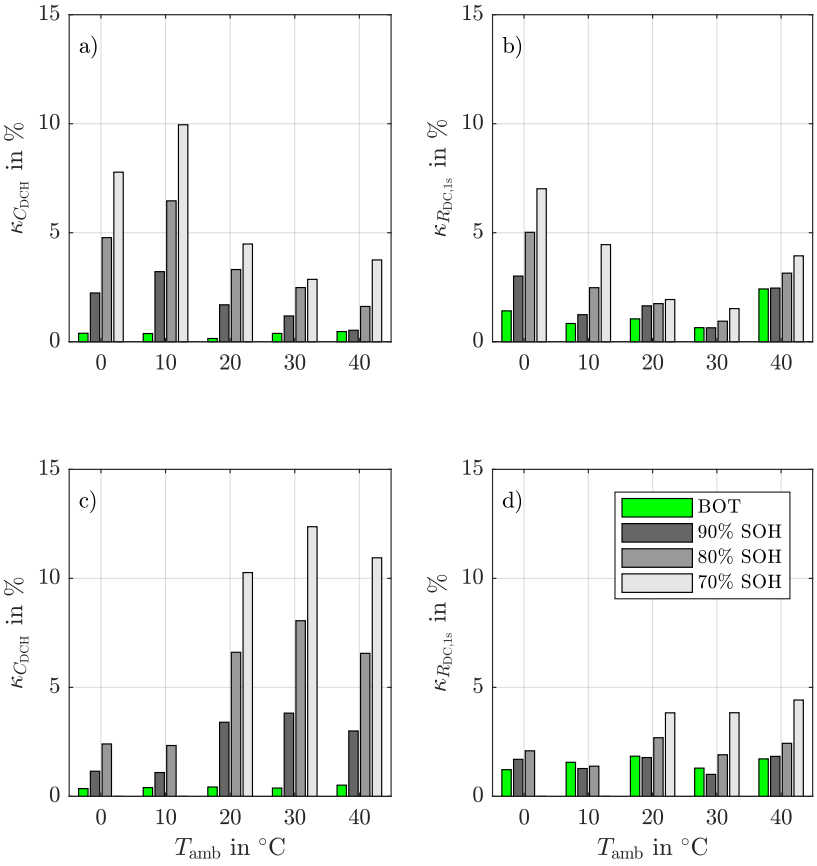

Figure 5.28: Summary of variation behaviour based on the COV. In a) and b) capacity and internal resistance variation of all 0.5C tests are shown. In c) and d) capacity and internal resistance variation of all 1.0C tests are shown. For the test conditions 1.0C/0°C, 10°C the comparison values only exist up to 80% SOH.

It can be clearly seen that the capacity variation $\kappa_{C_{\mathrm{DCH}}}$ increases under all test conditions compared to BOT. For a comprehensive interpretation of the results, however, it is important to consider the achieved lifetime as well. Although $\kappa_{C_{\mathrm{DCH}}}$ can be similar for the same SOH, the lifetime achieved can differ significantly. For example, at 0.5C/30°C and 0.5C/40°C at 70% SOH $\kappa_{C_{\mathrm{DCH}}}$ equals to 2.9% and 3.7% respectively. The values are similar, but the lifetimes with 531 EFC and 835 EFC differ significantly. Overall, the test conditions 0.5C/20°C, 30°C, 40°C stand out as the best compromise in terms of capacity variation and lifetime. Test conditions 0.5C/10°C and 1.0C/20°C, 30°C, 40°C lead to the strongest capacity variations due to the reasons mentioned above.

As confirmed in the literature, $\kappa_{R_{\mathrm{DC,1s}}}$ at BOT is significantly greater than $\kappa_{C_{\mathrm{DCH}}}$. At the same time, the measurements show that $\kappa_{R_{\mathrm{DC,1s}}}$ usually develops much more slowly and even decreases slightly for a short time under some test conditions. Thus, in this overview it becomes clear once again that the variation of C_{DCH} and $R_{\mathrm{DC,1s}}$ is not or only slightly coupled. Further ageing mechanisms may therefore be responsible for the development of the internal resistance variation.

Influence of Internal Resistance on Capacity Variation

In the last section, it was shown that the cells not only have a capacity variation but also a low internal resistance variation. All capacity variation values presented so far have been calculated on the basis of C_{DCH}. In order to check how much the internal resistances of the cells influence the determined variation, $\Delta C_{\mathrm{DCH,CV}}$ is now evaluated and compared with ΔC_{DCH} in Table 5.2. Again the common reference value is the EFC value at which the worst cell reaches 80% SOH.

Observing Table 5.2, it can be seen that $\Delta C_{\mathrm{DCH,CV}}$ is slightly lower than ΔC_{DCH} in most test conditions. The values prove that in most cases the internal resistance slightly increases the underlying capacity variation. However, the significantly greater part of ΔC_{DCH} results from the capacity differences of the cells themselves. In practice, continuous operation of cells with additional CV-discharge is not recommended, as the high DOD leads to mechanical stress in the materials and thus to faster ageing.

Test condition	ΔC_{DCH} in Ah	$\Delta C_{\mathrm{DCH,CV}}$ in Ah
0.5C/0°C	0.31	0.26
0.5C/10°C	0.50	0.49
0.5C/20°C	0.23	0.20
0.5C/30°C	0.18	0.16
0.5C/40°C	0.11	0.10
1.0C/0°C	0.17	0.19
1.0C/10°C	0.13	0.15
1.0C/20°C	0.43	0.38
1.0C/30°C	0.50	0.47
1.0C/40°C	0.47	0.45

Table 5.2: Capacity variation determined with CC and CC-CV discharge to decouple the internal resistance from capacity. The values are evaluated at 2.08 Ah (80% SOH).

Influence of the Initial Cell Parameters on Parameter Variation

To investigate the influence of the initial cell parameters on the ageing of the cells, C_{DCH}, $R_{\mathrm{DC,1s}}$, U_{cell} at delivery and m_{cell} are used.

Neither the initial C_{DCH}, nor the initial $R_{\mathrm{DC,1s}}$ and also not a combination of both values provide any information about the possible ageing progress of the cells. Also on the basis of U_{cell} at delivery and m_{cell}, no statements can be made about the possible ageing progress. The results in this regard confirm the literature findings [57,103]. No meaningful correlation between the initial parameters and the lifetime can be found. It is assumed that the lifetime is determined by production-related circumstances, such as fluctuating and non-uniform AML or minor impurities in the active material, which affect local lithium plating. However, this production-related tendency towards lithium plating is not visible in the initial cell parameters.

Summary of Lifetime Variation based on COV

Since the lifetime variation κ_{EFC} is directly dependent on the capacity variation, the causes are the same and will not be discussed again. The lifetime variation can be interesting for manufacturers of battery-operated devices in order to better estimate the warranty period under certain test conditions.

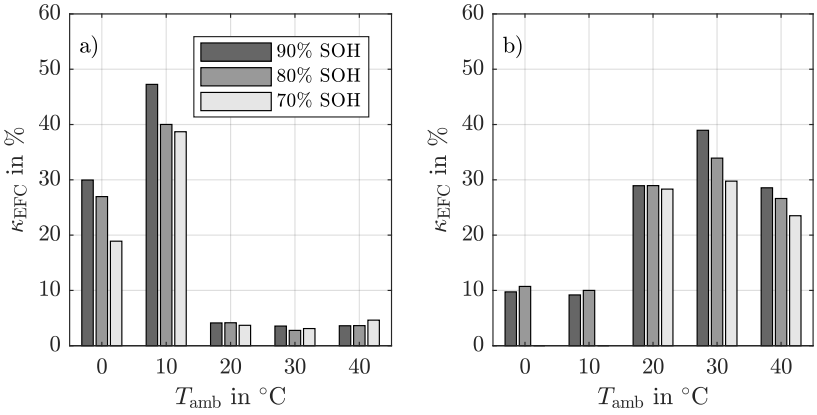

Figure 5.29: Lifetime variation based on COV. Plot a) contains all 0.5C tests, plot b) all 1.0C tests. For 1.0C/0°C, 10°C the values exist only up to 80% SOH.

Figure 5.29 clearly shows that the lifetime variation κ_{EFC} in the range from 20°C to 40°C at 0.5C is by far the lowest. Furthermore, it can be seen from the overview that κ_{EFC} of these test conditions remains similar over the entire ageing process. This means that the lifetime variation and the average lifetime develop in a similar ratio. For some test conditions, the lifetime variation drops further with decreasing SOH (e.g. 0.5C/10°C). This is due to the fact that the lifetime variation increases proportionally slower than the average lifetime itself. Similar to the capacity variation, the remaining test conditions perform significantly worse. Especially at 0.5C/10°C, as well as 1.0C/20°C, 30°C, 40°C, there is a very high κ_{EFC} due to the direct proximity to the lithium plating boundary.

5.4.2.2 Results from Stored Cells

During calendar ageing at approximately 20°C and 30% SOC, there is also a slight change in the parameter variation of the 137 cells (see Figure 5.30). The parameter variation of C_{DCH}, $C_{\mathrm{DCH,CV}}$ and $R_{\mathrm{DC,1s}}$ decreased slightly. The observed parameters of the cells have thus converged during the 2-year long storage period.

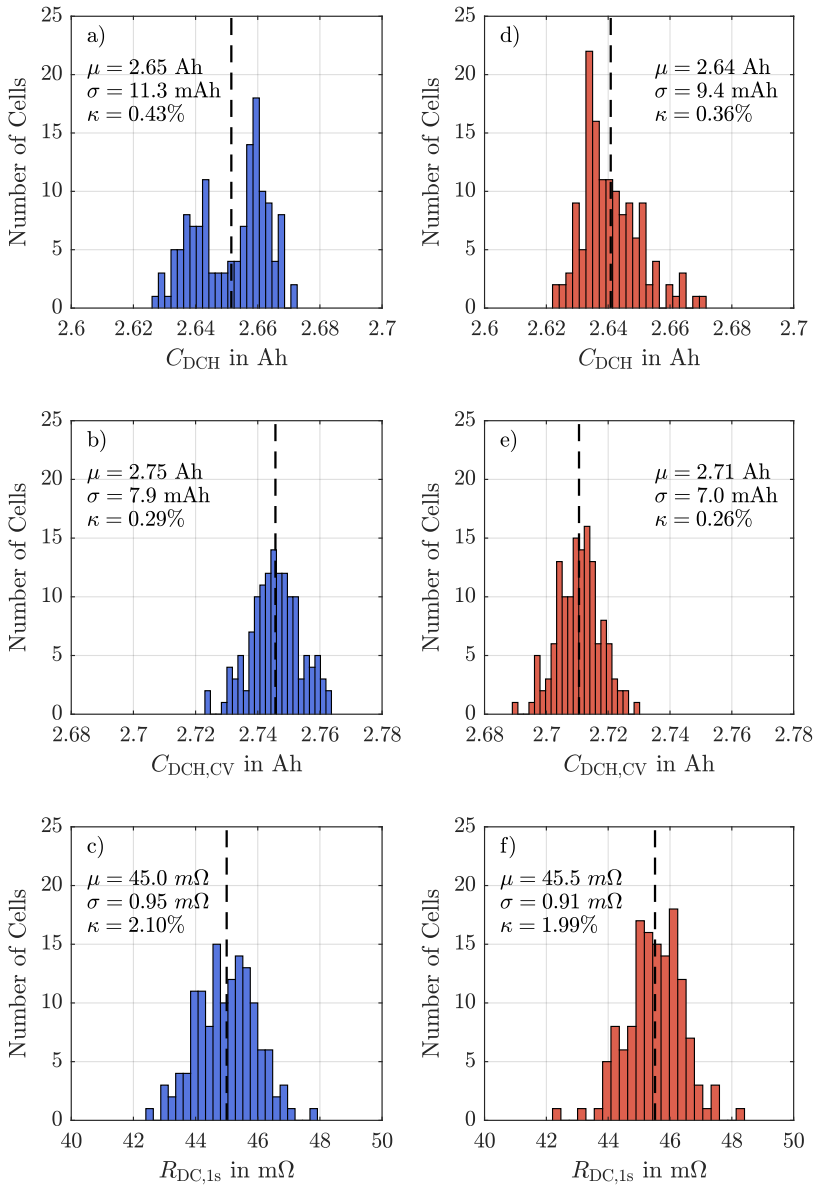

Figure 5.30: Results for the parameter variation during calendar ageing for 137 cells. Plots a) to c) show the parameters C_{DCH}, $C_{\mathrm{DCH,CV}}$ and $R_{\mathrm{DC,1s}}$ in November 2019. Plots d) to f) show the same parameters in November 2021.

The fact that the parameter variation has decreased can be explained by the calendar ageing behaviour of LICs. The capacity loss and the internal resistance increase, due to SEI growth follow a square root function of time [78,83,124]. Due to the square root function the slope of the respective ageing curve is steep at the beginning of calendar ageing and becomes flatter with time. This means that cells in the steeper part age faster for a certain time than cells that are already in the flatter section. Thus, the values for C_{DCH}, $C_{\mathrm{DCH,CV}}$ and $R_{\mathrm{DC,1s}}$ slowly converge due to the different ageing rates, which, however, decrease with time.

The change in the distribution of C_{DCH} is particularly apparent. Due to calendar ageing, the distribution has developed from a bimodal normal distribution to a right-skewed normal distribution (see Figure 5.30 a) and d)). The distribution of $C_{\mathrm{DCH,CV}}$ and $R_{\mathrm{DC,1s}}$, however, has not changed significantly (see Figure 5.30 b), c), e) and f)).

A reduction of the capacity variation during calendar ageing of NMC cells was also observed in [125]. In this study the cells were stored at 3.6 V and 50°C.

5.4.2.3 Summary

Based on the measurement data, it was possible to make statements about the parameter variation of aged single cells. For better clarity, they are summarised in bullet points.

Cyclic Ageing

- As long as all cells of a group age within the linear ageing section, ΔC_{DCH}, $\Delta R_{\mathrm{DC,1s}}$ and ΔEFC hardly change. The small differences in the ageing rates between the 8 cells cannot lead to a significantly higher variation within a few 100 EFC (see Figure 5.25 e.g. 0.5C/20°C, 30°C, 40°C).
- The change from the linear to the non-linear ageing section causes an increase in the ageing rates and massively promotes an increase in ΔC_{DCH} and ΔEFC, due to the different entry times of the cells. Which cell reaches this point first seems to be random and does not depend on the initial cell parameters in the test carried out (see Figure 5.25 e.g. 0.5C/20°C, 30°C, 40°C).
- Test conditions close to the lithium plating boundary at BOT are particularly prone to the development of a strong parameter variation. Here, small intrinsic or extrinsic factors can cause some cells to plate directly from the beginning, while other cells plate only weakly or even still age in the linear section without lithium plating. This coexistence of very different ageing rates, which is prevalent from BOT, leads to a large ΔC_{DCH} and thus also large ΔEFC (see Figure 5.25 0.5C/10°C and Figure 5.27 1.0C/20°C, 30°C, 40°C).
- If all cells of a test condition age mainly with lithium plating at BOT, a parameter variation develops mainly due to different lithium plating intensities. However, the difference in ageing rates is always smaller than that caused by changing from linear to non-linear ageing. Therefore, the parameter variation of the respective test conditions is smaller than for cells operated near the plating boundary. However, due to the low lifetime of these test conditions, no advantage can be gained (see Figure 5.25 0.5C/0°C and Figure 5.27 1.0C/0°C, 10°C).
- The lower the SOH of the cells at the onset of lithium plating, the lower the ageing rate in the non-linear section. Thus, for the respective test conditions, the different onset times of lithium plating in the 8 cells has a less pronounced effect on ΔC_{DCH} than for test conditions where

lithium plating starts at higher SOH values (see Figure 5.26).

- $\Delta R_{\mathrm{DC,1s}}$ does not develop simultaneously with ΔC_{DCH}. It is assumed that further capacity-independent ageing effects influence $\Delta R_{\mathrm{DC,1s}}$ (e.g. delamination of the active material from the current collector) (see Figure 5.25 and 5.27).
- $R_{\mathrm{DC,1s}}$ of the cells hardly influences ΔC_{DCH}. Most of ΔC_{DCH} results from the pure capacity differences of the cells themselves (see Table 5.2).
- Overall, the test conditions 0.5C/20°C, 30°C, 40°C stand out as the best compromise in terms of capacity variation and lifetime. Test conditions 0.5C/10°C and 1.0C/20°C, 30°C, 40°C lead to the strongest capacity variations (see Figure 5.28).

Calendar Ageing

- After 2 years of storage, the variation of the parameters C_{DCH}, $C_{\mathrm{DCH,CV}}$ and $R_{\mathrm{DC,1s}}$ decreased slightly (see Figure 5.30).
- The distribution of C_{DCH} has changed from a bimodal normal distribution to a right skewed normal distribution (see Figure 5.30).
- The distribution of $C_{\mathrm{DCH,CV}}$ and $R_{\mathrm{DC,1s}}$ has hardly changed (see Figure 5.30).

Chapter 6

Parameter Variation of Aged Lithium-Ion Modules

After examining the parameter variation of new cells and aged single cells, this chapter examines the parameter variation of cells in aged modules and serves as the final part of this thesis. The knowledge gained in the previous chapter serves as valuable basis for the interpretation of the results in this chapter.

Due to the series and parallel connection of cells in battery modules, extrinsic factors due to module assembly and module design now play a greater role in ageing in addition to the production-related intrinsic factors. These include, for example, electrical interactions between the cells in parallel connection or thermal interactions between the cells or with the immediate environment. In [58], various influences are summarised, which can lead to parameter variation of cells in modules (see Figure 6.1). They have an enduring effect on the development of the individual cell parameters and ultimately lead to an uneven ageing, to be examined in this chapter.

The modules aged in this chapter are self-designed and self-built. This has several advantages. On the one hand, inhomogeneous starting conditions can be excluded since the initial parameters of the cells are known precisely. On the other hand, the complex analysis of module ageing can be simplified by choosing a module architecture being as simple as possible.

6.1 Insights from Literature

This section deals with the results of parameter variation obtained from module ageing experiments. Again, less can be found about modules than new LICs. In particular, the focus is often on the impact of parallel connections of cells without series connections.

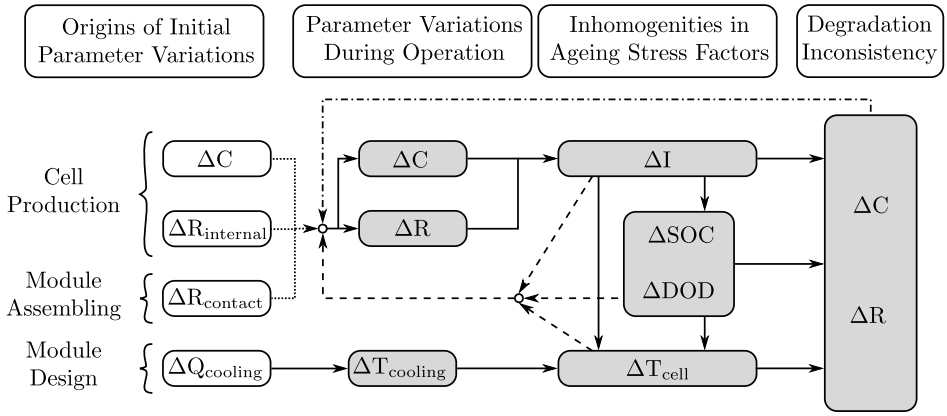

Figure 6.1: Overview of various influences that can lead to parameter variation of the cells in modules. Based on [58].

- Gogona et al. [126] investigated the effects of mismatched cells in parallel connection on the lifetime. For this purpose, two cells were connected in parallel and operated in an ageing experiment at a high C-Rate in the range between 3.65 V and 2.5 V. Special attention was paid to the internal resistance. The investigations showed that a difference in the internal resistance of the cells of 20% leads to a reduction of the lifetime of 40%. The investigated cells consist of a LFP cathode and a graphite anode and have a nominal capacity of 2.2 Ah.
- The study by Schuster et al. [93] was already mentioned in the chapter about brand-new cells. The variation of 1908 aged cells from two vehicles was determined. Since no inhomogeneities were found, neither in temperature nor in voltage, it is assumed that the parameter variation of the cells is only of intrinsic origin. Thus, the weak cells were randomly distributed in the modules. No thermal peculiarities are reported.
- The study by Campestrini et al. [95] deals with the ageing of self-built, passively balanced modules (8s14p) compared to the ageing of single cells. Capacity-based matching of the cells could significantly reduce the initial spread of the modules at BOT. However, in the ageing experiment the parameter variation increased measurably. In order to obtain more precise information about the ageing process, the modules were disassembled and analysed after EOT.

- Pastor-Fernandez et al. [127] deal with the ageing and interactions of cells connected in parallel. To perform the study, 4 cells with different SOH were selectively connected and aged at 25°C ambient temperature for 500 cycles. It was found that the parameters of the 4 cells converge during ageing. The parameter variation of the 4 parallel cells was therefore higher at BOT than at EOT. The nominal capacity of the cells used was 3 Ah.
- In an own study [128] the variation of 20 differently aged E-bike batteries with a 10s5p setup was investigated (approx. 40 to 1480 cycles). For this purpose, all batteries were disassembled and the 50 cells of each module were measured. Capacity and internal resistance were determined. A correlation was found between the number of cycles of the batteries and the variation of the parameters. In addition, it was found that the weaker cells were randomly distributed in the battery and could not be assigned to any hotspots. The examined cells consist of an NMC cathode and a graphite anode and had a nominal capacity of 2.6 Ah.

Although the parameter variation of cells within modules has been investigated in some of the studies presented, the author is not aware of any work that focuses on the parameter variation of aged modules depending on the load and the number of cells connected in parallel. The planned measurements are therefore intended to make a contribution to an area, with little knowledge about this so far.

6.2 Objectives and Tasks

The aim of this chapter is to investigate the ageing and cell parameter variation behaviour of modules. Therefore, not only the load but also the number of cells connected in parallel is varied. Based on the measurements, the most favourable combination of parallel-connected cells and the selected load will be identified with regard to lifetime and parameter variation. Furthermore, the transferability of the results from single cell ageing to module ageing will be investigated. The following tasks are carried out for this purpose:

- Ageing of modules at different loads with different numbers of cells connected in parallel.
- Analyse the influence of the number of cells connected in parallel and load on cell parameter variation and lifetime.

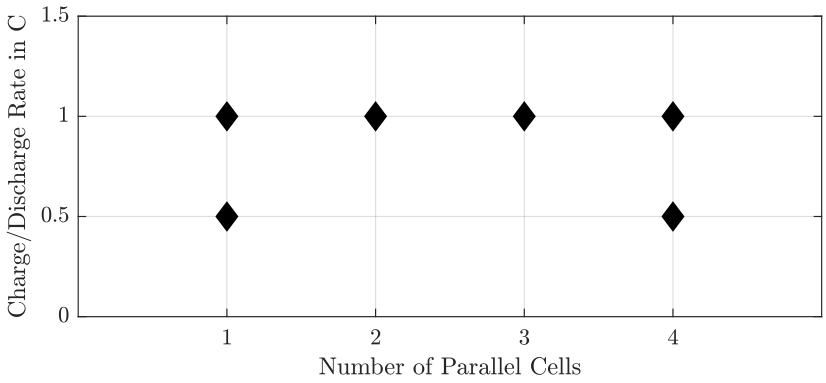

Figure 6.2: Test matrix of the performed cycle ageing module tests. Each module consists of six cells in series and a different number of cells connected in parallel.

- Analyse the influence of the module architecture on the results.
- Check comparability of single cell results with module ageing results.
- Interpretation of the results for real-world application.

6.3 Design of Study

In order to examine the ageing and the associated parameter variation behaviour of the modules, they are first aged under defined test conditions. Due to the time required and the limited measurement hardware available, all tests are carried out at one temperature. In the following, the cells connected parallel are referred to as Cell Level (CL) for p=1, 2, 3, 4.

6.3.1 Test Conditions

A total of 6 test conditions are selected. The charge/discharge rate and the number of cells connected in parallel are varied for each test condition. Each module consists of six cells in series. Since the single cell measurements at a charge/discharge rate of 1.0C showed a rapid ageing behaviour as well as a pronounced parameter variation behaviour, modules with 2 and 3 cells connected in parallel are additionally examined at 1.0C in order to study this test condition more closely. Figure 6.2 shows all planned test conditions.

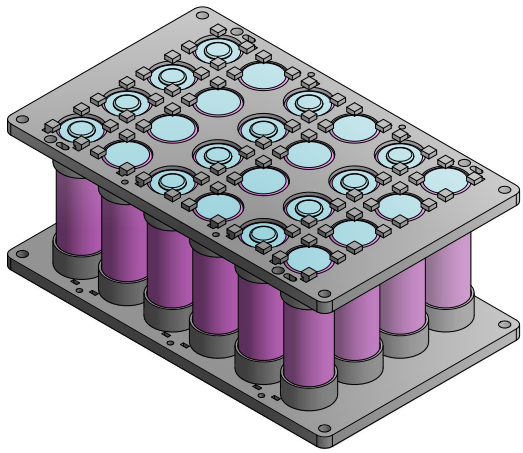

Figure 6.3: Construction view of the self-designed module. The example shows a 6s4p configuration without associated sheet metal connection.

Module Architecture

To simplify the interpretation of the test results, a simple 6x4 matrix is designed. Within this matrix, modules with up to 6 cells in series and 4 cells in parallel can be freely configured. All serially and parallel connected cells have a uniform spacing of 5 mm from cell surface to cell surface. The data sheet of the cells requires a safety-relevant minimum distance of 1 mm for use in modules. The module cages are made of Polylactic Acid (PLA) plastic with help of a 3D printer. Figure 6.3 shows the module in 6s4p configuration without cell connectors.

To protect the modules in the temperature chamber from air flow, they are completely surrounded by a plastic box. The only exception is an opening for cable routing.

A 0.2 mm thick nickel-plated steel sheet is used to connect the cells via spot welding with four welding points on each cell pole.

Battery Management System

For safety reasons and better utilisation of the modules, a passive balancing Battery Management System (BMS) system is used. The balancing resistor is connected to the cell as soon as a cell exceeds a voltage of 4.175 V. If the voltage drops, the balancing resistor is disconnected. When balancing is triggered, it remains active for 10 seconds, followed by a pause of 1 s. The

balancing current is set to approximately 100 mA.

Voltage/Current Range

To ensure comparability between the single cell and the module tests, the values for current and voltage range are not changed. The minimum and maximum voltage limit per cell/CL result in 2.75 V and 4.175 V respectively. This results in 16.5 V and 25.05 V as the lower and upper voltage limit for the module in a series connection of 6 cells.

Similarly, the currents are adjusted according to the number of cells connected in parallel. For example, in case of 2 parallel cells a current of 2.6 A ($= 2 \cdot 1.3$ A) is needed for 0.5C and a current of 5.2 A ($= 2 \cdot 2.6$ A) for 1.0C. Again, a simple cycle with CC discharge and subsequent CC-CV charge is used for ageing. The progress of a complete cycle is analogous to the single cell ageing and can be seen in Figure 5.4 in chapter 5.3.2.

Temperature

An ambient temperature of 20°C is chosen for the tests, which was also selected for the single cell test in chapter 5 and can thus provide comparative values. Lower temperatures (0°C and 10°C) are not investigated, since a sufficiently long lifetime of the modules is desired. Higher ambient temperatures (30°C and 40°C) can lead to premature shutdown of the test due to the maximum operating temperature of the cells (60°C) and are therefore not used.

6.3.2 Test Procedure

To carry out the investigations, the procedure shown in Figure 6.4 is run through once for all 6 modules. Before manufacturing, the cells stored at 3.6 V are tested again in an initial RPT to determine their status quo. The cells are then inserted into the module cages and welded, followed by the assembly of the BMS.

The module ageing progresses analogously to single cell ageing. After a 10-minute pause, the cycle begins with a CC discharge of the module until either the final discharge voltage of 16.5 V is reached or a cell/CL falls below a value of 2.75 V. After a further 10-minute pause, the CC-CV charging of the module begins. The transition to the CV phase in the charging process starts as soon as the module voltage reaches 25.05 V. The charging process is terminated as soon as the charging current falls below a C-Rate of 0.05C or a cell/CL exceeds 4.25 V.

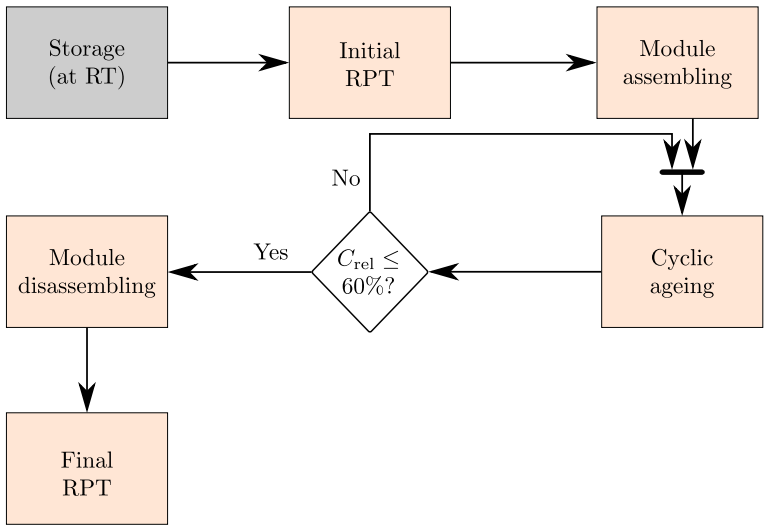

Figure 6.4: Module test procedure.

After each cycle, it is checked whether the module has reached 60% of its capacity in relation the first complete cycle ($C_{rel} \leq 60\%$). If the value is reached, the test is terminated and the module is disassembled. A final RPT then takes place, which determines the current state of the individual cells at EOT.

The RPT at BOT and EOT is carried out identically to the measurement of the new cells in chapter 4 and to the measurement of the aged single cells in chapter 5 in order to ensure comparability between the tests.

All measurements and cyclic ageing take place in IPP55 temperature chambers from Memmert. The RPT is carried out again at 25°C. Modules are aged at 20°C. A BaSyTec High Power System (HPS) is used to perform the cyclic ageing of the modules. To run the RPT of the single cells, BaSyTec CTS devices are used. Table 6.1 shows the specifications of the used BaSyTec HPS.

Device	**Variable**	**Accuracy**	**Range**
BaSyTec HPS	Voltage	±1 mV	[3 V, 60 V]
	Current	±20 mA	[-40 A, 20 A]

Table 6.1: Accuracy of the used BaSyTec HPS test system.

6.3.3 Measured Cell Parameters

During all measurements, various parameters are recorded and used for the later evaluation of the modules and the individual cells. These are summarised here in a brief overview and grouped thematically by module and cell.

Capacity (Module)

During each complete cycle, the module capacity is recorded by integrating the current flow over the entire duration of the discharge process. The value from each discharge cycle is set in relation to the first complete discharge of the module in order to quantify the ageing state (C_{rel}).

Internal Resistance (Module)

At the beginning of each discharge process (approximately 100% SOC), the applied discharge current is used as a current pulse and the resulting voltage is evaluated after 1 s. Just as with C_{rel}, the resistance value calculated is set in relation to the resistance value from the first discharge process (R_{rel}).

Cell Level Voltage (Module)

Since it is not possible to independently determine the capacity or the internal resistance of the individual cells during module ageing and thus also the parameter variation, the cell/CL voltages at EOD are recorded as an alternative. The voltage differences at EOD give an indirect insight into the variation of the parameters. The calculation of a comparable capacity variation/internal resistance variation is then carried out with the individual single cells by means of RPT after EOT.

Capacity (Cell)

To evaluate the single cell capacity, an RPT is performed before BOT and after EOT, where C_{DCH} and $C_{\mathrm{DCH,CV}}$ are recorded, which include the usable capacity during the CC discharge and an additional CV discharge.

Internal Resistance (Cell)

In the RPT $R_{\mathrm{DC,1s}}$ is recorded again at 100% SOC.

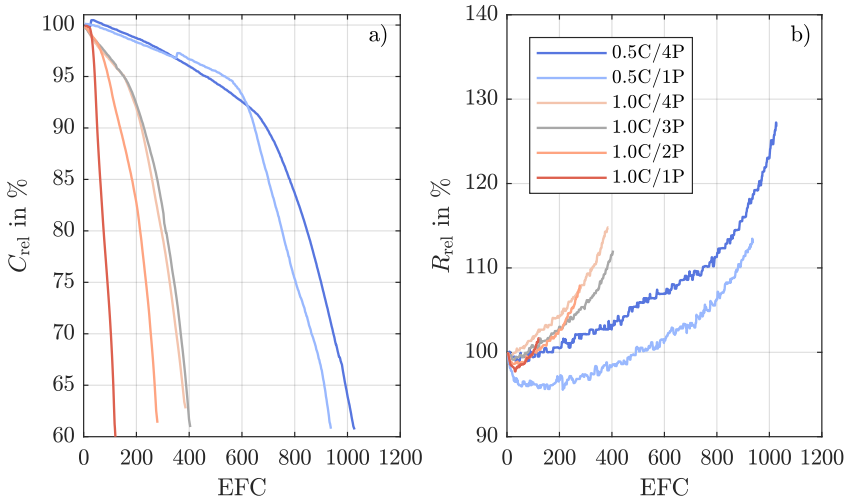

Figure 6.5: Result of cyclic module ageing. Plot a) shows the development of C_{rel} and plot b) the development of R_{rel} of all 6 modules. The colouring of the curves from red to blue is based on the achieved lifetime.

6.4 Results and Discussion

In the following sections, the results of module ageing and the resulting parameter variation are presented.

6.4.1 Results from Module Ageing Data

The results of cyclic ageing for modules operated with 0.5C as well as with 1.0C are shown in Figure 6.5. For some modules, the targeted 60% C_{rel} is not exactly reached. However, this is not a disadvantage for the following evaluation.

Results from 0.5C Modules

Both modules tested at 0.5C/1P and 0.5C/4P are characterised by a higher lifetime in the range of 1000 EFC due to the lower load compared to the modules operated with 1.0C. Both modules show a pronounced linear ageing section, which changes to a non-linear section after ca. 560 EFC (0.5C/1P) and ca. 650 EFC (0.5C/4P) respectively.

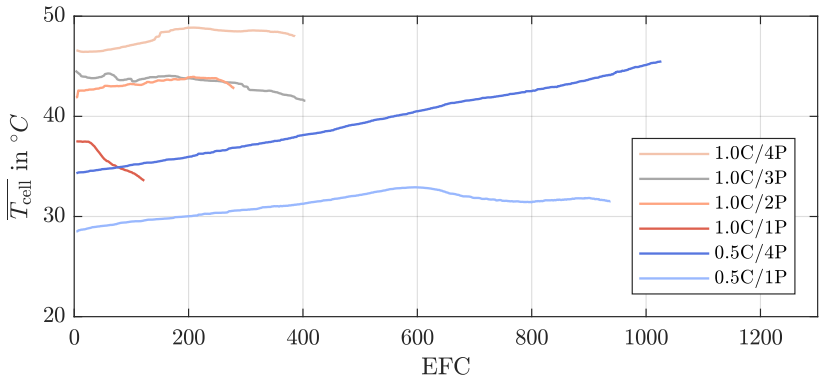

Figure 6.6: Mean cell surface temperature of the modules at EOD. The values shown are calculated from the arithmetic mean of three temperature sensors, each attached to the centre of three different cells on the outside.

Due to the slopes of the linear and non-linear sections, it can be assumed analogously to chapter 5.4.1.2 that the cells of module 0.5C/4P are exposed to a higher temperature than the cells of module 0.5C/1P. It becomes clear that in addition to the specified T_{amb} of 20°C, the actual cell temperature T_{cell} is of great importance for the evaluation of the ageing progress and the achieved lifetime.

To record the cell temperature T_{cell} during ageing, three different cells on the outside of each module are equipped with a PT100 temperature sensor. The arithmetic mean of the three temperature sensors ($\overline{T_{\text{cell}}}$) at EOD is shown in Figure 6.6 over the progress of the EFC. Here it can be seen that the cells of module 0.5C/4P are approximately 4°C warmer than those of module 0.5C/1P already after the first discharge cycle. This seems plausible due to the proximity of many cells and explains the different ageing rates in the linear and non-linear sections. Since temperatures of module 0.5C/4P are measured on the outside, an even higher temperature can be assumed for the cells inside.

The value R_{rel} of module 0.5C/1P (see Figure 6.5 b)) first decreases significantly to 95.5% and reaches its initial value again at approximately 490 EFC. At EOT, a final value of approximately 113% is reached. With module 0.5C/4P there is a significantly smaller decrease of R_{rel} to 99%, which returns to its initial value after approximately 125 EFC. A final value of approximately 127% is reached at EOT. Based on the findings of the single

cell tests, both the lower decrease of R_{rel} and the significantly higher end value of R_{rel} at module 0.5C/4P can be attributed to a higher T_{cell} during ageing. The warmer the cells were in the single cell test during ageing, the lower was the decrease in R_{rel} and the higher was the final value of R_{rel}.

Again, according to the literature, the decrease of R_{rel} in the modules can be attributed to an initial reduction of the anode impedance of the individual cells in the module. However, due to numerous interactions between the cells, the interpretation of the results at module level is significantly more complex than with single cells. Since the individual cells in the module do not age in the same way, the various ageing effects of the individual cells overlap and the visible progress of R_{rel} or C_{rel} reflects a combination of many different ageing states of all assembled cells.

Despite the same ambient temperature, the lifetimes of the modules 0.5C/1P and 0.5C/4P show that module and single cell tests are poorly comparable. In the single cell test at 0.5C/20°C, the maximum lifetime up to 60% C_{rel} was only 583 EFC, which deviates significantly from the lifetime of the modules. This fact is also a result of different cell temperatures between the single cell and module test. While the cells in the single cell test only heated up slightly above the set T_{amb} of 20°C, $\overline{T_{\mathrm{cell}}}$ in the module is clearly above T_{amb} (see Figure 6.6). In order to be able to compare module and single cell tests, a single cell test with similar temperature conditions must be used.

However, a comprehensive comparison between the single cell tests and the module tests operated with 0.5C shows large differences in the achieved lifetime and the general ageing process. This unexpected behaviour can not be clarified with help of the recorded data and possibly indicates inconsistent operating conditions between the module and single cell test.

A difference possibly results from air convection, which can cause a temperature gradient within the cells. In the used temperature chamber, a fan causes a low airflow. The module housing protects the cells from this air flow during the module test. This may result in a longer lifetime due to more homogeneous operating conditions inside the module. In contrast the cells in the single cell test were directly exposed to the airflow. According to the literature, an inhomogeneous temperature distribution within a cell can lead to accelerated ageing. This was investigated in [129]. In order to improve the comparability of tests with homogeneous temperature conditions with tests of inhomogeneous temperature conditions, a so-called "equivalent ageing temperature" was introduced here.

Results from 1.0C Modules

Four modules are aged at a C-Rate of 1.0C. Lifetimes of about 120 EFC to 405 EFC are achieved. A dependence of the lifetime on the number of cells connected in parallel can be detected (see Figure 6.5). The lowest lifetime of 120 EFC is achieved by module 1.0C/1P. By adding another parallel cell (1.0C/2P), the lifetime more than doubles, resulting in 280 EFC. Another parallel cell (1.0C/3P) increases the lifetime by approximately 120 EFC. However, this trend cannot be continued with module 1.0C/4P. The lifetime and ageing progress is very similar to this of module 1.0C/3P. Whether or not the reason for the increased lifetime depending on the number of parallel connected cells is temperature-related or based on other effects will be examined later, taking into account the module architecture and the cell parameter variation.

In analogy to the single cell test, the detection of ageing sections is difficult for modules aged with 1.0C. Due to the strong tendency towards lithium plating detected at 1.0C, only short linear ageing sections are expected, which quickly turn into non-linear sections with lithium plating.

The mean cell temperature $\overline{T_{\mathrm{cell}}}$ of the four modules aged with 1.0C is significantly higher than this of the modules aged with 0.5C due to the higher C-Rate (see Figure 6.6). While module 1.0C/1P is slightly below 40°C at BOT, the temperature rises further to 47°C for module 1.0C/4P due to the higher number of parallel cells. The mean cell temperature $\overline{T_{\mathrm{cell}}}$ of module 1.0C/2P and 1.0C/3P is particularly interesting. Although $\overline{T_{\mathrm{cell}}}$ during ageing is very similar, module 1.0C/3P has a lifetime advantage of 125 EFC. This is an indication that the number of cells connected in parallel can positively influence the lifetime of the modules. This will be investigated in more detail in the next subsection with the help of the single cell parameters.

In the first cycles, a drop in R_{rel} can again be observed for all modules operated with 1.0C. It is noticeable that the intensity and duration of the drop correlates with the number of parallel cells. The more cells are connected in parallel, the shorter the duration and the smaller the drop in R_{rel} (see Figure 6.5 b)). Once again, this behaviour can be explained by the temperature of the cells. Due to the increasing number of parallel cells, T_{cell} inside the modules increases steadily. In the single cell test, an increasing T_{cell} also led to a decrease of the internal resistance drop in the first cycles. The final value of R_{rel} shows a dependence on the cell temperature. During ageing the hotter the cells in the module are, the higher R_{rel} develops until 60% C_{rel} is reached. This also explains the different end value of R_{rel} of module

1.0C/4P and 1.0C/3P despite the very similar lifetime and the very similar ageing process (see Figure 6.6).

Again, the comparability of the module ageing with the ageing of the single cells is tested. As with the 0.5C modules, however, there are significant differences in the lifetime achieved and the ageing curves. In summary, the overall comparability is insufficient. A further comparison is therefore not meaningful. However, the ageing effects and mechanisms prevalent in the single cell tests are generally also found in the module tests.

6.4.1.1 Summary

For better clarity, the findings on module ageing are summarised again in bullet points.

- The different load of the modules with 0.5C and 1.0C leads to significantly different lifetimes. The worst module (1.0C/1P) reached a lifetime of 120 EFC, the best module (0.5C/4P) achieved 1027 EFC.
- There is a correlation between the number of parallel connected cells and the achieved lifetime for both 0.5C and 1.0C. In general, the more cells connected in parallel, the higher the achieved lifetime. The significantly greater gain in lifetime through the connection of several parallel cells resulted from operation with 1.0C. Here, the lifetime can be increased from 1p to 4p by a factor of 3.8. For the 0.5C modules, the lifetime can only be extended by a factor of 1.1.
- $\overline{T_{\text{cell}}}$ in the module depends on the number of parallel connected cells and the load. In general, $\overline{T_{\text{cell}}}$ increased by increasing the load from 0.5C to 1.0C and by increasing the number of parallel cells.
- The increased lifetime with a higher number of parallel cells cannot be attributed to a higher cell temperature alone. Despite a very similar $\overline{T_{\text{cell}}}$ in the first cycles between module 1.0C/2P and 1.0C/3P, a lifetime advantage of 125 EFC is given for module 1.0C/3P.
- The comparability of the module lifetime with the single cell lifetime is limited despite similar temperature conditions. It is assumed that the plastic housing used extends the lifetime of the modules by protecting them from any forced convection in the temperature chamber.

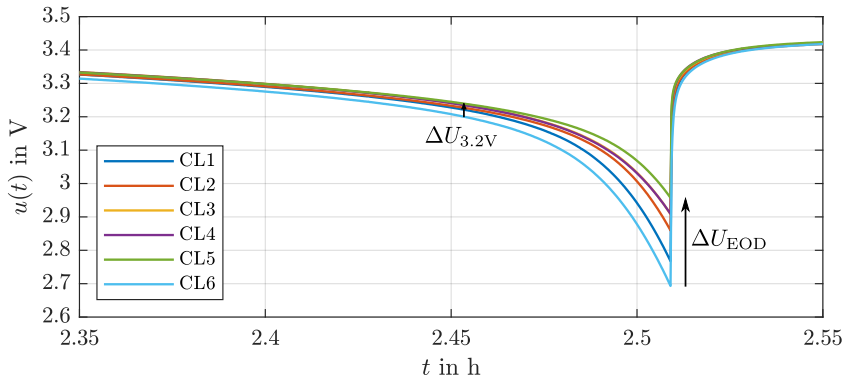

Figure 6.7: Due to the steep voltage curve at EOD, even small parameter variations between the CLs are visible. At higher cut-off voltages (e.g. 3.2 V) the parameter variations are hardly visible.

6.4.2 Results from Module Parameter Variation

In this subsection, the variation behaviour of the cells on the modules is examined. For this purpose, the subsection is divided into two parts. In the first part, only data from cyclic ageing is considered, while in the second part, the parameters of the individual cells from the disassembled modules after EOT are presented.

6.4.2.1 Data from Cyclic Ageing

As already mentioned, the parameters of the single cells can only be determined after disassembling the modules and measuring them individually. To obtain information on the parameter variation of the CLs during cyclic ageing, the CL voltage is used.

Information about the capacity variation in connection with the internal resistance of the individual CLs can be obtained from the distribution of the CL voltages at EOD. Since the CLs are balanced to the same voltage at EOC with a passive BMS, there is a common starting point at approximately 100% SOC (4.175 V per level). Since the current flow through all CLs is identical, the CL that first reaches the final discharge voltage during the subsequent discharge therefore has the weakest combination of capacity and internal resistance. The position of the other CL voltages at EOD gives an indication of the current state of the other CLs. Due to the steep voltage

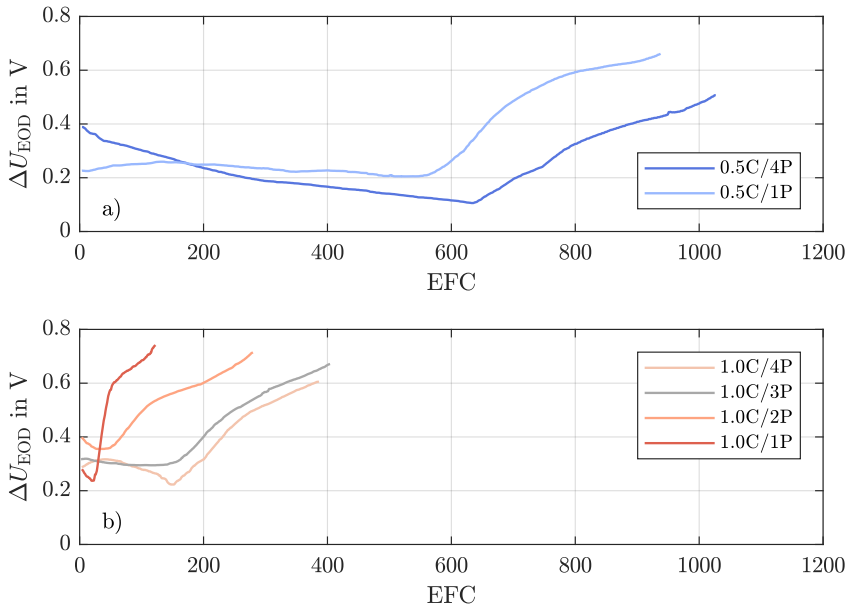

Figure 6.8: ΔU_{EOD} of all modules plotted over EFC.

curve towards EOD, this method is suitable for making even small parameter variations between the CLs visible. In contrast, this method is only suitable to a limited extent for higher cut-off voltages (e.g. >3.2 V). Due to the flattening voltage curve, a less pronounced voltage difference can result here even from larger parameter variations (see Figure 6.7).

In Figure 6.8 the difference of the maximum and minimum CL voltage at EOD ΔU_{EOD} for all modules over the complete lifetime in EFC is shown. In a) both 0.5C modules and in b) all 1.0C modules are shown.

For the modules aged with 0.5C as well as for the modules aged with 1.0C, similar starting values of ΔU_{EOD} in the range of 0.2 V to 0.4 V are obtained. The similarity of the values can be attributed to the cell matching before assembling. This ensures that the parameter variation among the cells is similar for each module at BOT. The similar parameter variation then leads to a similar ΔU_{EOD}. In total, ΔU_{EOD} is influenced by SOC, SOH and the internal resistance of the installed cells.

For most modules, there is initially a significant reduction of ΔU_{EOD} in the first ageing section (see Figure 6.8). Only for modules 0.5C/1P and 1.0C/3P

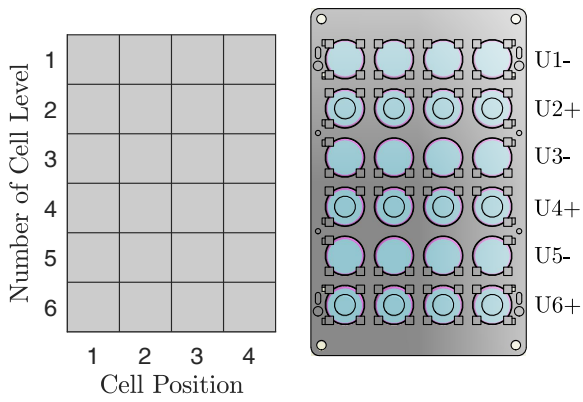

Figure 6.9: Schematic illustration of the module with the respective CLs (left), associated design view from above (right).

ΔU_{EOD} hardly changes at the beginning. Whether the major part of the reduction of ΔU_{EOD} results from the equalisation of the cell parameters (usable capacity and internal resistance) or the balancing of different SOCs of the CLs with passive balancing cannot be clarified on the basis of the measured data.

As soon as individual cells in the modules age faster than others, the performance of the affected CL collapses and ΔU_{EOD} increases suddenly. The stronger CLs in the module still have residual capacity and thus higher voltages at EOD.

To find out which CL causes the increase of ΔU_{EOD} in the 6 tested modules or whether different CLs are involved is now checked on the basis of all CL voltages.

To assign the individual CLs to the module design Figure 6.9 shows the schematic illustration of the module with the corresponding CLs (left) compared to the design view from above (right). In Figure 6.10 the voltages from CL1 to CL6 of all modules are shown.

At BOT, either CL1 or CL6 triggers the EOD for all modules in the first cycles (see Figure 6.10). However, this is not due to a lower capacity or a higher internal resistance of the cells in CL1 and CL6, but to the slightly higher resistance due to the connection with the BMS. This is therefore not a cell-specific but BMS-specific phenomenon.

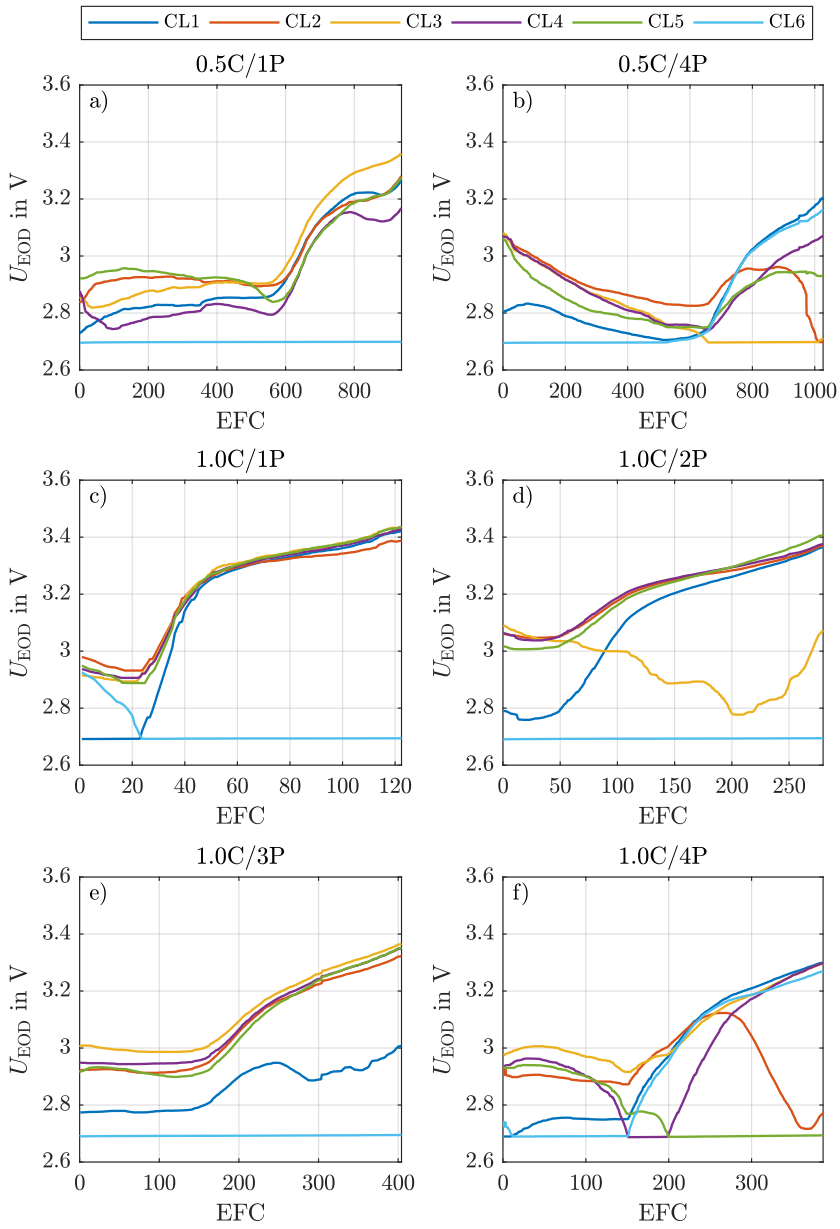

Figure 6.10: U_{EOD} of all CLs visualises in which cycle which CL triggers the EOD.

The behaviour of the CL voltages of module 0.5C/1P (Figure 6.10 a)) can be compared well with the behaviour of the single cells under the test conditions 0.5C/20°C, 30°C, 40°C. As long as the ageing of the cells is in the linear section, the parameter variation hardly changed. In the module test 0.5C/1P, too, the position of the CL voltages hardly changes until the non-linear section is reached after approximately 560 EFC. This indicates a constant ratio of capacity loss and internal resistance increase of the CLs. Finally, due to the change from linear to non-linear section, there is clearly a rapid decay of CL6, as the voltages of the other CLs are increasingly higher at EOD. Accordingly, CL6 determines the EOD over the entire lifetime.

For module 0.5C/4P (Figure 6.10 b)), CL6 initially determines the EOD. In the further ageing progress, the CL voltages then develop closer together until the module ageing switches to the non-linear section at approximately 650 EFC. Now, CL3 causes the EOD and is replaced by CL2 shortly before reaching 60% C_{rel}. The change in the parameters of CL2 can be recognized more than 100 EFC earlier by a rapid continuous drop in U_{EOD}.

With the 1.0C modules, the non-linear ageing section is reached much earlier (see Figure 6.10 c) to f)). The modules 1.0C/1P, 1.0C/2P and 1.0C/3P also behave very similarly. After different lengths of linear sections of about 25 EFC, 50 EFC and 150 EFC respectively, there is a collapse of the capacity or an increasing internal resistance at CL6, which permanently determines the EOD for all three modules. Module 1.0C/4P behaves more like module 0.5C/4P. Here, the EOD is determined by different CLs during the test. In the non-linear ageing section, first CL4 and then CL5 determines the EOD. Towards EOT, strong ageing can also be detected in CL2.

Based on the CL voltages, the ageing behaviour of the modules can be analysed more precisely without knowing the individual single cell parameters. With help of the position of the CL voltages at EOD, it is not only possible to detect the CL that lead to EOD, but also to estimate the parameters of the remaining CLs. It turns out that, especially in CL6, four of the six modules age significantly. Another characteristic can be seen in the modules 0.5C/4P and 1.0C/4P. Here, in contrast to the other modules, the EOD is triggered by different CLs. The module ageing is therefore dominated by several CLs here.

For a more detailed analysis of the cell parameter variation, the individual cells of the disassembled modules are examined in the following pages. The influence of the modular architecture is also investigated.

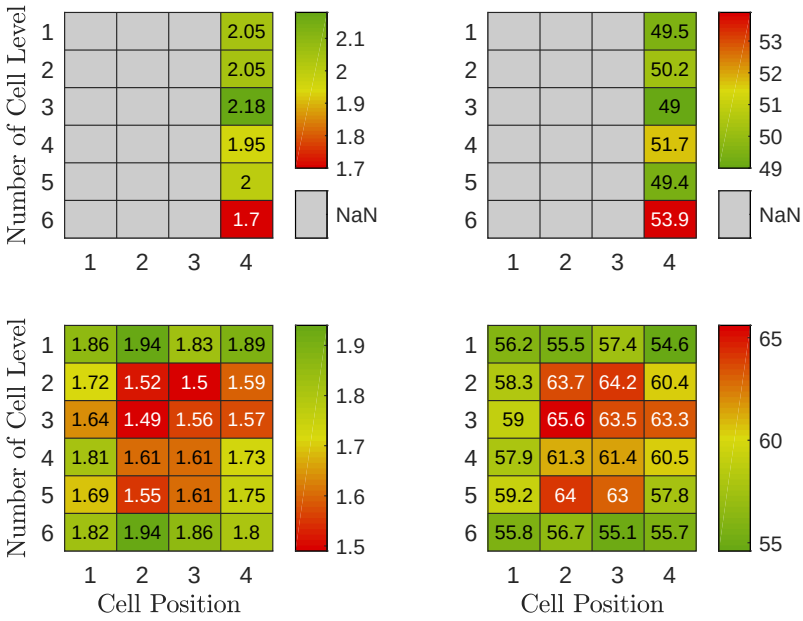

Figure 6.11: Single cell overview of all modules operated with 0.5C. The left part shows the values for C_{DCH} in Ah and the right part the corresponding internal resistance $R_{\mathrm{DC,1s}}$ in mΩ.

6.4.2.2 Data from Single Cells

The measurement of the individual cell parameters (see colour maps Figure 6.11 and Figure 6.12) reflects the estimates made by the CL voltages in Figure 6.10 very well. CLs that lead to EOD in the last EFC during module ageing generally exhibit the lowest capacity C_{DCH} and the highest internal resistance $R_{\mathrm{DC,1s}}$.

Impact of Module Architecture

With help of the colour maps, architecture-related correlations between the cell parameters and the position of the cells in the module can be recognised. Both for the 0.5C modules in Figure 6.11 as well as for the 1.0C modules in Figure 6.12, repetitive patterns appear.

In four of the six modules (0.5C/1P and 1.0C/1P, 2P, 3P), cell CL6/4 in the lower right corner is the weakest cell, regardless of the number of parallel connected cells.

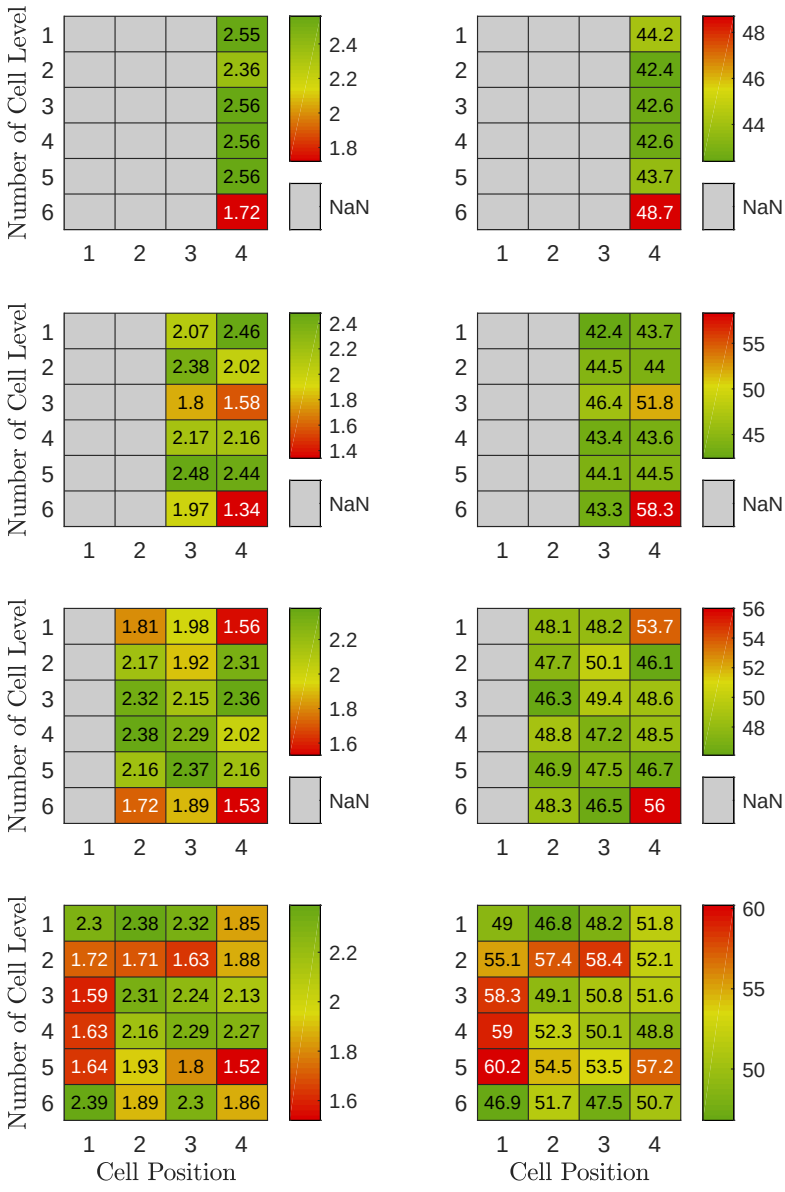

Figure 6.12: Single cell overview of all modules operated with 1.0C. The left part shows the values for C_{DCH} in Ah and the right part the corresponding values for $R_{\mathrm{DC,1s}}$ in mΩ.

The fact that cell CL6/4 in particular is the weakest cell in all mentioned modules is possibly due to the proximity to the cable duct. Here, all load and measuring cables connected to the module are led out of the module housing. This leads to contact with the cooler air of the temperature chamber at this area, which can lead to a temperature gradient within cell CL6/4 and thus to faster ageing.

In module 1.0C/3P, in addition to cell CL6/4, three other cells are affected, each located at the outer corners of the module (CL6/2, CL1/2, CL1/4). Here, too, the behaviour can possibly be explained by a temperature gradient within the affected corner cells, since the cell surface facing the module becomes hotter than the cell surface facing outwards. A temperature gradient within a cell leads to spatially different electrical impedances in the active material and thus ultimately to spatially different current densities, which accelerate the ageing of the complete cell [129, 130].

In module 0.5C/4P, another pattern emerges. Here, especially the inner cells show a lower C_{DCH} and a higher $R_{\mathrm{DC,1s}}$. As the inner cells of the module become hotter, their internal resistance decreases. Since the behaviour of the cells in parallel connection is comparable to an electrical current divider, the current through the hotter cells increases significantly, which leads to faster ageing of these cells. This behaviour has already been demonstrated in the literature for parallel connected cells [130, 131]. The ageing of module 0.5C/4P is thus mainly determined by the inner cells of different CLs.

In module 1.0C/4P, cells on the left edge are particularly affected. However, no explanation can be found for this, which can be attributed to the architecture of the module. Here, too, the ageing is determined by several CLs.

The causes mentioned for the distribution of the weaker cells are based on findings from the literature in combination with the module architecture used. However, the causes cannot be confirmed on the basis of the measured parameters. The contradictory findings regarding the distribution of the weaker cells (corner cells vs. inner cells) reveal a need for further research in this area. Regardless of the reasons for the distribution of the weaker cells, the colour maps shown in Figure 6.11 and Figure 6.12, however, provide important insights.

The colour maps show that the weaker cells are not distributed randomly, but a result from the module architecture. As already mentioned from literature, this is often attributed to thermal differences in the module ultimately leading to varying operating conditions among the affected cells

[130, 132–135].

Another important finding emerges when looking at the CLs. Not all cells of a CL age evenly. There are clear differences in cell parameters among the cells of a CL. It can not be observed that the cell parameters in a parallel circuit equalise over ageing, as described in some publications (e.g. [127]). In [58] it is concluded that the cell parameters in a parallel circuit do not equalise during ageing, too. According to [136], the equalising effect of cell parameters in a parallel circuit only takes place if the operating current is low enough that any SOC differences in a CL can be equalised. At higher operating currents, as in the test carried out here, the varying cell current in the parallel circuit clearly outweighs the compensating effect of parallel connected cells. The result is different ageing of the individual cells in one CL.

From the above findings, conclusions can thus be drawn about the lifetime of the modules depending on the number of parallel cells. Ideally, all cells of a module age evenly. However, due to intrinsic and, above all, extrinsic conditions (e.g. spatial temperature differences within the module architecture), there are inevitably different operating conditions in a real application, which lead to different ageing rates of the installed cells. As soon as in a 6s1p configuration (e.g. module 1.0C/1P) one CL ages faster than the other CLs due to a spatially limited thermal characteristic (e.g. a cable duct), the ageing process of the worse CL cannot be compensated. By adding more parallel cells, the architecture-related spatial temperature differences can be better compensated. While the weakest cell of the affected CL ages strongly (e.g. CL6/4), the ageing speed of the entire CL can be stabilised by lower ageing speeds of the parallel connected neighbouring cells. In the end, only the average ageing speed of the entire CL is decisive.

Based on the results shown, it is therefore assumed that the number of cells connected in parallel is only indirectly responsible for the improvement in lifetime. Rather, a positive effect is assumed due to the spatial distribution of the CL. With help of this, thermal differences in the module can be spatially compensated. The same effect can thus also be achieved with a single cell of larger dimensions, e.g. with a pouch cell.

Overall, the positive effect of parallel connected cells on the lifetime is significantly greater in the 1.0C modules than in the 0.5C modules. The stabilising effect comes into play especially when cells of one CL show high differences in the ageing rate. It is known from the single-cell test that very pronounced ageing differences could develop very quickly during operation

with 1.0C. The probability that cells in the module will age at significantly different rates at 1.0C is therefore significantly higher than for the 0.5C modules. Thus, the averaging effect of parallel connected cells has a significantly greater benefit.

Based on the results, it can therefore be concluded that parallel connected cells have a positive effect on the lifetime of the modules, especially if the test condition tends to develop a pronounced parameter variation.

Parameter Variation of Aged Modules

The parameter variation of the modules is calculated in two different scenarios. On the one hand, the individual cells installed in the module are observed in total in a theoretical observation independent of the interconnection ($xsy\mathrm{p}$), and on the other hand, the parameter variation of the CLs is evaluated. For this purpose, the parameters of the CLs are calculated from the parameters of the measured single cells. For comparability of the variation values, these are again presented on the basis of the COV (κ_x).

In Figure 6.13, the capacity variation of the single cells in a) and the capacity variation of the CLs in c) at BOT and at EOT can be seen.

At BOT, the capacity variation $\kappa_{C_{\mathrm{DCH}}}$ of the individual cells in a) is between 0.24% and 0.51% at a very low level. By connecting the cells in parallel, this value can be further reduced to BOT, since production-related differences among the CLs are statistically averaged (see Figure 6.13 c)). Thus, the parallel connection of cells already has a positive influence at BOT. This was also confirmed in [91].

At EOT, the capacity variation of the individual cells of all six modules in a) significantly increases. Distinct differences between the modules operated at 0.5C and 1.0C can be seen. As in the single cell test conducted in chapter 5, the capacity variation for the modules aged with 0.5C is significantly lower than for the modules aged with 1.0C.

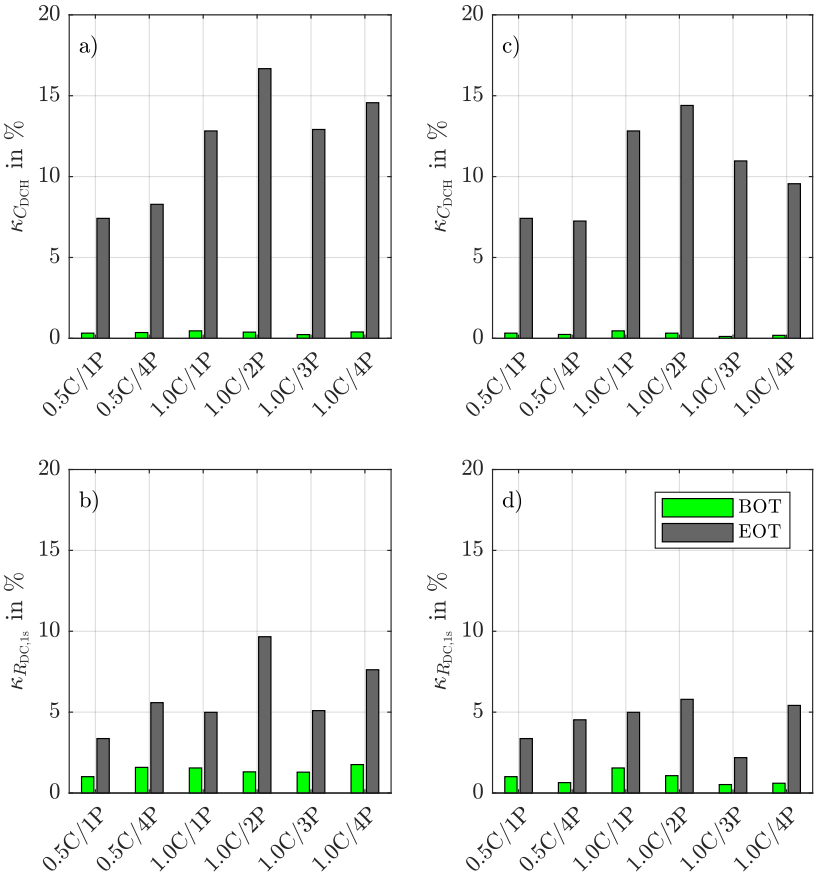

Figure 6.13: Summary of the variation behaviour based on the COV at BOT and EOT. In a) and b) the parameter variation of single cells; in c) and d) the parameter variation of CLs can be seen.

By considering the capacity variation of the CLs in c), further findings can be obtained. The variation of module 0.5C/4P hardly changed (-0.52 percentage points) by interconnection compared to the single cell observation in a). This indicates that in this case there is hardly any additional benefit from the parallel connection in terms of capacity variation. In the 1.0C modules, however, the capacity variation of the CLs decreases significantly compared to the single cell observation in a). As a tendency, the capacity variation of the CLs in c) significantly reduces with an increasing number of parallel connected cells, while at the same time the achieved lifetime of the modules also increases. The parallel connection of cells therefore has a positive effect on the capacity variation. This effect is significantly more pronounced for the 1.0C modules than for the 0.5C modules.

Finally, the variation of the internal resistances of the single cells in b) and of the CLs in d) is considered. Due to production-related reasons, the variation of the internal resistances at BOT is again higher than the capacity variation (compare with Table 4.1). Here, too, the resistance variation of the CLs can be initially reduced by connecting the individual cells in parallel. At EOT, the variation values again increase significantly. Neither by observing the individual cells (Figure 6.13 b)) nor by looking at the CLs (Figure 6.13 d)) significant differences can be detected that indicate operation of the modules with 0.5C or 1.0C.

6.4.2.3 Summary

The results regarding the parameter variation of the modules are now summarised in bullet points:

Data from Cyclic Ageing

- ΔU_{EOD} generally decreases during the first cycles. As soon as at least one cell of a CL ages faster, ΔU_{EOD} increases abruptly. A further reduction of ΔU_{EOD} can not measured in any of the modules from this point on, thus the parameter variation grows until EOT.
- The value of the CL voltages at EOD in the last ageing cycle shows a high correlation with the single cell parameters measured in the RPT after disassembling.

Data from Single Cells

- The spatial distribution of the weak cells in the module can usually be traced back to the module architecture and does not happen randomly in the test carried out.
- Within a CL, there are often clear differences between the cells in C_{DCH} and $R_{\mathrm{DC,1s}}$. Thus, the parameters of the cells of a CL do not equalise during module ageing, as often described in the literature.
- Based on the results, it can be assumed that the number of cells connected in parallel only indirectly influences the lifetime of the modules. Rather, it is assumed that the spatial dimensions of a CL can compensate thermal peculiarities in a module. Ultimately, only the average ageing rate of a CL is decisive. This average ageing rate can be reduced by better cells in the affected CL. The same effect can therefore also be achieved with a single cell of the same spatial dimension (e.g. a pouch cell).
- The parameter variation of the modules can be reduced by connecting cells in parallel at BOT, due to statistical averaging.
- The variation of C_{DCH} at EOT is significantly higher for the 1.0C modules than for the 0.5C modules despite their shorter lifetime, thus confirming the findings from the single cell ageing. The variation of $R_{\mathrm{DC,1s}}$ again develops more slowly than the variation of C_{DCH}.
- Especially the 1.0C modules, which develop a greater parameter variation, benefit from the parallel connection of many cells. The variation of the CL parameters is significantly lower than the variation of the individual single cell parameters, since there is an averaging effect of the single cell parameters. Since the 0.5C modules have a significantly lower variation of the single cell parameters, the positive averaging effect of the parallel connection in CL is hardly noticeable.
- As with the single cell ageing tests, no significant dependencies on the values of the initial parameters of the single cells could be determined for the future module ageing.

Chapter 7

Conclusion and Outlook

7.1 Conclusions and Contributions

Lithium-ion batteries consist of a large number of interconnected cells. Due to technical production reasons, there is already a parameter variation among new cells when the module is assembled. During the ageing of the module, different and overlapping factors affect the ageing of the individual cells and lead to increasing parameter variation. Although first studies from the literature present the effects of parameter variation during ageing in some empirical studies, the focus lies not on the cause of the variation. An investigation of the parameter variation as a function of different test conditions is also missing. This thesis makes a first contribution to this gap in the literature.

Using an empirical approach, investigations are carried out on unconnected single cells and on self-built modules. With help of the unconnected cells, the development of the parameter variation at different test conditions (load and temperature) without interacting influences is examined. The test results enable analysing the dominant intrinsic development of the parameter variation of cells during ageing. In a further experiment, the development of the variation of cell parameters in modules is investigated. Here, the modules are aged under different loads (0.5C and 1.0C) at 20°C ambient temperature. In order to determine the influence of the cell configuration, the number of cells connected in parallel is varied from 1 to 4 in the tested modules.

Overview of empirical tests:

- Parameters from 480 brand-new cells are collected and evaluated.
- 137 cells undergo calendar ageing for 2 years at 20°C.
- 80 single cells are aged with 0.5C and 1.0C at 0°C, 10°C, 20°C, 30°C

and 40°C in groups of 8 cells.

- 90 cells are installed in 6 modules of different configurations (6s1p, 6s2p, 6s3p, 6s4p) and aged with 0.5C, as well as 1.0C at 20°C. After completion of the tests, all cells are removed from the modules and measured again.

The most important findings from the empirical tests are summarised. They are divided into single-cell tests and module tests. Finally, recommendations for minimising the parameter variation are given on the basis of the measurement data.

Findings from Single Cell Ageing

- While the investigated cell groups age in the linear section without lithium plating, ΔC_{DCH}, $\Delta R_{\mathrm{DC,1s}}$ and ΔEFC hardly change. The different, seemingly arbitrary, onset time of lithium plating finally leads to faster non-linear ageing and an increase in ΔC_{DCH} and ΔEFC. The observed value $\Delta R_{\mathrm{DC,1s}}$, on the other hand, behaves differently. $\Delta R_{\mathrm{DC,1s}}$ develops significantly slower than ΔC_{DCH} and probably depends on further factors that were not recorded in this work.
- Test conditions close to the lithium plating boundary at BOT are particularly prone to the development of a strong parameter variation (0.5C/10°C and 1.0C/20°C, 30°C, 40°C). Smallest intrinsic and extrinsic factors can cause some cells to age already very fast with lithium plating while other cells still age linear without lithium plating. This coexistence of different ageing rates, already prevalent from the BOT, leads to a large ΔC_{DCH} and thus also ΔEFC. This behaviour was observed for ageing with 0.5C and with 1.0C.
- If all cells of the test group age from BOT on with lithium plating (e.g. at 0.5C/0°C), the development of the of parameter variation of all cells is relatively slow, since there is no non-uniform transition to different ageing mechanisms. However, no advantage can be gained from this, as the lifetime under these test conditions is extremely short.
- The majority of ΔC_{DCH} results from the capacity differences of the cells themselves. Decoupling ΔC_{DCH} from the internal resistance ($\Delta C_{\mathrm{DCH,CV}}$) hardly reduced the capacity variation.
- During pure calendar ageing of the remaining 137 cells over 2 years, the variation of C_{DCH}, $C_{\mathrm{DCH,CV}}$ and $R_{\mathrm{DC,1s}}$ slightly decreased.

Findings from Module Ageing

- At EOT, the variation of C_{DCH} among the single cells was significantly larger for modules aged with 1.0C than for modules aged with 0.5C. The variation of $R_{\mathrm{DC,1s}}$ showed hardly any dependence on the C-Rate.
- The spatial distribution of the weak cells in the modules can usually be traced back to the modular architecture and does not happen randomly in the test carried out.
- Within a CL, there are often clear differences in the C_{DCH} and $R_{\mathrm{DC,1s}}$ values of the single cells at EOT. Thus, the parameters of the cells of a CL do not equalise during ageing.
- The lifetime of the modules can be increased by connecting cells in parallel. This is on the one hand due to thermal effects and on the other hand due to an average ageing effect caused by the parallel-connected cells.
- Based on the results, it is assumed that the number of cells connected in parallel in the test only indirectly influences the lifetime of the modules. Rather, it is assumed that the spatial dimensions of a CL can compensate thermal peculiarities in a module. Ultimately, only the average ageing rate of the complete CL is decisive. This average ageing rate can be reduced by stronger cells in the affected CL. The same effect is therefore assumed to be achieved with a single cell of the same spatial dimension (e.g. a pouch cell). Since the variation of the cell parameters is much more pronounced in the modules aged with 1.0C, these modules in particular benefit from the averaging effect of the parallel connection of cells.

Recommendations for Minimising Parameter Variation

- Operating conditions close to the lithium plating boundary at BOT are to be avoided. With the help of the relaxation measurement, the plating boundary at BOT can be determined.
- Lower operating currents (e.g. 0.5C) and warmer temperatures (e.g. 40°C) are recommended, since such operating conditions are less prone to parameter variation and shift the onset of lithium plating to much later times or to a lower SOH (longer linear section). The lower the SOH when lithium plating occurs, the lower the slope of the non-linear ageing section. Accordingly, varying onset times of lithium plating of the different cells have a weaker effect on the parameter variation. It is

recommended to delay the onset of lithium plating as much as possible in order to mitigate the negative effect of an increasing parameter variation.

- Remaining in the linear ageing section leads to the smallest increase in parameter variation. By setting the EOL to a higher SOH (if possible), the non-linear section can be completely avoided and therefore also a pronounced parameter variation.
- In modules with high operating currents (e.g. 1.0C) combined with significant temperature gradients the use of several parallel cells is advantageous. In case of spatially stronger ageing of some cells, other cells in the same CL can reduce the average ageing rate and extend the lifetime of CL and thus the module.

7.2 Future Works

With the help of the measurements carried out, a basic understanding of the parameter variation of single cells and modules was gained. When analysing the measured data, further questions and findings arise that require further research:

- Since lithium plating in particular played a significant role in the development of the parameter variation, the charging current has a major influence on the parameter variation. Future studies should investigate the influence of charging and discharging current separately. For example, the effects of different discharge rates on the development of the parameter variation can be investigated at a uniformly low charging current.
- In order not to increase the test duration any further, the minimum and maximum voltage limits during cyclic operation were set to 2.75 V and 4.175 V respectively. Especially the maximum voltage limit of 4.175 V leads to a low anode potential during charging, which in turn is responsible for the onset of lithium plating. In further tests, the effects of limiting the SOC range to, for example, 20% to 80% should be investigated. In real applications, the maximum possible voltage limits are rarely used.
- For reasons of limited test capacity, only 8 cells per test group were used for single cell ageing. In order to increase the statistical significance of the results, the number of cells tested should be increased in

future studies.

- The investigations carried out are based on the ageing of a high-energy cell. High-power cells can react differently to the selected test conditions. The results are also not generally transferable to other high-energy cells. In further investigations, different high-energy cells and high-performance cells should therefore be examined in a similar way.
- It has been shown that $\Delta R_{\mathrm{DC,1s}}$ developed largely independently, or with a significant delay, from ΔC_{DCH}. Further investigations can concentrate more on the development of the internal resistance variation.
- The effect of the spatial dimensions of a cell on module ageing needs further research.

7.3 Publications and Patent Applications of the Author

7.3.1 Results Related to Battery Management Systems

1. A. Ziegler, D. Oeser, T. Hein, D. Montesinos-Miracle and A. Ackva, "Reducing Cell to Cell Variation of Lithium-Ion Battery Packs During Operation", *IEEE Access, vol. 9, pp. 24994-25001, 2021*

   Abstract - In this work, an experimental approach to reduce the variation from cell to cell during battery operation is evaluated to reach a better battery utilization. Numerous theoretical considerations of intelligent battery management systems without long-term experimental validation of their capabilities lead to a gap in the literature, which this work aims to address. For this purpose, the ageing behaviour of two batteries is investigated over a period of almost 1.5 years. One battery is connected to an active balancing battery management system (BMS) and the other to a conventional passive balancing BMS. Important battery parameters, such as capacity and internal resistance, are recorded in each cycle. The battery behaviour is evaluated in detail by observing the voltage difference of the individual cells at the end of discharge and by calculating the amount of charge actually balanced by the BMS. Significant differences between the BMS systems used are elucidated, which illustrate the advantages of active balancing. In contrast to passive balancing, active balancing is able to reduce the ageing rate of the battery and achieve better utilization with a more

than five times lower voltage spread at end of discharge, a up to 3.1% higher discharge capacity and a 7.7% longer service life.

2. T. Hein, A. Ziegler, D. Oeser, A. Ackva, "A capacity-based equalization method for aged lithium-ion batteries in electric vehicles", *Electric Power Systems Research, vol. 191, 2021*

   Abstract - A capacity-based equalization method for active balancing is proposed to increase the usable capacity of aged lithium-ion batteries within a minimum of balancing effort. The main goal of the presented algorithm is to predict the equalization charge for each cell, which is needed to fully charge and discharge every cell of the battery in the next cycle. For this, State-Of-Charge (SOC) and State-Of-Health (SOH) of each cell must be determined. The predicted energy is balanced at the beginning of the cycle and further balancing is performed only if the parameters of the cells change. This ensures that the minimum possible balancing effort is achieved. To validate the performance of the proposed method, a simulation is carried out. For this purpose, a battery model and Battery Management System (BMS) model are built in Matlab/Simulink. The parameters of the simulated cells differ in capacity and initial SOC to imitate an aged battery. The simulation results verify that the developed balancing method can improve the usage of aged batteries compared to conventional methods. This algorithm for active balancing can be used in second life cases of battery systems.

3. A. Ziegler, D. Oeser, T. Hein, A. Ackva, "Development and Application of an Active Balancing System for Lithium-Ion Cells", *IEEE Vehicle Power and Propulsion Conference, Hanoi, Vietnam, VPPC 2019*

   Abstract - This paper describes the development of an active battery management system for lithium-ion cells and its comparison with passive battery management. For this purpose, the structure of the test hardware is described and its universal possibilities are explained. An iterative balancing algorithm is presented as a central component of the active balancing system. The algorithm is able to determine the capacitance deviations between the individual cells by measuring cell voltages and battery current. In order to compare the system built up in this work with a conventional battery management system, a realistic test is carried out on aged lithium-ion batteries. In this test, the active balancing system is able to significantly increase the removable

battery capacity compared to conventional passive balancing. In addition, the disadvantage of passive balancing in second-life applications is clarified.

4. A. Ziegler, D. Oeser, B. Arndt, A. Ackva, "A Universal, Modular and Bidirectional Active Balancing System for Lithium-Ion Cells", *Proceedings of the 10th International Scientific Symposium on Electrical Power Engineering ELEKTROENERGETIKA, Stará Lesná, Slowakia, EE 2019*

   Abstract - This paper introduces a new, modular and universal active balancing system that is able to gain significantly more energy from aged and unbalanced batteries compared to other balancing concepts. One of the major issues when using battery packs is the possible unbalance within single battery cells. As this problem worsens with increasing age state of the art passive balancing methods reach their limits in terms of energy efficiency and applicability. After identifying the issues of standard balancing systems, requirements to overcome those problems are derived. To meet those requirements a new balancing hardware and the corresponding algorithm is implemented. The applicability and energy efficiency is proofed in the laboratory on a real hardware system and demonstrated by measurement results. Furthermore, a evaluation of a realistic application with a traction battery is executed.

5. A. Ziegler, D. Oeser, B. Arndt, A. Ackva, "Comparison of Active and Passive Balancing by a Long Term Test Including a Post-Mortem Analysis of all Single Battery Cells", *IEEE International Conference and Workshop in Óbuda on Electrical and Power Engineering, Budapest, Hungary, IEEE CANDO-EPE 2018*

   Abstract - Due to the fact, that there are basically no practical test comparisons between active and passive lithium-ion battery balancing systems, a long term test is carried out. Therefore two batteries with an active and a passive balancing system are cycled. After about 2600 cycles test is stopped to start with further investigations. Capacity decrease and the increase of internal resistance of the two used battery packs are presented. To investigate the influence of load cycles in combination with different battery management systems (BMS) a detailed single cell investigation is executed. Finally, active balancing increases the usable capacity by a maximum of 2balancing and reduces the cell to cell deviation of capacity and internal resistance. Furthermore it is

shown that the additional stress due to frequent energy redistribution in active balancing systems has no negative ageing effects to the cells compared to passive balancing.

6. D. Oeser, A. Ziegler, B. Arndt, A. Ackva, "Effectiveness of Active Balancing on High Dispersion Batteries", *IEEE International Conference and Workshop in Óbuda on Electrical and Power Engineering, Budapest, Hungary, IEEE CANDO-EPE 2018*

   Abstract - These investigations examine the benefit of an active balancing system based on an LTC-3300 IC with help of an arbitrarily configurable battery. The used structure allows creating batteries with different cell to cell variations in a 12S1P setup and to test it with the active balancing system. In total, three different combinations with varying degrees of cell to cell variation are tested. The usable capacity of the cell combinations is compared with and without balancing. In all three tests, the capacity could be significantly increased and stabilized with help of the active system. These studies indicate that the additional benefit of an active balancing system could play a major role in the field of second-life batteries. Furthermore, the system can ensure the usability of a battery in case of cell failure.

7.3.2 Results Related to Battery Ageing

1. A. Ziegler, D. Oeser, T. Hein, D. Montesinos-Miracle, A. Ackva, "Run to Failure: Aging of Commercial Battery Cells beyond Their End of Life" *Journal of Energies, vol. 13, no. 8: 1858, 2020*

   Abstract - The aim of this work is to age commercial battery cells far beyond their expected lifetime. There is a gap in the literature regarding run to failure tests of lithium-ion batteries that this work intends to address. Therefore, twenty new Samsung ICR18650-26F cells were aged as a battery pack in a run to failure test. Aging took place with a constant load current and a constant charge current to accelerate capacity decrease. Important aging parameters such as capacity and internal resistance were measured at each cycle to monitor their development. The end of the test was initiated by the explosion of a single battery cell, after which the battery pack was disassembled and all parameters of the still intact single cells were measured. The distribution of all measured capacities and internal resistances is displayed graphically. This clearly shows the influence of the exploded cell on the cells in its immediate vicinity. Selected cells from this area of the battery were subjected to computed tomography (CT) to detect internal defects. The X-rays taken with computed tomography showed clear damage within the jelly roll, as well as the triggered safety mechanisms.

2. G. Bohn, J. Taub, A. Linke, S. Bayer, D. Oeser, A. Ziegler, P. Ettl, A. Ackva, "High-resolution interferometric measurement of thickness change on a lithium-ion pouch battery", *3^{rd} International Conference on Environmental and Energy Engineering, IOP Conference Series Vol. 281, Nr. 012030, Shanghai, China, IC3E 2019*

   Abstract - Volume change of graphite leads to change in thickness of battery storage layers during discharging and charging. Pouch cell lithium ion batteries are used in the field of electric vehicles and solar home storage. This paper shows a measurement setup for the three-dimensional measurement of thickness change on a flat 6.7 mm thick pouch cell using a white light interferometer. With a measuring field of 7.05 mm diameter the resulting 3D thickness change record contains 226000 3D readings. The measuring points have a lateral distance of 13.1 μm. The repeatability of the measurement is 312.8 nm for the individual values and 64.1 nm for the average value. In addition, this paper shows how the storage capacity of this pouch cell drops over 30

charge cycles.

3. D. Oeser, A. Ziegler, A. Ackva, "Single Cell Analysis of Lithium-Ion E-Bike Batteries Aged under Various Conditions", *Journal of Power Sources, vol. 397, pp. 25-31, 2018*

   Abstract - In most cases, batteries consist of multiple cells with different interconnections in which the weakest cells determine the usable capacity, performance and lifetime. Since data on initial production-related cell to cell parameter variance is well known, only little data on variance change over lifetime is available. This work investigates how variance spreads with age. Twenty differently aged electric bike (pedelec) batteries are disassembled and the state of health, as well as the internal resistance, are measured cell by cell for each of these batteries. The results show the development of cell to cell variation of aged batteries. Gathered data is also used to calculate capacity limitations through progressed variation. The methodology of the investigation can be used to analyse potential use cases for active balancing systems.

4. S. Bayer, D. Oeser, A. Ziegler, A. Ackva, "Laboratory ageing of commercial e-bike battery packs", *15th Design&Elektronik Batterieforum, 2018, Munich, Germany*

   Abstract - Due to the growing market for e-bikes in Europe and a gap in the knowledge about Li-ion technology a set of aging tests has been carried out using Li-ion batteries. The integrated NMC (Nickel Manganese Cobaltoxide) cells are manufactured by Samsung, labelled as ICR18650-26F. These cells are a commercial off-the-shelf product. The tests comprise of cycling in the field and laboratory. The laboratory aging concentrates on testing at different ambient temperatures. Discharging is done with an average from collected field-test data. The study shows impact of the ambient temperature on the remaining capacity and the internal resistance. In addition a post-mortem analysis of one battery has been done.

7.3.3 Patent Applications

1. Patent Application: A. Ziegler, A. Molchanov, D. Oeser, P. Ponomarov, "Verfahren und Vorrichtung zum Zellspanungsausgleich von Batteriezellen mehrzelliger Energiespeicher",
   Application Number: DE 10 2019 108 579.9
2. Patent Application: A. Ziegler, D. Oeser, "Verfahren zur Bestimmung eines bevorstehenden Fehlerfalls einer Batteriezelle sowie Batterie-Management-System",
   Application Number: DE 10 2019 134 510.3
3. Patent Application: A. Ziegler, D. Oeser, T. Hein, P. Ponomarov, "Verfahren und Vorrichtung zum aktiven Balancieren von Batteriezellen mehrzelliger Energiespeicher" (Part I),
   Application Number: DE 10 2020 123 864.9
4. Patent Application: A. Ziegler, D. Oeser, T. Hein, P. Ponomarov, "Verfahren und Vorrichtung zum aktiven Balancieren von Batteriezellen mehrzelliger Energiespeicher" (Part II),
   Application Number: DE 10 2021 119 237.4

Bibliography

[1] David Spiers. Batteries in PV Systems. In *Practical Handbook of Photovoltaics*, pages 721–776. Elsevier Ltd, 2012.

[2] Peter Kurzweil and Otto K. Dietlmeier. *Elektrochemische Speicher*. Springer, 2015.

[3] Reiner Korthauer. *Lithium-ion batteries: Basics and applications*. Springer, 2018.

[4] K. Mizushima, P. C. Jones, P. J. Wiseman, and J. B. Goodenough. Li_xCoO_2 ($0<x\leq1$): A new cathode material for batteries of high energy density. *Materials Research Bulletin*, 15(6):783–789, 1980.

[5] Naoki Nitta, Feixiang Wu, Jung Tae Lee, and Gleb Yushin. Li-ion battery materials: present and future. *Materials Today*, 18(5):252–264, 2015.

[6] Bote Zhao, Ran Ran, Meilin Liu, and Zongping Shao. A comprehensive review of $Li_4Ti_5O_{12}$-based electrodes for lithium-ion batteries: The latest advancements and future perspectives, 2015.

[7] Reiner Korthauer. *Handbuch Lithium-Ionen-Batterien*. Springer Berlin Heidelberg, Berlin, Heidelberg, 2013.

[8] Hannes Hopp. *Thermomanagement von Hochleistungsfahrzeug-Traktionsbatterien anhand gekoppelter Simulationsmodelle*. SpringerVieweg, 2016.

[9] Tim Hettesheimer, Axel Thielmann, Christoph Neef, Kai-Christian Möller, Mareike Wolter, Vincent Lorentz, Martin Miller, Markus Hagen, Patrik Fanz, Prof. Dr. Jens Tübke, Markus Gepp, Martin Wenger, Torben Prill, Jochen Zausch, Peter Kitzler, and Joachim Montnacher. Entwicklungsperspektiven für Zellformate von Lithium-Ionen-Batterien in der Elektromobilität. Technical report, Fraunhofer, 2017.

[10] Jan Schmitt. *Untersuchungen zum Herstellungsprozess des Elektrode-Separator-Verbunds für Lithium-Ionen Batteriezellen*. PhD thesis, TU Braunschweig, Essen, 2015.

[11] Victor A. Agubra and Jeffrey W. Fergus. The formation and stability of the solid electrolyte interface on the graphite anode. *Journal of Power Sources*, 2014.

[12] Seong Jin An, Jianlin Li, Claus Daniel, Debasish Mohanty, Shrikant Nagpure, and David L. Wood. The state of understanding of the lithium-ion-battery graphite solid electrolyte interphase (SEI) and its relationship to formation cycling. *Carbon*, 2016.

[13] Christoph R. Birkl, Matthew R. Roberts, Euan McTurk, Peter G. Bruce, and David A. Howey. Degradation diagnostics for lithium ion cells. *Journal of Power Sources*, 341:373–386, 2017.

[14] Chemie.de. Wasserstoffelektrode.

[15] J. Vetter, P. Novák, M. R. Wagner, C. Veit, K.-C. C. Möller, J. O. Besenhard, M. Winter, M. Wohlfahrt-Mehrens, C. Vogler, and A. Hammouche. Ageing mechanisms in lithium-ion batteries. *Journal of Power Sources*, 147(1-2):269–281, 2005.

[16] John B. Goodenough and Youngsik Kim. Challenges for rechargeable Li batteries. *Chemistry of Materials*, 2010.

[17] Fu Ming Wang, Meng Han Yu, Yi Ju Hsiao, Ying Tsai, Bing Joe Hwang, Yung Yun Wang, and Chi Chao Wan. Aging effects to solid electrolyte interface (SEI) membrane formation and the performance analysis of lithium ion batteries. *International Journal of Electrochemical Science*, 6(4):1014–1026, 2011.

[18] Mengyun Nie, Dinesh Chalasani, Daniel P. Abraham, Yanjing Chen, Arijit Bose, and Brett L. Lucht. Lithium ion battery graphite solid electrolyte interphase revealed by microscopy and spectroscopy. *Journal of Physical Chemistry C*, 2013.

[19] Toshihiro Yoshida, Michio Takahashi, Satoshi Morikawa, Chikashi Ihara, Hiroyuki Katsukawa, Tomoyuki Shiratsuchi, and Jun-ichi Yamaki. Degradation Mechanism and Life Prediction of Lithium-Ion Batteries. *Journal of The Electrochemical Society*, 153(3):A576, 2006.

[20] Jung Tae Lee, Naoki Nitta, James Benson, Alexandre Magasinski, Thomas F. Fuller, and Gleb Yushin. Comparative study of the solid electrolyte interphase on graphite in full Li-ion battery cells using X-ray photoelectron spectroscopy, secondary ion mass spectrometry, and electron microscopy. *Carbon*, 2013.

[21] Xiao Guang Yang, Yongjun Leng, Guangsheng Zhang, Shanhai Ge, and Chao Yang Wang. Modeling of lithium plating induced aging

of lithium-ion batteries: Transition from linear to nonlinear aging. *Journal of Power Sources*, 2017.

[22] Christian Von Lüders. *Experimentelle und simulative Untersuchung von Lithium-Plating und Lithium-Stripping in Lithium-Ionen-Zellen.* PhD thesis, Technische Universität München, 2019.

[23] Andreas Jossen and Wolfgang Weydanz. *Moderne Akkumulatoren richtig einsetzen*, volume 49. Cuvillier Verlag, 2021.

[24] Thomas Waldmann and Margret Wohlfahrt-Mehrens. Effects of rest time after Li plating on safety behavior - ARC tests with commercial high-energy 18650 Li-ion cells. *Electrochimica Acta*, 230:454–460, 2017.

[25] Johannes Sieg, Jochen Bandlow, Tim Mitsch, Daniel Dragicevic, Torben Materna, Bernd Spier, Heiko Witzenhausen, Madeleine Ecker, and Dirk Uwe Sauer. Fast charging of an electric vehicle lithium-ion battery at the limit of the lithium deposition process. *Journal of Power Sources*, 2019.

[26] Tobias C. Bach, Simon F. Schuster, Elena Fleder, Jana Müller, Martin J. Brand, Henning Lorrmann, Andreas Jossen, and Gerhard Sextl. Nonlinear aging of cylindrical lithium-ion cells linked to heterogeneous compression. *Journal of Energy Storage*, 2016.

[27] Victor Agubra and Jeffrey Fergus. Lithium ion battery anode aging mechanisms. *Materials*, 6(4):1310–1325, 2013.

[28] Simon F. Schuster, Tobias Bach, Elena Fleder, Jana Müller, Martin Brand, Gerhard Sextl, and Andreas Jossen. Nonlinear aging characteristics of lithium-ion cells under different operational conditions. *Journal of Energy Storage*, 2015.

[29] Timo Danner, Madhav Singh, Simon Hein, Jörg Kaiser, Horst Hahn, and Arnulf Latz. Thick electrodes for Li-ion batteries: A model based analysis. *Journal of Power Sources*, 2016.

[30] D. Anseán, M. Dubarry, A. Devie, B. Y. Liaw, V. M. García, J. C. Viera, and M. González. Operando lithium plating quantification and early detection of a commercial $LiFePO_4$ cell cycled under dynamic driving schedule. *Journal of Power Sources*, 2017.

[31] Jens Steiger, Dominik Kramer, and Reiner Mönig. Mechanisms of dendritic growth investigated by in situ light microscopy during electrodeposition and dissolution of lithium. *Journal of Power Sources*, 2014.

[32] Jiang Fan and Steven Tan. Studies on Charging Lithium-Ion Cells at Low Temperatures. *Journal of The Electrochemical Society*, 153(6):A1081, 2006.

[33] Christian von Lüders, Veronika Zinth, Simon V. Erhard, Patrick J. Osswald, Michael Hofmann, Ralph Gilles, and Andreas Jossen. Lithium plating in lithium-ion batteries investigated by voltage relaxation and in situ neutron diffraction. *Journal of Power Sources*, 342:17–23, 2017.

[34] B. Rieger, S. Schlueter, S.V. Erhard, J. Schmalz, G. Reinhart, and A. Jossen. Multi-scale investigation of thickness changes in a commercial pouch type lithium-ion battery. *Journal of Energy Storage*, 6:213–221, 2016.

[35] Vijay A. Sethuraman, Laurence J. Hardwick, Venkat Srinivasan, and Robert Kostecki. Surface structural disordering in graphite upon lithium intercalation/deintercalation. *Journal of Power Sources*, 2010.

[36] Leonard Jahn, Felix Katzer, and Michael A Danzer. Combined dilatometry and voltage analysis for a reliable detection of lithium deposition on graphitic anodes. *Journal of Power Sources*, 520:230870, 2022.

[37] G Bohn, J Taub, A Linke, S Bayer, D Oeser, A Ziegler, P Ettl, and A Ackva. High-resolution Interferometric Measurement of Thickness Change on a Lithium-Ion Pouch Battery. *IOP Conference Series: Earth and Environmental Science*, 281:012030, 2019.

[38] Jiagang Xu, Rutooj D. Deshpande, Jie Pan, Yang-Tse Cheng, and Vincent S. Battaglia. Electrode Side Reactions, Capacity Loss and Mechanical Degradation in Lithium-Ion Batteries. *Journal of The Electrochemical Society*, 162(10):A2026–A2035, 2015.

[39] Ping Liu, John Wang, Jocelyn Hicks-Garner, Elena Sherman, Souren Soukiazian, Mark Verbrugge, Harshad Tataria, James Musser, and Peter Finamore. Aging Mechanisms of $LiFePO_4$ Batteries Deduced by Electrochemical and Structural Analyses. *Journal of The Electrochemical Society*, 2010.

[40] Cheng Lin, Aihua Tang, Hao Mu, Wenwei Wang, and Chun Wang. Aging mechanisms of electrode materials in lithium-ion batteries for electric vehicles. *Journal of Chemistry*, 2015, 2015.

[41] Shinichi Komaba, Naoaki Kumagai, Tomoya Sasaki, and Yuko Miki. Manganese dissolution from lithium doped Li-Mn-O spinel cathode materials into electrolyte solution. *Electrochemistry*, 69(10):784–787,

2001.

[42] S.-C Yin, Y.-H Rho, I Swainson, and L F Nazar. X-ray/Neutron Diffraction and Electrochemical Studies of Lithium De/Re-Intercalation in $Li_{1-x}Co_{1/3}Ni_{1/3}Mn_{1/3}O_2$ ($x = 0 \rightarrow 1$). *ACS Publications*, 2006.

[43] Zongyi Wang, Yun Zhang, Baojun Chen, and Chao Lu. Study on decrystallization of cathode material and decomposition of electrolyte in $LiNi_{1/3}Co_{1/3}Mn_{1/3}O_2$-based cells. *Journal of Solid State Electrochemistry*, 18(6):1757–1762, 2014.

[44] K. Edström, T. Gustafsson, and J.O. Thomas. The cathode-electrolyte interface in the Li-ion battery. *Electrochimica Acta*, 50(2-3):397–403, 2004.

[45] Li Li, Jing Ge, Feng Wu, Renjie Chen, Shi Chen, and Borong Wu. Recovery of cobalt and lithium from spent lithium ion batteries using organic citric acid as leachant. *Journal of Hazardous Materials*, 176(1-3):288–293, 2010.

[46] Lydia Terborg, Sascha Weber, Franziska Blaske, Stefano Passerini, Martin Winter, Uwe Karst, and Sascha Nowak. Investigation of thermal aging and hydrolysis mechanisms in commercial lithium ion battery electrolyte. *Journal of Power Sources*, 242:832–837, 2013.

[47] Michael Stich. *Wasserverunreinigungen in Lithium-Ionen-Batterien*. PhD thesis, Technische Universität Ilmenau, 2019.

[48] Martin Grützke, Vadim Kraft, Björn Hoffmann, Sebastian Klamor, Jan Diekmann, Arno Kwade, Martin Winter, and Sascha Nowak. Aging investigations of a lithium-ion battery electrolyte from a field-tested hybrid electric vehicle. *Journal of Power Sources*, 273:83–88, 2015.

[49] Patricia Handel, Gisela Fauler, Katja Kapper, Martin Schmuck, Christoph Stangl, Roland Fischer, Frank Uhlig, and Stefan Koller. Thermal aging of electrolytes used in lithium-ion batteries - An investigation of the impact of protic impurities and different housing materials. *Journal of Power Sources*, 267:255–259, 2014.

[50] D. Aurbach, I. Weissman, A. Zaban, and P. Dan. On the role of water contamination in rechargeable Li batteries. *Electrochimica Acta*, 45(7):1135–1140, 1999.

[51] Gerardine G. Botte, Ralph E. White, and Zhengming Zhang. Thermal stability of $LiPF_6$-EC:EMC electrolyte for lithium ion batteries.

Journal of Power Sources, 97-98:570–575, 2001.

[52] Christina Peabody and Craig B. Arnold. The role of mechanically induced separator creep in lithium-ion battery capacity fade. *Journal of Power Sources*, 196(19):8147–8153, 2011.

[53] Danghe Shi, Xinran Xiao, Xiaosong Huang, and Hamid Kia. Modeling stresses in the separator of a pouch lithium-ion cell. *Journal of Power Sources*, 196(19):8129–8139, 2011.

[54] Robert Kostecki, Laura Norin, Xiangyun Song, and Frank McLarnon. Diagnostic Studies of Polyolefin Separators in High-Power Li-Ion Cells. *Journal of The Electrochemical Society*, 151(4):A522, 2004.

[55] T. Waldmann, S. Gorse, T. Samtleben, G. Schneider, V. Knoblauch, and M. Wohlfahrt-Mehrens. A Mechanical Aging Mechanism in Lithium-Ion Batteries. *Journal of The Electrochemical Society*, 2014.

[56] John Cannarella and Craig B. Arnold. Ion transport restriction in mechanically strained separator membranes. *Journal of Power Sources*, 226:149–155, 2013.

[57] Arnaud Devie, George Baure, and Matthieu Dubarry. Intrinsic Variability in the Degradation of a Batch of Commercial 18650 Lithium-Ion Cells. *Energies*, 11(5):1031, 2018.

[58] Michael Baumann, Leo Wildfeuer, Stephan Rohr, and Markus Lienkamp. Parameter variations within Li-Ion battery packs - Theoretical investigations and experimental quantification. *Journal of Energy Storage*, 18:295–307, 2018.

[59] Katharina Rumpf, Maik Naumann, and Andreas Jossen. Experimental investigation of parametric cell-to-cell variation and correlation based on 1100 commercial lithium-ion cells. *Journal of Energy Storage*, 14:224–243, 2017.

[60] Susanne Rothgang, Thorsten Baumhöfer, and Dirk Uwe Sauer. Diversion of aging of battery cells in automotive systems. In *2014 IEEE Vehicle Power and Propulsion Conference, VPPC 2014*, 2014.

[61] Wladislaw Waag, Stefan Käbitz, and Dirk Uwe Sauer. Experimental investigation of the lithium-ion battery impedance characteristic at various conditions and aging states and its influence on the application. *Applied Energy*, 102:885–897, 2013.

[62] D. Andre, M. Meiler, K. Steiner, Ch Wimmer, T. Soczka-Guth, and D. U. Sauer. Characterization of high-power lithium-ion batteries

by electrochemical impedance spectroscopy. I. Experimental investigation. *Journal of Power Sources*, 196(12):5334–5341, 2011.

[63] Peter Keil. *Aging of lithium-ion batteries in electric vehicles.* Phd thesis, Technische Universität München, 2015.

[64] Andreas Jossen. Fundamentals of battery dynamics. *Journal of Power Sources*, 2006.

[65] Eckhard Karden, Stephan Buller, and Rik W. De Doncker. A method for measurement and interpretation of impedance spectra for industrial batteries. *Journal of Power Sources*, 85(1):72–78, 2000.

[66] Jan Philipp Schmidt. *Verfahren zur Charakterisierung und Modellierung von Lithium-Ionen Zellen.* PhD thesis, Karlsruher Institut für Technologie, 2013.

[67] Nils Lohmann, Patrick Weßkamp, Peter Haußmann, Joachim Melbert, and Thomas Musch. Electrochemical impedance spectroscopy for lithium-ion cells: Test equipment and procedures for aging and fast characterization in time and frequency domain. *Journal of Power Sources*, 273:613–623, 2015.

[68] F . C. Laman, M. W. Matsen, and J . A. R. Stiles. Inductive Impedance of a Spirally Wound Li / MoS_2 Cell. *Journal of The Electrochemical Society*, pages 2441–2446, 1986.

[69] Anup Barai, Gael H. Chouchelamane, Yue Guo, Andrew McGordon, and Paul Jennings. A study on the impact of lithium-ion cell relaxation on electrochemical impedance spectroscopy. *Journal of Power Sources*, 280:74–80, 2015.

[70] Heider Lilia Levi, M. D., Salitra G., Markovsky B.; Teller H., Aurbach D., Heider Udo. Solid-State Electrochemical Kinetics of Li-Ion Intercalation into $LiCoO_2$. *Journal of The Electrochemical Society*, 1999.

[71] Jun Huang, Zhe Li, Jianbo Zhang, Shaoling Song, Zhongliang Lou, and Ningning Wu. An Analytical Three-Scale Impedance Model for Porous Electrode with Agglomerates in Lithium-Ion Batteries. *Journal of The Electrochemical Society*, 162(4):A585–A595, 2015.

[72] KIT. Batteriemodellierung in MATLAB, Grundlagen Batterien II.

[73] Thorsten Baumhöfer, Manuel Brühl, Susanne Rothgang, and Dirk Uwe Sauer. Production caused variation in capacity aging trend and correlation to initial cell performance. *Journal of Power Sources*,

247:332–338, 2014.

[74] Frank M. Kindermann, Andreas Noel, Simon V. Erhard, and Andreas Jossen. Long-term equalization effects in Li-ion batteries due to local state of charge inhomogeneities and their impact on impedance measurements. *Electrochimica Acta*, 185:107–116, 2015.

[75] See How Ng, Fabio La Mantia, and Petr Novák. A multiple working electrode for electrochemical cells: A tool for current density distribution studies. *Angewandte Chemie - International Edition*, 48(3):528–532, 2009.

[76] Jan Becker, Markus Lelie, Markus Jansen, and Dirk Uwe Sauer. Impact of low Temperatures on Performance and Ageing of Lithium-Ion Batteries and Strategies for Heating. In *Hybrid and electric vehicles : 11th Symposium*, 2014.

[77] L. H.J. Raijmakers, D. L. Danilov, J. P.M. Van Lammeren, M. J.G. Lammers, and P. H.L. Notten. Sensorless battery temperature measurements based on electrochemical impedance spectroscopy. *Journal of Power Sources*, 247:539–544, 2014.

[78] Ira Bloom, Lee K. Walker, John K. Basco, Daniel P. Abraham, Jon P. Christophersen, and Chinh D. Ho. Differential voltage analyses of high-power lithium-ion cells. 4. Cells containing NMC. *Journal of Power Sources*, 195(3):877–882, 2010.

[79] Ira Bloom, Andrew N. Jansen, Daniel P. Abraham, Jamie Knuth, Scott A. Jones, Vincent S. Battaglia, and Gary L. Henriksen. Differential voltage analyses of high-power, lithium-ion cells. *Journal of Power Sources*, 139(1-2):295–303, 2005.

[80] Matthieu Dubarry, Cyril Truchot, Bor Yann Liaw, Kevin Gering, Sergiy Sazhin, David Jamison, and Christopher Michelbacher. Evaluation of commercial lithium-ion cells based on composite positive electrode for plug-in hybrid electric vehicle applications. Part II. Degradation mechanism under 2 C cycle aging. *Journal of Power Sources*, 196(23):10336–10343, 2011.

[81] Matthieu Dubarry, Vojtech Svoboda, Ruey Hwu, and Bor Yann Liaw. Incremental capacity analysis and close-to-equilibrium OCV measurements to quantify capacity fade in commercial rechargeable lithium batteries. *Electrochemical and Solid-State Letters*, 2006.

[82] Meinert Lewerenz, Georg Fuchs, Lisa Becker, and Dirk Uwe Sauer. Irreversible calendar aging and quantification of the reversible ca-

pacity loss caused by anode overhang. *Journal of Energy Storage*, 18(May):149–159, 2018.

[83] Peter Keil, Simon F. Schuster, Jörn Wilhelm, Julian Travi, Andreas Hauser, Ralph C. Karl, and Andreas Jossen. Calendar Aging of Lithium-Ion Batteries. *Journal of The Electrochemical Society*, 2016.

[84] Michael Heß and Petr Novák. Shrinking annuli mechanism and stage-dependent rate capability of thin-layer graphite electrodes for lithium-ion batteries. *Electrochimica Acta*, 106:149–158, 2013.

[85] Marius Bauer. *Elektrische und mechanische Verfahren zur Detektion von Alterungseffekten in Lithium-Ionen-Batterien.* PhD thesis, Technische Universität München, 2017.

[86] Andreas Klein. *Untersuchungen zur Erhöhung der Strombelastbarkeit manganbasierter Kathodenmaterialien für Lithium-Ionen Batterien.* PhD thesis, Universität Ulm, 2016.

[87] Meinert Lewerenz, Andrea Marongiu, Alexander Warnecke, and Dirk Uwe Sauer. Differential voltage analysis as a tool for analyzing inhomogeneous aging: A case study for $LiFePO_4$—Graphite cylindrical cells. *Journal of Power Sources*, 368:57–67, 2017.

[88] Matthieu Dubarry, Nicolas Vuillaume, and Bor Yann Liaw. Origins and accommodation of cell variations in Li-ion battery pack modeling. *International Journal of Energy Research*, 34(2):216–231, 2010.

[89] Matthieu Dubarry, Cyril Truchot, Mikaël Cugnet, Bor Yann Liaw, Kevin Gering, Sergiy Sazhin, David Jamison, and Christopher Michelbacher. Evaluation of commercial lithium-ion cells based on composite positive electrode for plug-in hybrid electric vehicle applications. Part I: Initial characterizations. *Journal of Power Sources*, 196(23):10328–10335, 2011.

[90] Sebastian Paul, Christian Diegelmann, Herbert Kabza, and Werner Tillmetz. Analysis of ageing inhomogeneities in lithium-ion battery systems. *Journal of Power Sources*, 239:642–650, 2013.

[91] Susanne Rothgang, Thorsten Baumhöfer, and Dirk Uwe Sauer. Necessity and Methods to Improve Battery Lifetime on System Level. In *EVS28*, 2015.

[92] Dirk Uwe Sauer, Thorsten Baumhöfer, and Susanne Lehner. Disparity in initial and lifetime parameters of lithium-ion cells. *IET Electrical Systems in Transportation*, 2016.

[93] Simon F. Schuster, Martin J. Brand, Philipp Berg, Markus Gleissenberger, and Andreas Jossen. Lithium-ion cell-to-cell variation during battery electric vehicle operation. *Journal of Power Sources*, 297:242–251, 2015.

[94] Fuqiang An, Lufan Chen, Jun Huang, Jianbo Zhang, and Ping Li. Rate dependence of cell-to-cell variations of lithium-ion cells. *Scientific Reports*, 6:4–10, 2016.

[95] Christian Campestrini, Peter Keil, Simon F. Schuster, and Andreas Jossen. Ageing of lithium-ion battery modules with dissipative balancing compared with single-cell ageing. *Journal of Energy Storage*, 6:142–152, 2016.

[96] Christoph Lienemann. Produktionsprozess einer Lithium-Ionen-Zelle, 2018.

[97] Dirk Kehrwald, Paul R. Shearing, Nigel P. Brandon, Puneet K. Sinha, and Stephen J. Harris. Local Tortuosity Inhomogeneities in a Lithium Battery Composite Electrode. *Journal of The Electrochemical Society*, 2011.

[98] Georg Lenze, Henrike Bockholt, Christiane Schilcher, Linus Froböse, Dietmar Jansen, Ulrike Krewer, and Arno Kwade. Impacts of Variations in Manufacturing Parameters on Performance of Lithium-Ion-Batteries. *Journal of the Electrochemical Society*, 2018.

[99] Marcel Wilka, Alice Hoffmann, and Rainer Stern. Influence of Anode/Cathode Balancing on Cycling Stability of Lithium Ion Cells. *ECS Meeting Abstracts*, pages 2–3, 2012.

[100] Ludwig Fahrmeir, Christian Heumann, Rita Künstler, Iris Pigeot, and Gerhard Tutz. *Statistik - Der Weg zur Datenanalyse, 8. Auflage.* Springer Spektrum, 2016.

[101] Katharina Rumpf. *Causes and effects of inhomogeneity in lithium-ion battery modules : A physicochemical modelling approach.* PhD thesis, Technische Universität München, 2018.

[102] Madeleine Ecker, Nerea Nieto, Stefan Käbitz, Johannes Schmalstieg, Holger Blanke, Alexander Warnecke, and Dirk Uwe Sauer. Calendar and cycle life study of Li(NiMnCo)O_2-based 18650 lithium-ion batteries. *Journal of Power Sources*, 2014.

[103] Stephen J. Harris, David J. Harris, and Chen Li. Failure statistics for commercial lithium ion batteries: A study of 24 pouch cells. *Journal of Power Sources*, 2017.

[104] Seung Wook Eom, Min Kyu Kim, Ick Jun Kim, Seong In Moon, Yang Kook Sun, and Hyun Soo Kim. Life prediction and reliability assessment of lithium secondary batteries. *Journal of Power Sources*, 2007.

[105] Kristen A. Severson, Peter M. Attia, Norman Jin, Nicholas Perkins, Benben Jiang, Zi Yang, Michael H. Chen, Muratahan Aykol, Patrick K. Herring, Dimitrios Fraggedakis, Martin Z. Bazant, Stephen J. Harris, William C. Chueh, and Richard D. Braatz. Data-driven prediction of battery cycle life before capacity degradation. *Nature Energy*, 4(5):383–391, 2019.

[106] Thorsten Baumhöfer, Susanne Rothgang, and Dirk Uwe Sauer. The Necessity and Methods for Choosing the Best Performing Lithium-Ion Cells from a Production Batch. In *European Space Power Conference*, 2014.

[107] Johannes Schmalstieg, Stefan Käbitz, Madeleine Ecker, and Dirk Uwe Sauer. A holistic aging model for Li(NiMnCo)O_2 based 18650 lithium-ion batteries. *Journal of Power Sources*, 2014.

[108] Peter Keil and Andreas Jossen. Charging protocols for lithium-ion batteries and their impact on cycle life-An experimental study with different 18650 high-power cells. *Journal of Energy Storage*, 2016.

[109] Xiao Guang Yang and Chao Yang Wang. Understanding the trilemma of fast charging, energy density and cycle life of lithium-ion batteries. *Journal of Power Sources*, 402:489–498, 2018.

[110] Alexander Johannes Warnecke. *Degradation Mechanisms in NMC-Based Lithium-Ion Batteries*. PhD thesis, RWTH Aachen, 2017.

[111] Meinert Lewerenz, Jens Münnix, Johannes Schmalstieg, Stefan Käbitz, Marcus Knips, and Dirk Uwe Sauer. Systematic aging of commercial $LiFePO_4$ —Graphite cylindrical cells including a theory explaining rise of capacity during aging. *Journal of Power Sources*, 345:254–263, 2017.

[112] Thomas Waldmann, Marcel Wilka, Michael Kasper, Meike Fleischhammer, and Margret Wohlfahrt-Mehrens. Temperature dependent ageing mechanisms in Lithium-ion batteries - A Post-Mortem study. *Journal of Power Sources*, 2014.

[113] Barbara Stiaszny, Jörg C. Ziegler, Elke E. Krauß, Jan P. Schmidt, and Ellen Ivers-Tiffée. Electrochemical characterization and post-mortem analysis of aged $LiMn_2O_4$-Li($Ni_{0.5}Mn_{0.3}Co_{0.2}$)O_2/graphite lithium ion batteries. Part I: Cycle aging. *Journal of Power Sources*, 251:439–450,

2014.

[114] Sophia Gantenbein. *Impedanzbasierte Modellierung von Lithium-Ionen Zellen und deren Degradationsverhalten*. PhD thesis, KIT, 2019.

[115] Pouyan Shafiei Sabet and Dirk Uwe Sauer. Separation of predominant processes in electrochemical impedance spectra of lithium-ion batteries with nickel-manganese-cobalt cathodes. *Journal of Power Sources*, 2019.

[116] Käbitz Stefan R. *Untersuchung der Alterung von Lithium-Ionen-Batterien mittels Elektroanalytik und elektrochemischer Impedanzspektroskopie*. PhD thesis, RWTH Aachen, 2013.

[117] Alex Friesen, Jan Haetge, Falko M Schappacher, and Martin Winter. Influence of temperature on the aging behavior of 18650-type lithium ion cells: A comprehensive approach combining electrochemical characterization and post-mortem analysis. *Journal of Power Sources*, 342:88–97, 2017.

[118] Arpit Maheshwari, Michael Heck, and Massimo Santarelli. Cycle aging studies of lithium nickel manganese cobalt oxide-based batteries using electrochemical impedance spectroscopy. *Electrochimica Acta*, 273:335–348, 2018.

[119] T. Matsuda, M. Myojin, K. Ando, and D. Imamura. Degradation Analyses of Commercial Lithium-Ion Cells by Temperature/C-rate Controlled Cycle Test. *ECS Transactions*, 64(22):69–75, 2015.

[120] B. Rieger, S. F. Schuster, S. V. Erhard, P. J. Osswald, A. Rheinfeld, C. Willmann, and A. Jossen. Multi-directional laser scanning as innovative method to detect local cell damage during fast charging of lithium-ion cells. *Journal of Energy Storage*, 8:1–5, 2016.

[121] Alex Friesen, Fabian Horsthemke, Xaver Mönnighoff, Gunther Brunklaus, Roman Krafft, Markus Börner, Tim Risthaus, Martin Winter, and Falko M. Schappacher. Impact of cycling at low temperatures on the safety behavior of 18650-type lithium ion cells: Combined study of mechanical and thermal abuse testing accompanied by post-mortem analysis. *Journal of Power Sources*, 2016.

[122] Johannes Philipp Fath, Daniel Dragicevic, Laura Bittel, Adnan Nuhic, Johannes Sieg, Severin Hahn, Lennart Alsheimer, Bernd Spier, and Thomas Wetzel. Quantification of aging mechanisms and inhomogeneity in cycled lithium-ion cells by differential voltage analysis. *Journal of Energy Storage*, 25:100813, 2019.

[123] Matthieu Dubarry, Nan Qin, and Paul Brooker. Calendar aging of commercial Li-ion cells of different chemistries - A review. *Current Opinion in Electrochemistry*, 9:106–113, 2018.

[124] John Wang, Justin Purewal, Ping Liu, Jocelyn Hicks-Garner, Souren Soukazian, Elena Sherman, Adam Sorenson, Luan Vu, Harshad Tataria, and Mark W. Verbrugge. Degradation of lithium ion batteries employing graphite negatives and nickel-cobalt-manganese oxide + spinel manganese oxide positives: Part 1, aging mechanisms and life estimation. *Journal of Power Sources*, 269:937–948, 2014.

[125] Christian Geisbauer, Katharina Wöhrl, Daniel Koch, Gudrun Wilhelm, Gerhard Schneider, and Hans-Georg Schweiger. Comparative Study on the Calendar Aging Behavior of Six Different Lithium-Ion Cell Chemistries in Terms of Parameter Variation. *MDPI Energies*, 14:3358, 2021.

[126] Radu Gogoana, Matthew B. Pinson, Martin Z. Bazant, and Sanjay E. Sarma. Internal resistance matching for parallel-connected lithium-ion cells and impacts on battery pack cycle life. *Journal of Power Sources*, 252:8–13, 2014.

[127] C. Pastor-Fernández, T. Bruen, W. D. Widanage, M. A. Gama-Valdez, and J. Marco. A Study of Cell-to-Cell Interactions and Degradation in Parallel Strings: Implications for the Battery Management System. *Journal of Power Sources*, 329:574–585, 2016.

[128] David Oeser, Andreas Ziegler, and Ansgar Ackva. Single cell analysis of lithium-ion e-bike batteries aged under various conditions. *Journal of Power Sources*, 397:25–31, 2018.

[129] Daniel Werner, Sabine Paarmann, Achim Wiebelt, and Thomas Wetzel. Inhomogeneous temperature distribution affecting cyclic aging of Li-ion cells. Part ii: Analysis and correlation. *Batteries*, 6(1), 2020.

[130] Matthias Fleckenstein, Oliver Bohlen, Michael A. Roscher, and Bernard Bäker. Current density and state of charge inhomogeneities in Li-ion battery cells with $LiFePO_4$ as cathode material due to temperature gradients. *Journal of Power Sources*, 196(10):4769–4778, 2011.

[131] Yichao Zhang, Ruxiu Zhao, Jacob Dubie, Thomas Jahns, and Larry Juang. Investigation of current sharing and heat dissipation in parallel-connected lithium-ion battery packs. *IEEE Energy Conversion Congress and Exposition (ECCE)*, 2016.

[132] Naixing Yang, Xiongwen Zhang, Binbin Shang, and Guojun Li. Unbal-

anced discharging and aging due to temperature differences among the cells in a lithium-ion battery pack with parallel combination. *Journal of Power Sources*, 306:733–741, 2016.

[133] Tao Wang, K. J. Tseng, Jiyun Zhao, and Zhongbao Wei. Thermal investigation of lithium-ion battery module with different cell arrangement structures and forced air-cooling strategies. *Applied Energy*, 2014.

[134] Kuan Cheng Chiu, Chi Hao Lin, Sheng Fa Yeh, Yu Han Lin, Chih Sheng Huang, and Kuo Ching Chen. Cycle life analysis of series connected lithium-ion batteries with temperature difference. *Journal of Power Sources*, 263:75–84, 2014.

[135] Ziyou Song, Niankai Yang, Xinfan Lin, Fanny Pinto Delgado, Heath Hofmann, and Jing Sun. Progression of cell-to-cell variation within battery modules under different cooling structures. *Applied Energy*, 2022.

[136] Thomas Bruen and James Marco. Modelling and experimental evaluation of parallel connected lithium ion cells for an electric vehicle battery system. *Journal of Power Sources*, 310:91–101, 2016.

Appendix A

Additional Measurement Data

A.1 Single Cell Ageing Curves (RPT)

In chapter 5, the ageing curves of all 80 individual cells are presented on the basis of the cyclic data. The cyclic data are characterised by a high information content, as the data are recorded every cycle. The RPT data are only recorded every 50 cycles. Accordingly, the ageing process under most test conditions cannot be accurately presented. However, the advantage of the RPT data is the complete comparability between the test conditions. On the following pages, all ageing curves are therefore also presented on the basis of the RPT data.

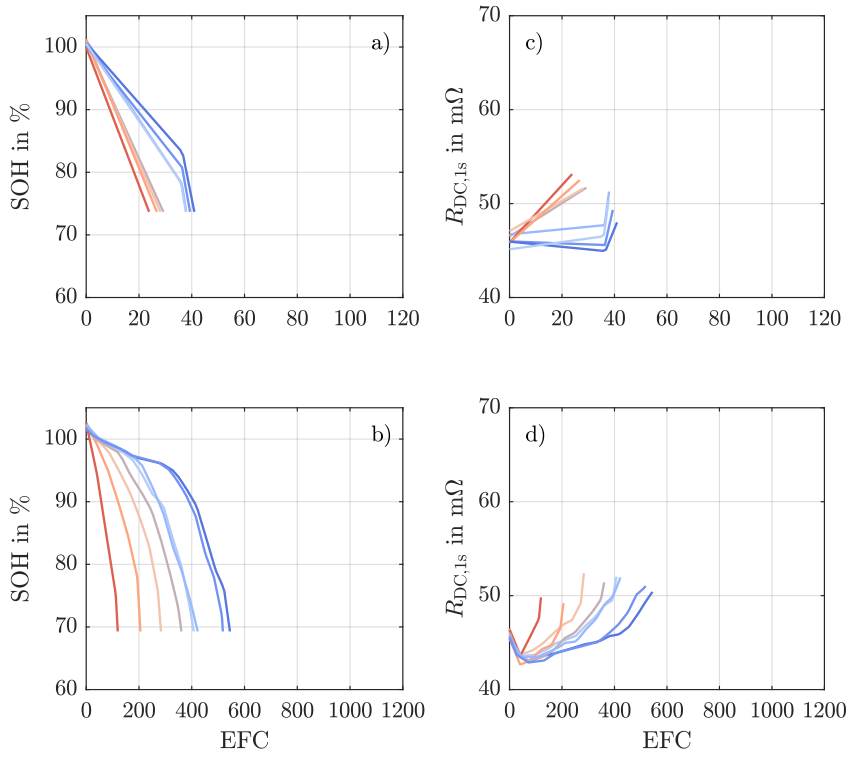

Figure A.1: Plots a) and b) show the SOH under the test conditions 0.5C/0°C, 10°C respectively. Plots c) and d) show the corresponding curves of $R_{DC,1s}$. The colouring of the curves from red to blue is based on the lifetime within the respective test condition.

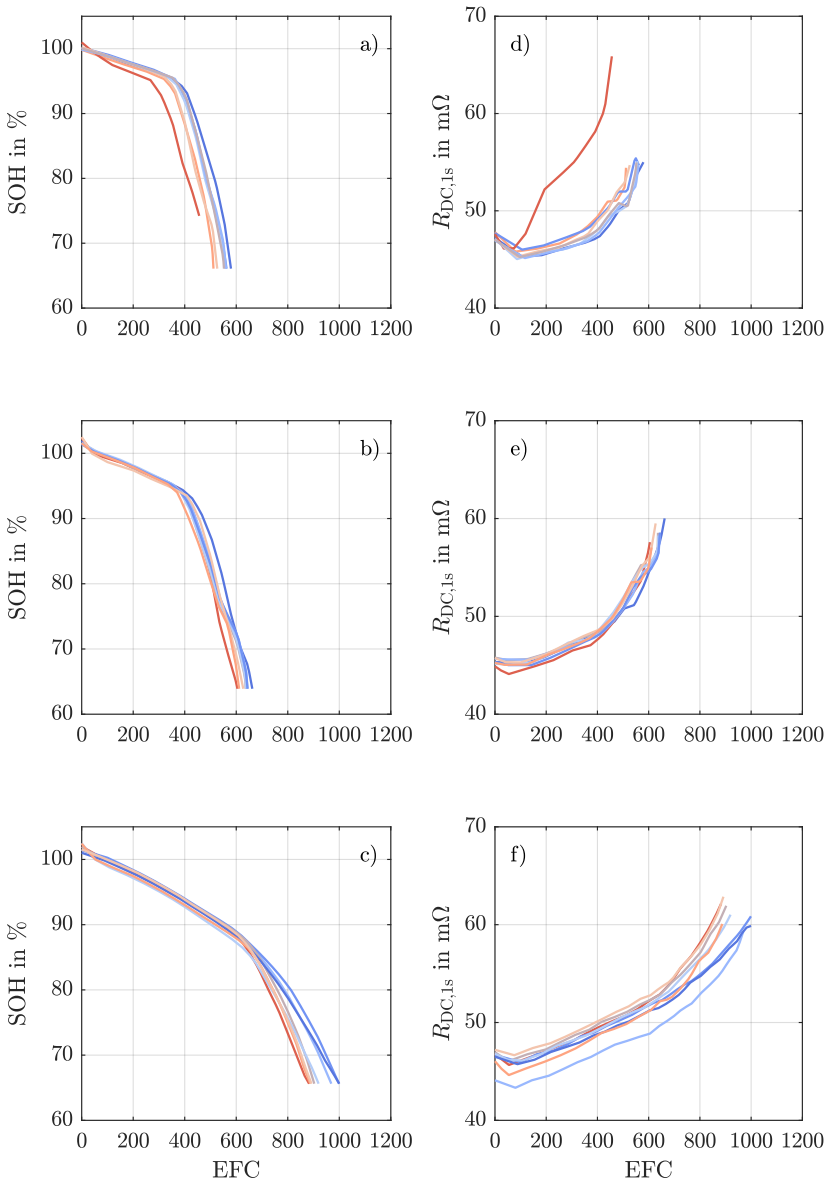

Figure A.2: Plots a) to c) show the SOH under the test conditions 0.5C/20°C, 30°C, 40°C, respectively. Plots d) to f) show the corresponding curves of $R_{DC,1s}$. The colouring of the curves from red to blue is based on the lifetime within the respective test condition.

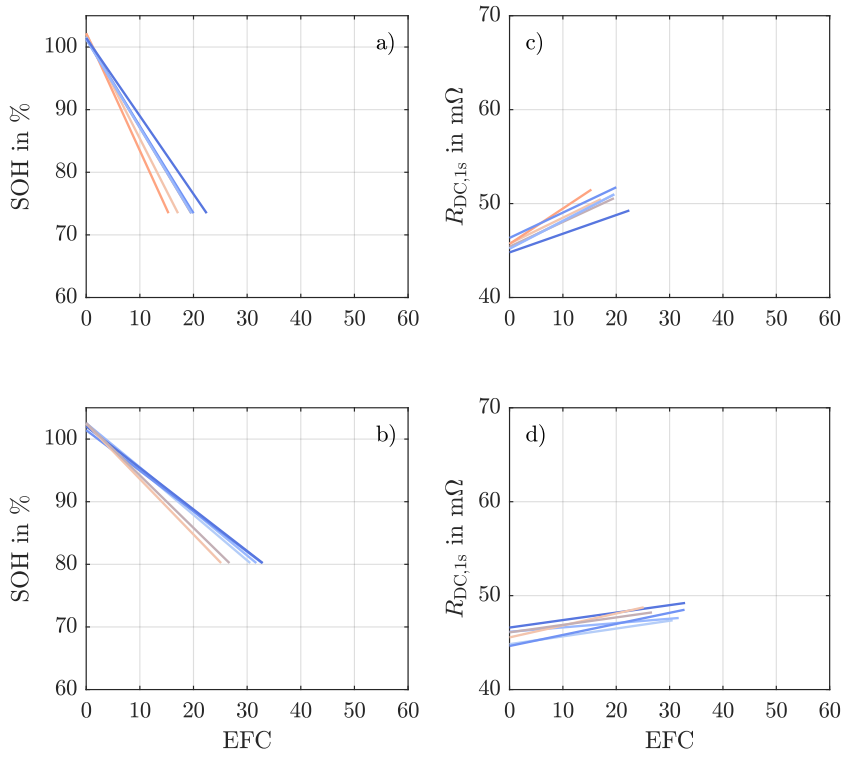

Figure A.3: Plots a) and b) show the SOH under the test conditions 1.0C/0°C, 10°C respectively. Plots c) and d) show the corresponding curves of $R_{DC,1s}$. The colouring of the curves from red to blue is based on the lifetime within the respective test condition.

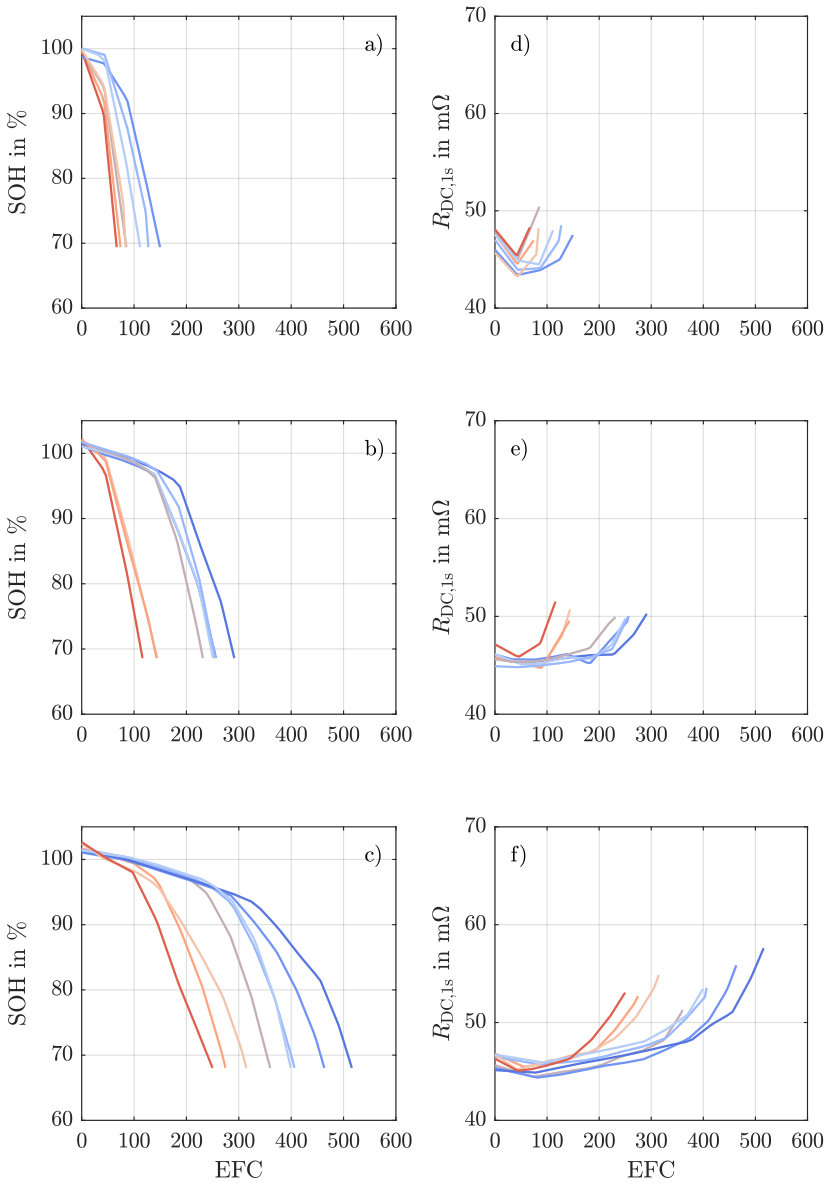

Figure A.4: Plots a) to c) show the SOH under the test conditions 1.0C/20°C, 30°C, 40°C, respectively. Plots d) to f) show the corresponding curves of $R_{DC,1s}$. The colouring of the curves from red to blue is based on the lifetime within the respective test condition.

A.2 DVA of Aged Single Cells (Absolute Values)

In chapter 5, the DVA at EOT is presented over the SOC. The representation via the SOC has the advantage of showing the shift of the middle anode peak in a visually simple way. Thus, it can be quickly checked whether the anode has a limiting effect on the cell capacity. For the sake of completeness, the DVA is also shown on the basis of the absolute values in Ah on the following pages.

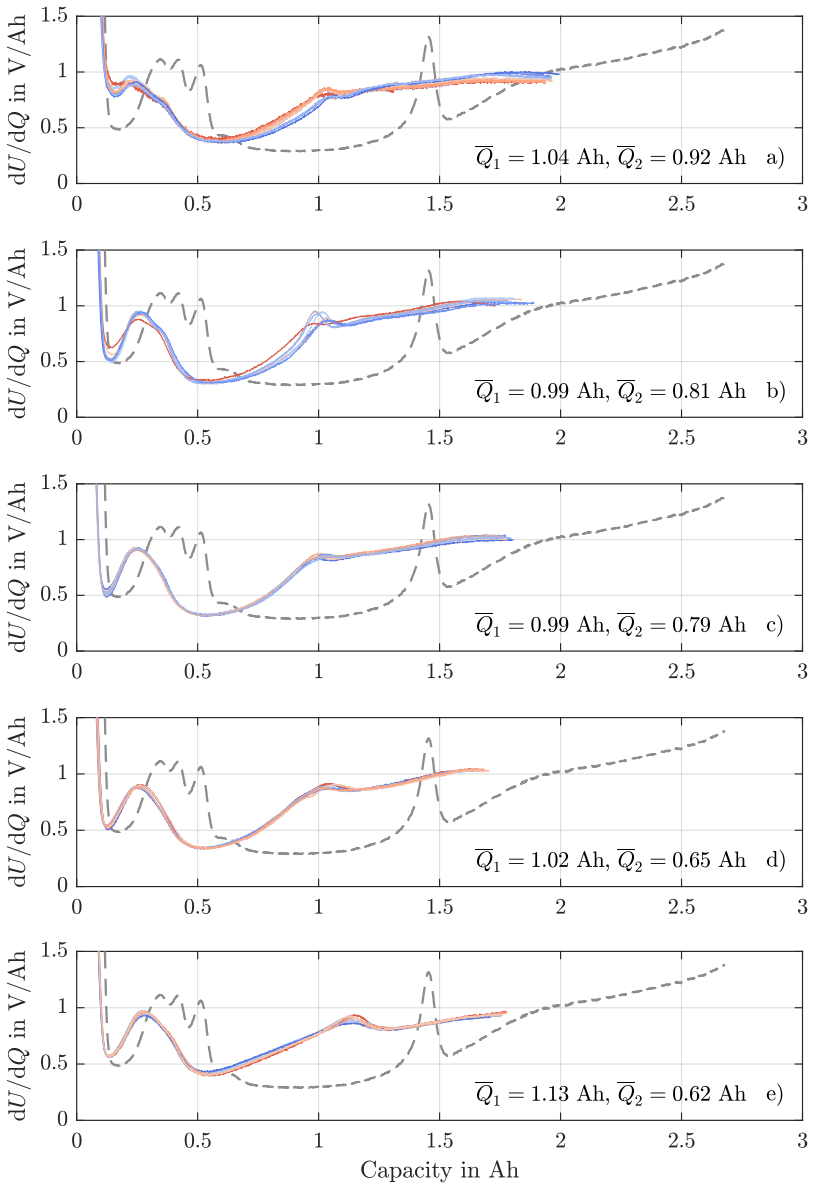

Figure A.5: DVA of cells aged with 0.5C (absolute values). In a) to e), the temperatures from 0°C to 40°C in steps of 10°C are shown in ascending order. The colouring of the curves matches that of the cyclic data plots and represents the achieved lifetime.

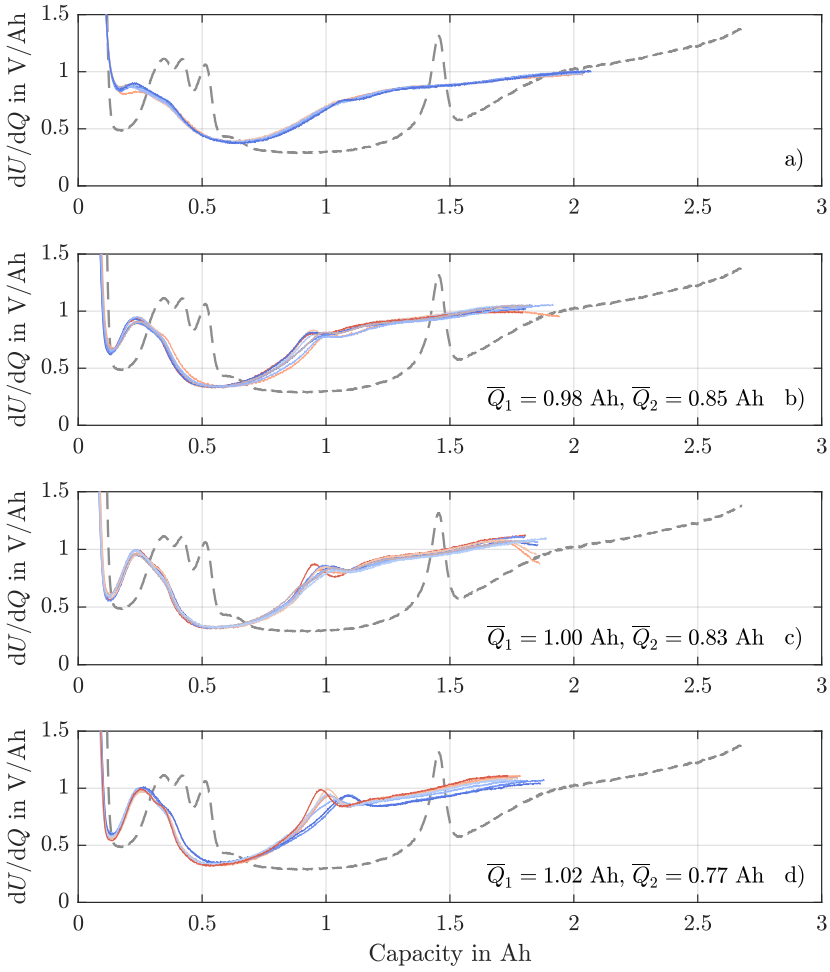

Figure A.6: DVA of cells aged with 1.0C (absolute values). In a) the cells aged at 0°C are shown in b) to d) the cells from 20°C to 40°C in steps of 10°C are shown in ascending order. DVA for 1.0C/10°C is not possible due to triggered CIDs. The colouring of the curves matches that of the cyclic data plots and represents the achieved lifetime.